LS-DYNA Validation Booklet

ARUP

Date   July 2016

Editors   Jan van Elk & Dirk Doornhof

General Introduction

As part of the investigations into the seismic response of unreinforced masonry (URM) buildings, measurements and experiments have been carried out on building materials, wall elements and wall units to establish the material properties of building materials and the behaviour of masonry walls units (Ref. 1 to 6). This knowledge is used to calibrate numerical models for buildings (Ref. 7 and 8).

The current report describes the development and calibration of a new masonry material model plug-in for the modelling software LS-DYNA. This validation book also shows that with the modelling software LS-DYNA reliable simulations can be performed, which reasonably replicate the recent experiments performed by TU Delft and Eucentre in Pavia.

References

1. In-situ testing of URM houses (building unit: Loppersum, Zijlvest 25), Eucentre (F. Graziotti, A. Rossi, I. Senaldi, S. Peloso), 5th December 2014.
2. Summary report for the characterisation of original Groningen masonry, TU Delft (S. Safari, J. Rots), 18th December 2015.
3. Laboratory component testing: Modelling post-test predictions and analysis cross-validation, ARUP, TU Delft and Eucentre (several staff members from all three institutions), 16th February 2016.
4. Tests for the characterisation of replicated masonry and wall ties, TU Delft (R. Esposito, F. Messali, J. Rots), 18th April 2016.
5. In-plane tests of replicated masonry walls, TU Delft (G. Ravenshorst, F. Messali), 18th April 2016.
6. Experimental campaign on cavity walls systems representative of the Groningen building stock (incl. EUC-BUILD1), Eucentre (F. Graziotti, U. Tomassetti, A. Rossi, S. Kallioras, M. Mandirola, E. Cenja, A. Penna, G. Magenes), 16th June 2016.
7. URM Modelling and Analysis Cross Validation – Arup, Eucentre, TU Delft, Reference 229746_032.0_REP127_Rev.0.03 April 2015.
8. Eucentre Shake-table Test of Terraced House Modelling Predictions and Analysis Cross Validation, staff from ARUP, Eucentre (Pavia) and TU Delft, November 2015 [this document also includes; (1) Instruments full-scale test-house Eucentre Laboratory, (2) Protocol for Shaking Table Test on Full Scale Building (Eucentre) V_1, and (3) Selection of Acceleration Time-Series for Shake Table Testing of Groningen Masonry Building at the EUCENTRE, Pavia, all three by staff from Eucentre (Pavia)].

Title	**LS-DYNA Validation Booklet**		Date	July 2016
			Initiator	NAM
Autor(s)	**Staff of ARUP**	**Editors**	Jan van Elk and Dirk Doornhof	
Organisation	ARUP	**Organisation**	NAM	
Place in the Study and Data Acquisition Plan	Study Theme: Seismic Response of Buildings (URM) Comment: As part of the investigations into the seismic response of unreinforced masonry (URM) buildings, measurements and experiments have been carried out on building materials, wall elements and wall units to establish the material properties of building materials and the behaviour of masonry walls units. This knowledge is used to calibrate numerical models for buildings. The current report describes the development and calibration of a new masonry material model plug-in for the modelling software LS-DYNA. This validation book also shows that with the modelling software LS-DYNA reliable simulations can be performed, which reasonably replicate the recent experiments performed by TU Delft and Eucentre in Pavia.			
Directliy linked research	(1) Building Material properties (2) Shake table tests (3) Fragility curves for building typologies (URM) (4) Risk Assessment			
Used data	Experiments			
Associated organisation	NAM			
Assurance	ARUP			

Client: Nederlandse Aardolie
Maatschappij

**Arup Project Title: Groningen
Earthquakes - Structural Upgrading**

LS-DYNA Validation Booklet

229746_031.0_REP1020

Rev.A.01 | 01 July 2016

This report was prepared by Arup in July 2016 on the basis of a scope of services agreed with our client. It is not intended for and should not be relied upon by any third party and no responsibility or liability is undertaken to any third party.

Job number   229746

Arup bv
Naritaweg 118
1043 CA Amsterdam
PO box 57145
1040 BA Amsterdam
The Netherlands
www.arup.com

ARUP

Contents

1   Introduction

1.1   Purpose

Arup has been developing modelling techniques and contributing to the LS-DYNA source code for seismic engineering applications over the past 25 years, and continues to expand the range of features available and to improve modelling practices and software algorithms. This document intends to demonstrate that simulation with LS-DYNA can reasonably replicate an extensive series of experimental tests and/or theoretical solutions relevant to non-linear dynamic seismic performance of structures and soils. The following topics are covered:

- Masonry walls

- Reinforced concrete slabs and shear walls

- Foundation resistance with soil modelled as 3D elements

- Pile/soil interaction

- Non-linear site response with soil modelled as 3D elements

- Timber Diaphragms

1.2   Software version

This Validation Book sets out the performance of the Development Version of LS-DYNA with masonry material model plug-in dated 25 May 2016.

Improvements to the LS-DYNA code and recommended modelling practices continue to be made in order to achieve increasing levels of accuracy in calibration against physical tests. As new versions of LS-DYNA and modelling guidance are released (incorporating consolidated sets of improvements) they will be accompanied by new versions of this Validation Book.

1.3   Context

The validation examples in each class are modelled using recommended (consistent) procedures in terms of element formulation, assignment of material parameters etc. that are also to be applied to practical project cases. For this reason the comparisons between simulations and individual test results are not 'perfect'; no attempt has been made to 'fine-tune' input parameters to obtain the best fit to individual tests.

Rather, the examples intend to demonstrate that a consistent approach to modelling and parameter selection can reproduce reasonably well a wide range of material/component behaviours.

It should also be recognised that considerable variation can be observed in experimental results for notionally identical specimens, especially for brittle behaviours and materials having high intrinsic variability (e.g. masonry).

2 Masonry Modelled with *MAT_SHELL_MASONRY

The masonry material model is the subject of ongoing development efforts by Arup. The masonry material model plug-in dated 25 May 2016 is used for the simulations reported below. This incorporates a number of enhancements relative to previous versions to improve prediction of near-collapse states arising from loss of capacity to carry vertical loads following toe-crushing or shearing failures. The developments of these enhancements has been informed by the results of recent physical tests performed at TU Delft and Eucentre, Pavia.

2.1 In-Plane Diagonal Damage Mode – Clay Brick – LOWSTA

2.1.1 Test Description

LOWSTA was a quasi-static in-plane cyclic test administered at the University of Pavia, Italy. The specimen was a 250 mm thick double-wythe wall with aspect ratio of 1.35 constructed of clay brick units. The applied overburden stress was 0.6 MPa. The wall was tested under double clamped boundary conditions [1].
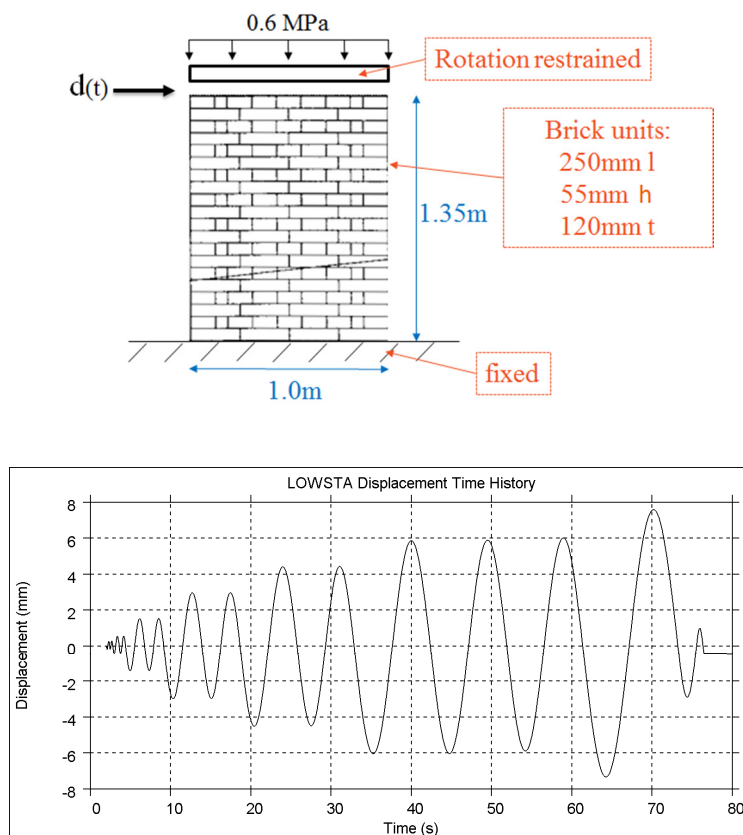

Figure 1 LOWSTA – Diagram of test set up (top) and displacement time history (bottom)

The material properties tabulated below are taken from the laboratory material characterization tests.

Table 1 LOWSTA Material Properties [2]

Mass density	1652 kg/m^3
Masonry Young's modulus perpendicular to bed joints	1491 MPa
Masonry compressive strength perpendicular to bed joints	6.2 MPa
Tensile strength (flexural bond strength) of mortar joints	0.04 MPa
Initial shear strength of mortar joints	0.23 MPa
Coefficient of friction for sliding of joints	0.58

2.1.2　　Test Results

The predominant deformation mode of LOWSTA was shear damage characterized by diagonal cracking.
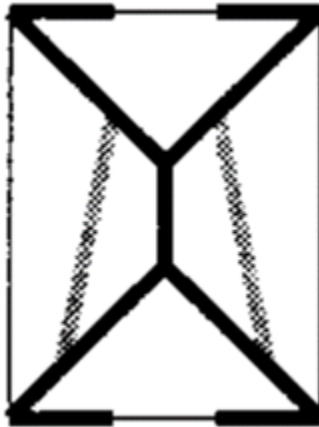

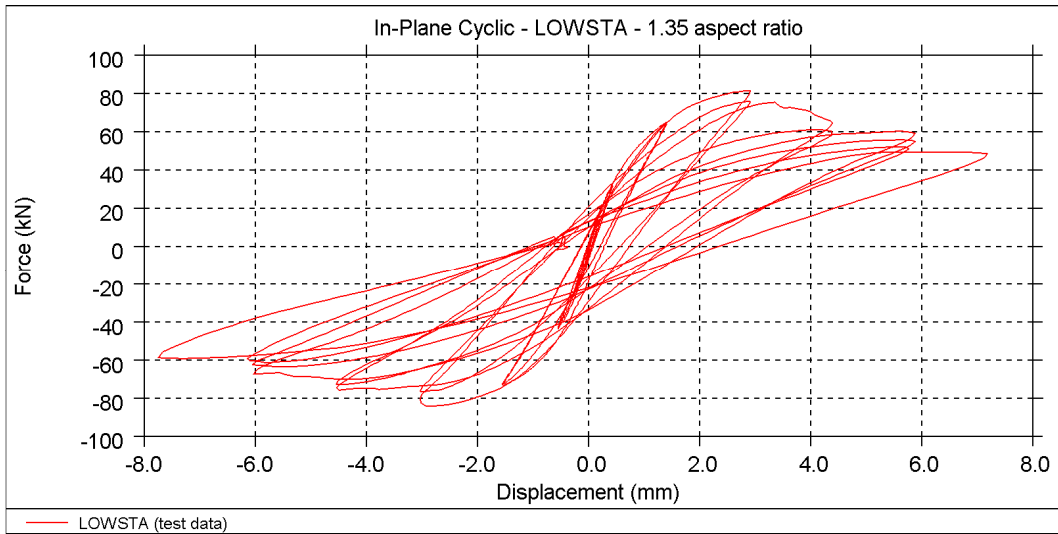Figure 2 LOWSTA – Observed crack pattern

Figure 3 LOWSTA –Shear force-displacement plot from test data

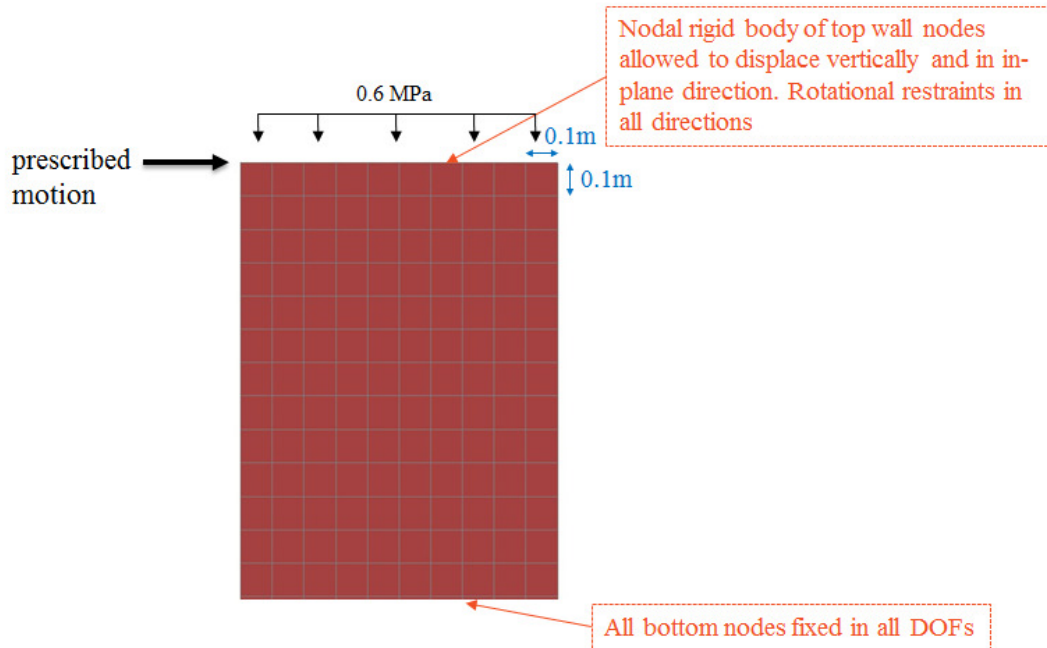### 2.1.3   LS-DYNA: Model Description

Figure 4 LS-DYNA shell model description

2.1.4   LS-DYNA: Results & Validation

The results presented below were obtained using the 25-May-2016 version of the MAT_SHELL_MASONRY.
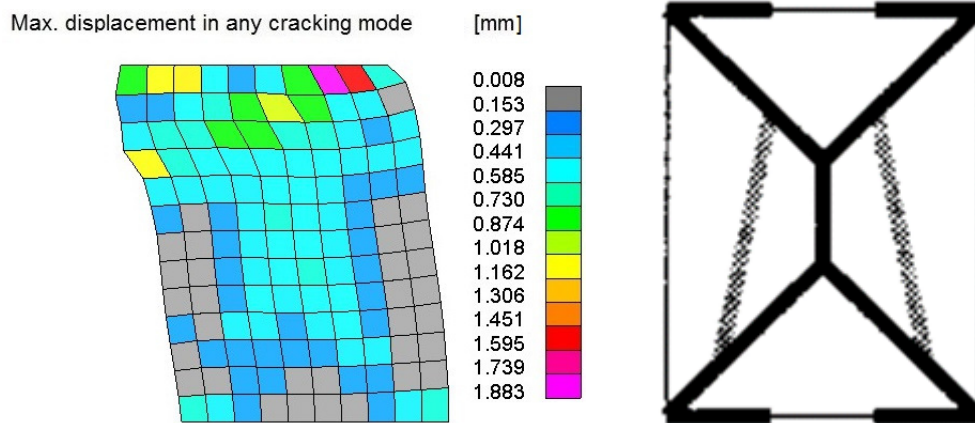

Figure 5 LOWSTA – Final crack pattern—comparison between LS-DYNA shell element model (left) and laboratory test (right)
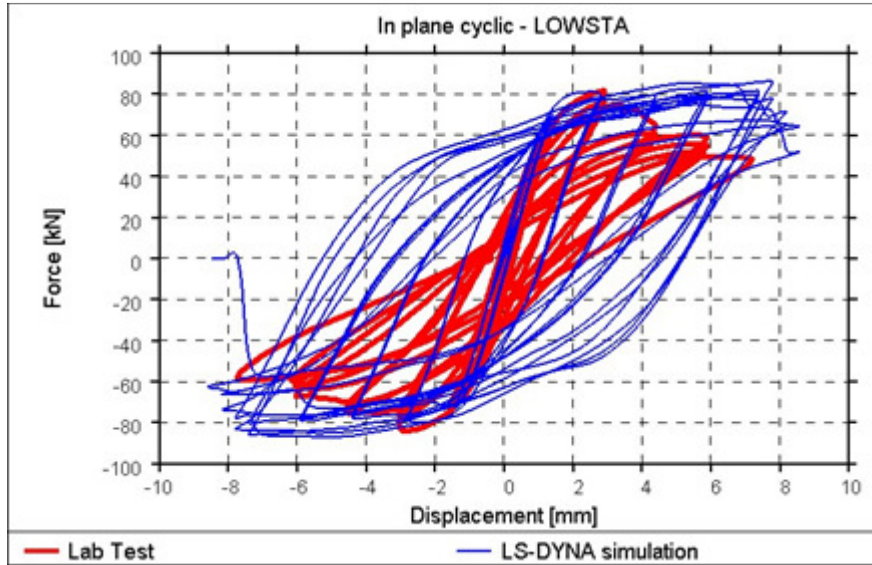
Figure 6 LOWSTA – Shear force-displacement comparison plot: collapse in the LS-DYNA simulation occurs at a drift of 0.6% (8mm deflection).

2.1.5 Conclusion

The LS-DYNA simulation exhibits an approximately diagonal crack pattern but the damage is less concentrated than observed in the experiment. The peak lateral strength and initial stiffness are well predicted, but the model does not capture the modest degradation of strength at higher applied deformation cycles or the reduced unloading stiffness. The model over-predicts the energy dissipation of the specimen.

It is not clear how far the test specimen was from collapse under the final loading cycles even though a partial drop of base shear capacity occurs at a drift of 0.6% (8mm deflection). The LS-DYNA simulation indicate collapse at a drift value of 0.6% (8mm deflection).

2.2 In-Plane Diagonal Damage Mode – Calcium Silicate Brick – EUC-COMP-3

2.2.1 Test Description

EUC-COMP-3 was a quasi-static in-plane cyclic test administered in the Eucentre laboratory at the University of Pavia, Italy. The specimen was a 100 mm thick single-wythe wall with aspect ratio of 0.69 constructed of calcium-silicate brick units. The applied overburden stress was 0.3 MPa. The wall was tested under cantilever boundary conditions [3].
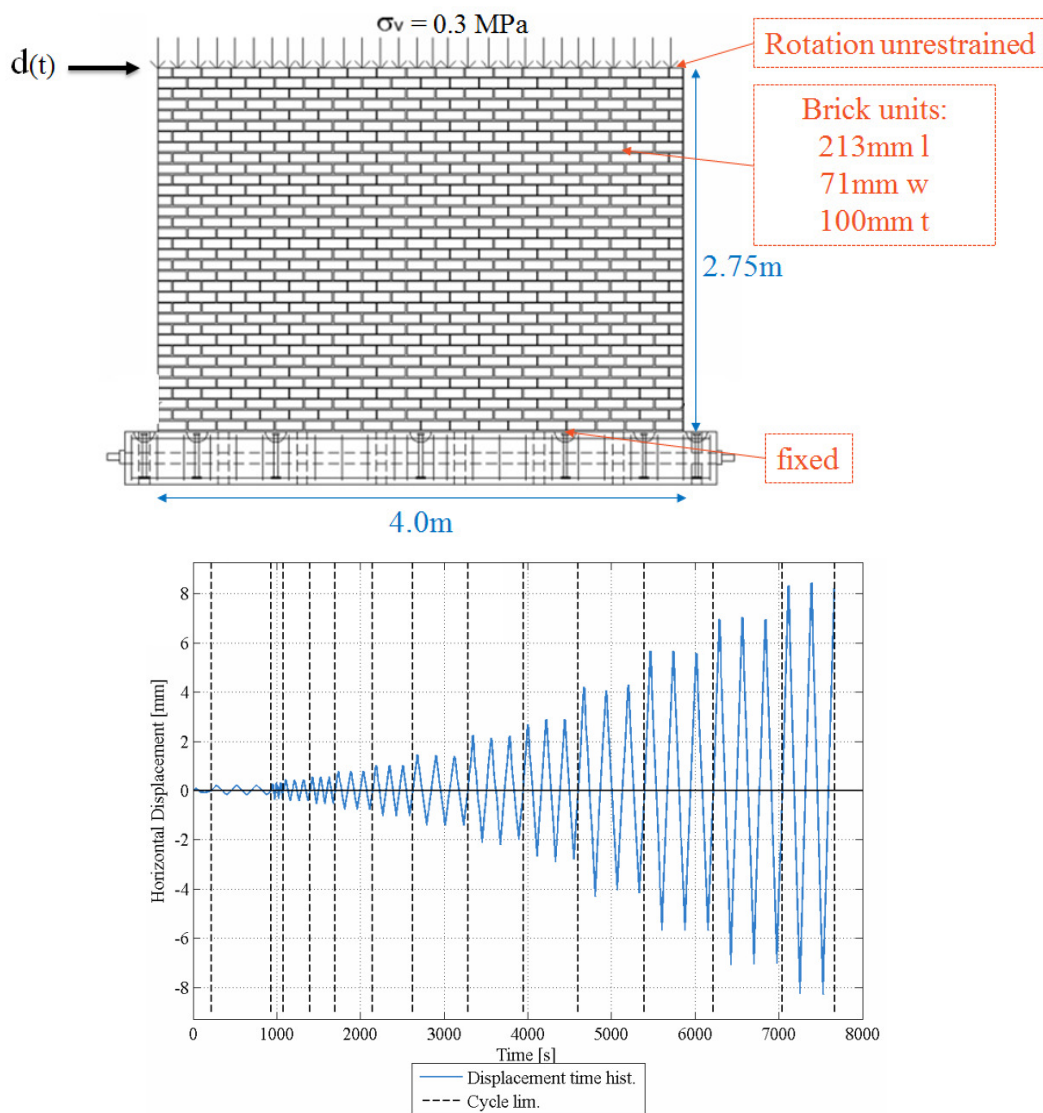

Figure 7 EUC-COMP-3 – Diagram of test set up (top) and displacement time history (bottom)

The material properties tabulated below are taken from the laboratory material characterization tests.

Table 2 EUC-COMP-3 Material Properties

Mass density	1852 kg/m^3
Masonry Young's modulus perpendicular to bed joints	4182 MPa
Masonry compressive strength perpendicular to bed joints	6.2 MPa
Tensile strength (flexural bond strength) of mortar joints	0.238 MPa
Initial shear strength of mortar joints	0.21 MPa
Coefficient of friction for sliding of joints	0.42

2.2.2   Test Results

The predominant deformation mode of EUC-COMP-3 was shear damage characterized by diagonal cracking.

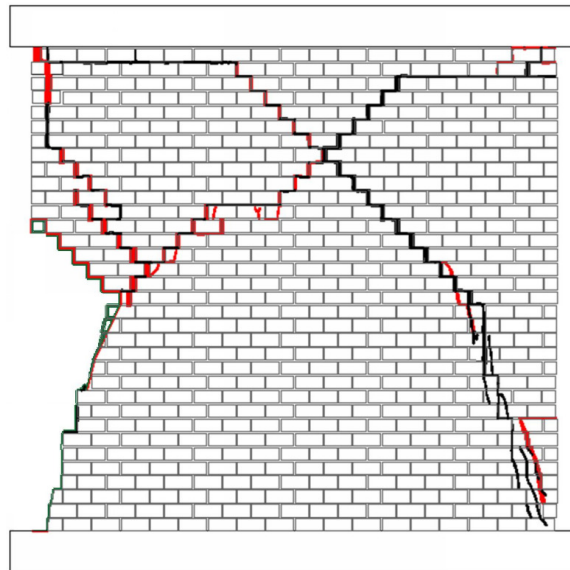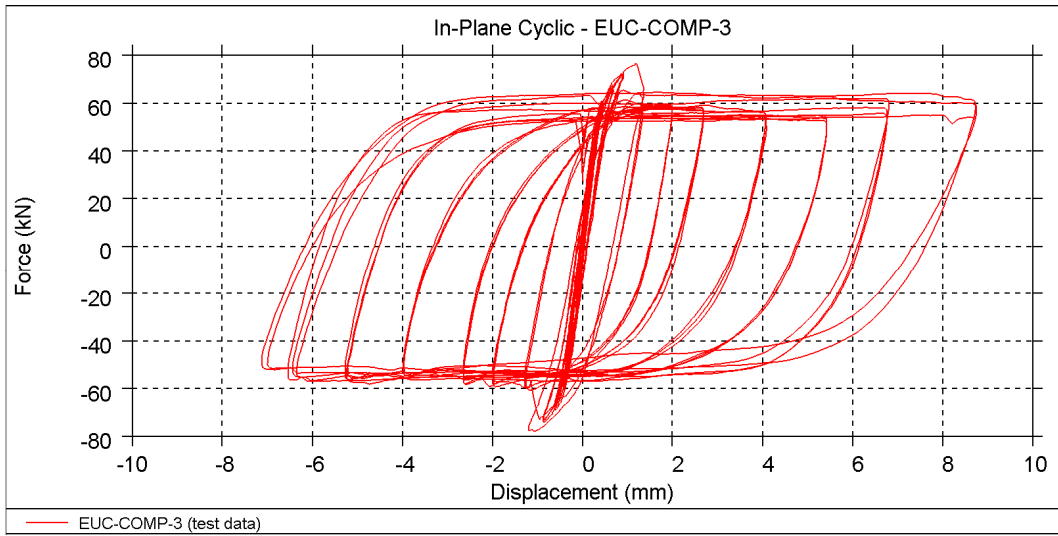Figure 8 EUC-COMP-3 – Observed crack pattern

Figure 9 EUC-COMP-3 – shear force-displacement plot from test data
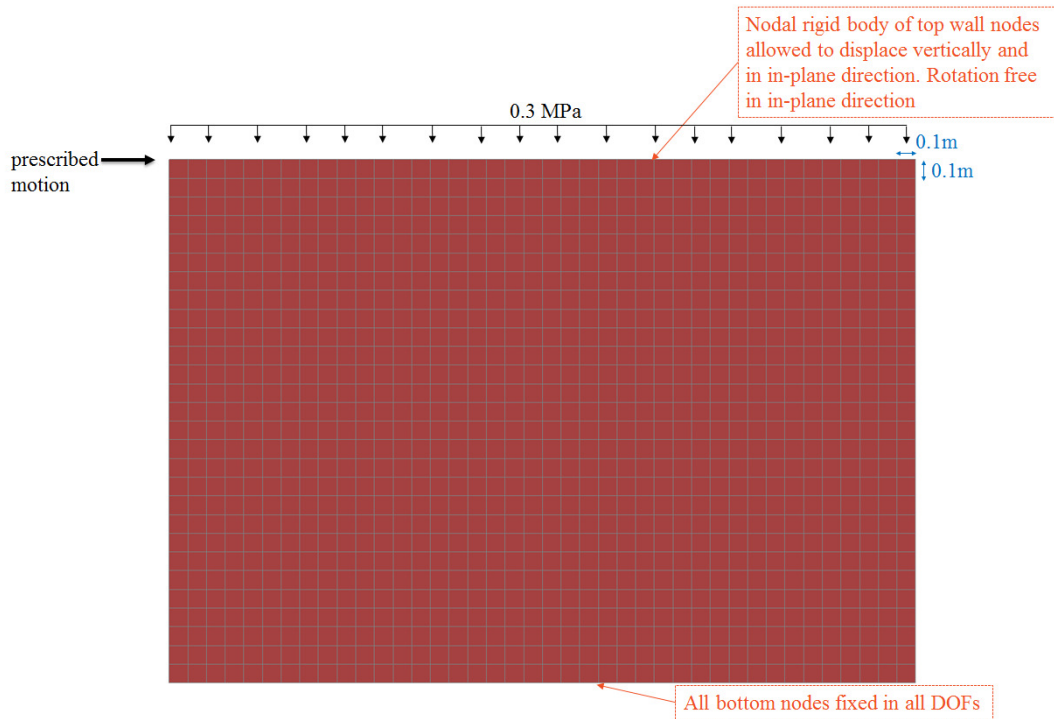
2.2.3   LS-DYNA: Model Description

Figure 10 LS-DYNA shell model description

The loading protocol applied to the model is the same as in the physical experiment, except that additional larger cycles were added to the end of the protocol to capture the point at which collapse occurs.

2.2.4 LS-DYNA: Results & Validation

The results presented below were obtained using the 25-May-2016 version of the *MAT_SHELL_MASONRY.
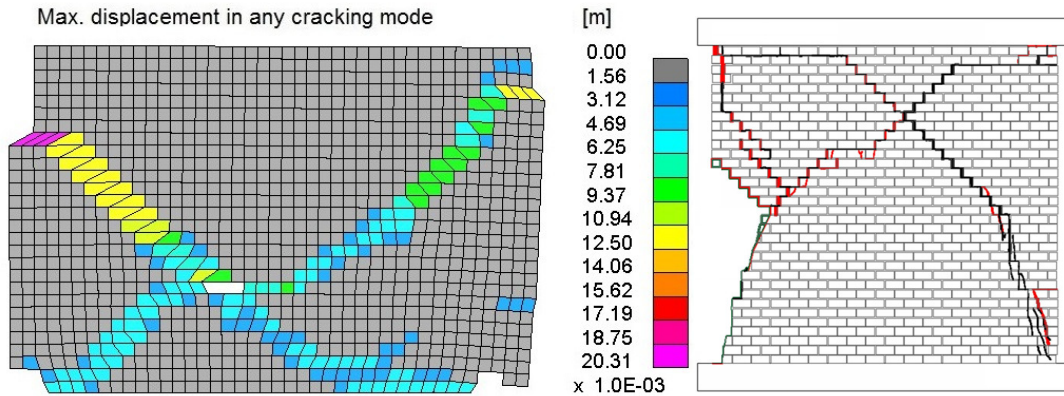
Figure 11 EUC-COMP-3 – Final crack pattern—comparison between LS-DYNA shell element model (left) and laboratory test (right)
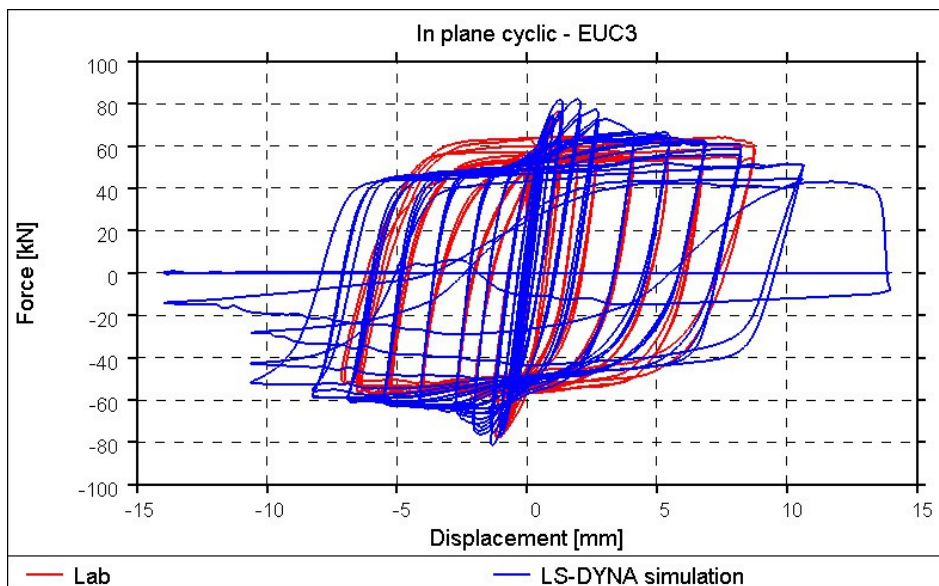
Figure 12 EUC-COMP-3 – Shear force-displacement comparison plot: near collapse conditions of the LS-DYNA simulation at 0.35% drift (10mm deflection), lab test near collapse conditions at 0.3% drift (8mm deflection).

2.2.5 Conclusion

The LS-DYNA simulation predicts the diagonal tensile failure mode with toe-crushing at the corners.

The peak lateral strength, initial stiffness, unloading stiffness and energy dissipation are all well predicted.

The analysis predicts a substantial drop of base shear capacity at a drift of about 0.35% (10mm deflection). This well correlates with the test results where the capacity to carry overburden drops at a drift of 0.3% (8mm deflection). It is noted that similarly to the drop of overburden bearing capacity of the test, LS-DYNA shows a significant downward displacement when the base shear capacity drops.

2.3 In-Plane Crushing Damage Mode – Historic Masonry – PMW2

2.3.1 Test Description

PMW2 was a quasi-static in-plane cyclic test administered at the University of Civil Engineering, Bucharest (UTCB) [4]. The specimen was a 115 mm thick single-wythe wall with aspect ratio of 0.80 constructed of old clay brick units with relatively weak lime mortar. The applied overburden stress was 0.6 MPa. The wall was tested under double clamped boundary conditions.
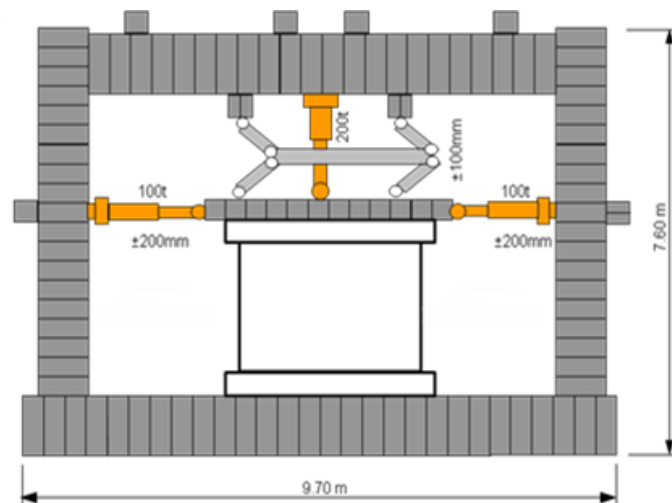
Figure 13 PMW2 – Diagram of test set up

Of the various material properties required for the simulations, only the compressive strength of masonry was available. The other properties were therefore assumed, based upon typical correlations. Therefore a close match with the measured behaviour should not be expected.

Table 3 PMW2 Material Properties

Mass density	1867 kg/m3 (*)
Masonry Young's modulus perpendicular to bed joints	4030 MPa (*)
Masonry compressive strength perpendicular to bed joints	7 MPa (from laboratory test)
Tensile strength (flexural bond strength) of mortar joints (of bed joints)	0.115 MPa (*)
Initial shear strength of mortar joints (of bed joints)	87.3 kPa (*)
Coefficient of friction for sliding of joints	0.75 (*)

(*)Test data not available. The reported value was assumed in order to carry out the LS-DYNA simulation.

2.3.2   Test Results

The predominant failure mode of PMW2 was collapse arising from compression/crushing failure. At 0.6% drift the specimen became incapable of supporting the vertical load.

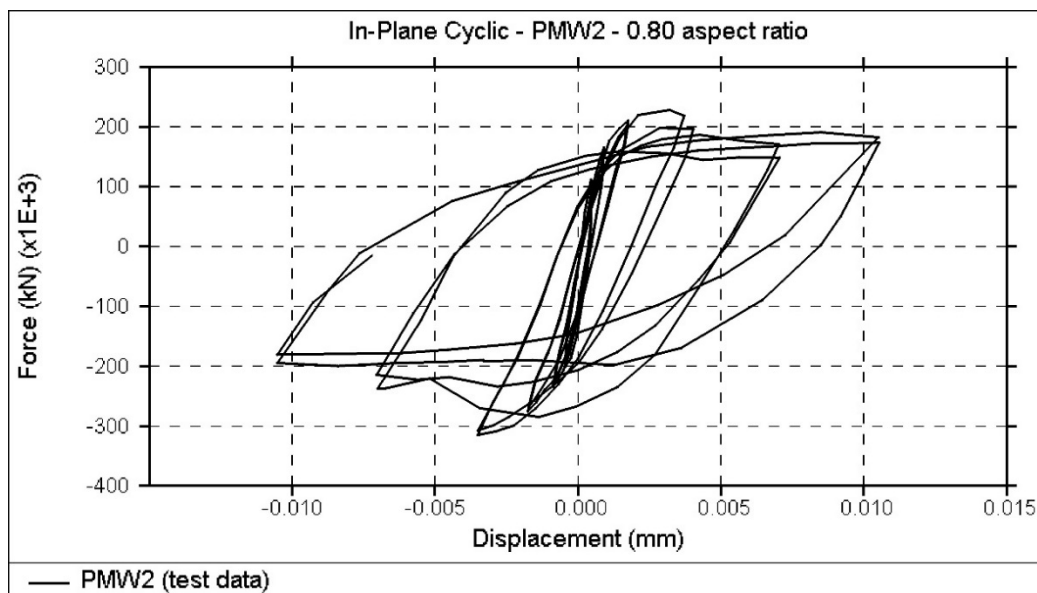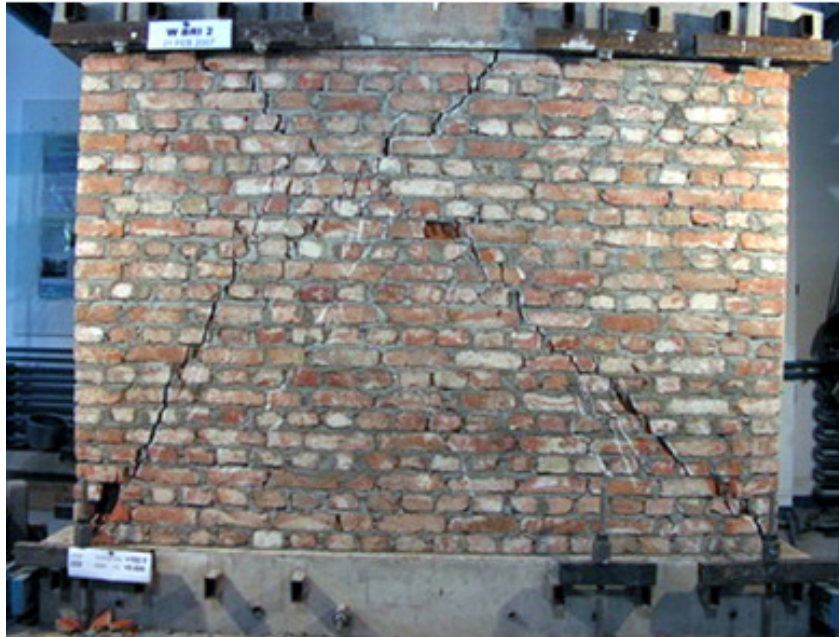Figure 14 PMW2 – Observed crack pattern (top) and shear force-displacement plot from test data (bottom)
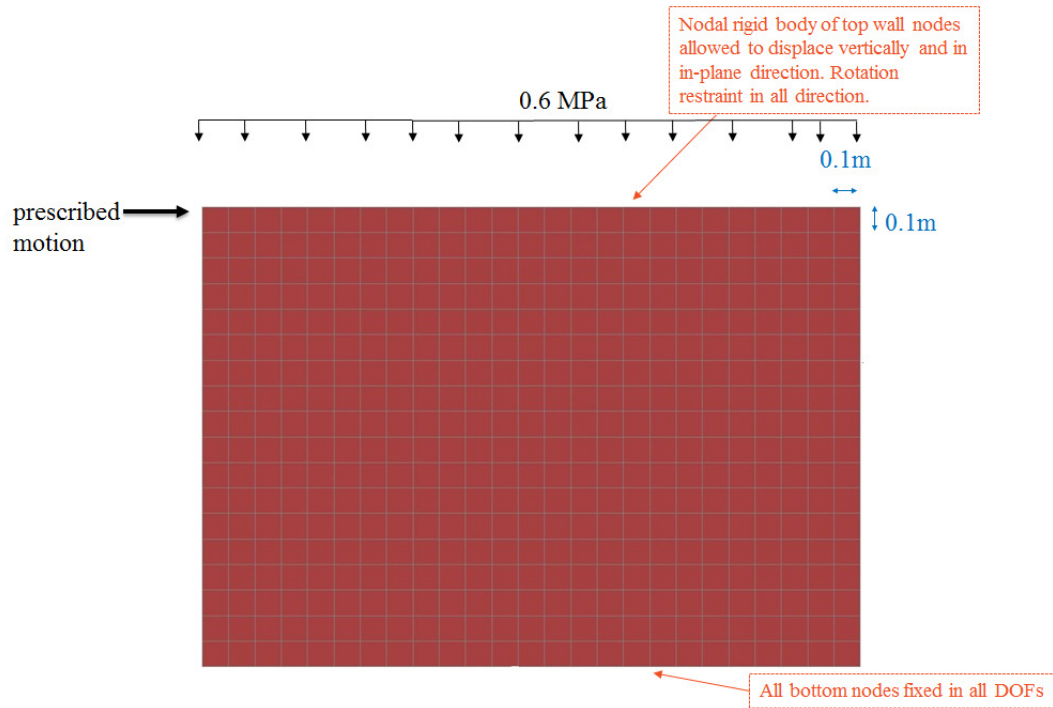
2.3.3   LS-DYNA: Model Description

Figure 15 LS-DYNA shell model description

The loading protocol applied to the model is the same as in the physical experiment, except that additional larger cycles were added to the end of the protocol to capture the point at which collapse occurs.

2.3.4   LS-DYNA: Results & Validation

The results presented below were obtained using the 25-May-2016 version of the MAT_SHELL_MASONRY.
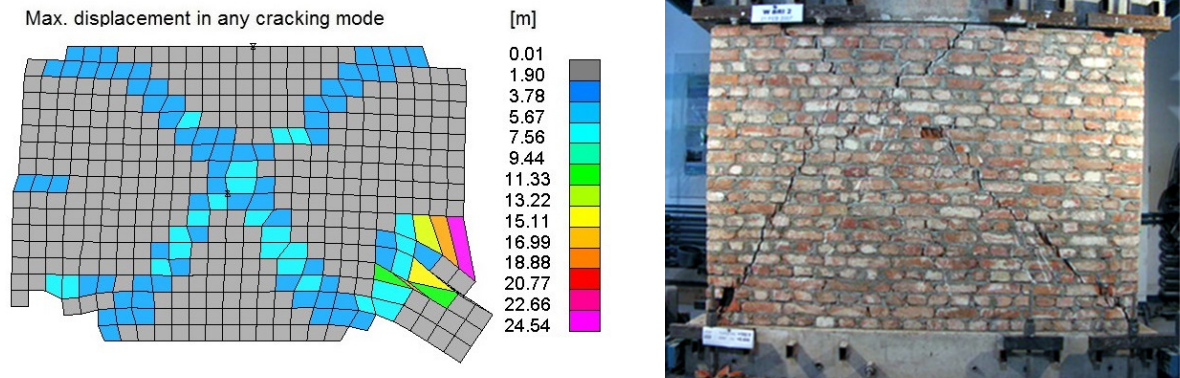
Figure 16 PMW2 – Final crack pattern—comparison between LS-DYNA shell element model (left) and laboratory test (right)
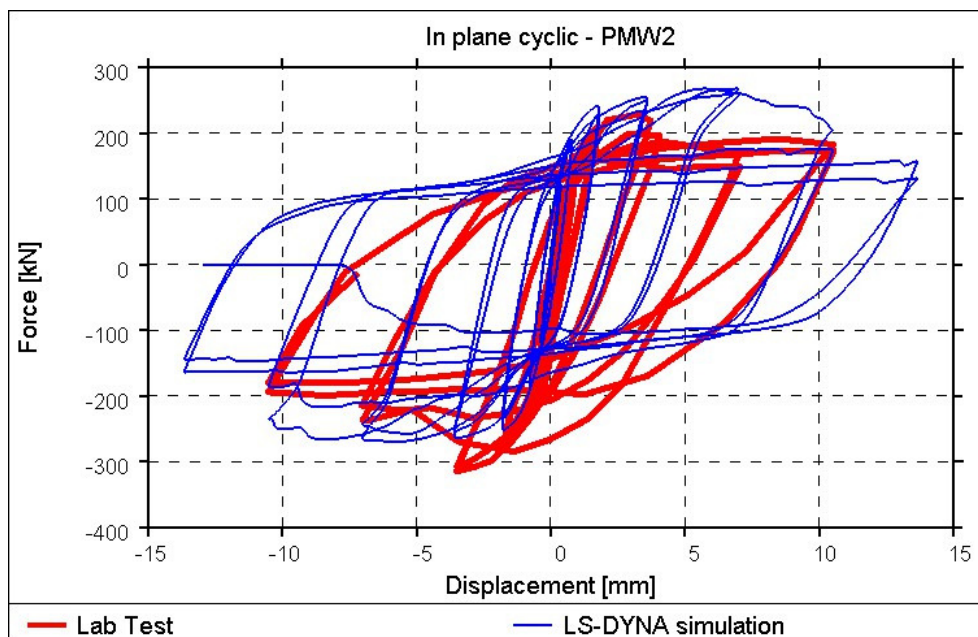
Figure 17 PMW2 – Shear force-displacement comparison plot: near collapse conditions of the LS-DYNA simulation at 0.6% drift (10mm deflection), lab test near collapse conditions at 0.6% drift (10mm deflection).

2.3.5   Conclusion

The LS-DYNA simulation predicts a compression failure at the corners of the wall and a diagonal type of failure similar to the test. The peak lateral strength, initial and unloading stiffness, and energy dissipation are all well predicted.

The analysis predicts near collapse conditions with a drop of base shear capacity at a drift of 0.6% (10mm deflection). Complete collapse of the specimen follows

at a drift of 0.75% (13mm deflection). The drift of the simulation at near collapse conditions correlates well with the experiment: the test was interrupted due to loss of capacity to carry vertical loads at a drift of 0.6%.

2.4   In-Plane Pier Rocking – Clay Brick – HIGSTA1

2.4.1   Test Description

HIGSTA1 was a quasi-static in-plane cyclic test administered at the University of Pavia, Italy. The specimen was a 250 mm thick double-wythe wall with aspect ratio of 2.0 constructed of clay brick units. The applied overburden stress was 0.6 MPa. The wall was tested under double clamped boundary conditions [1].
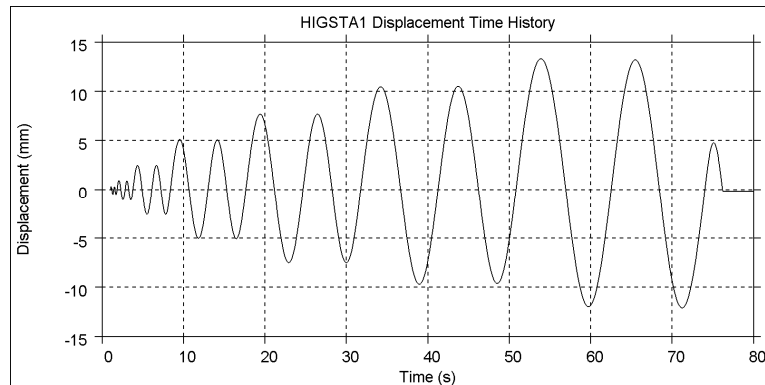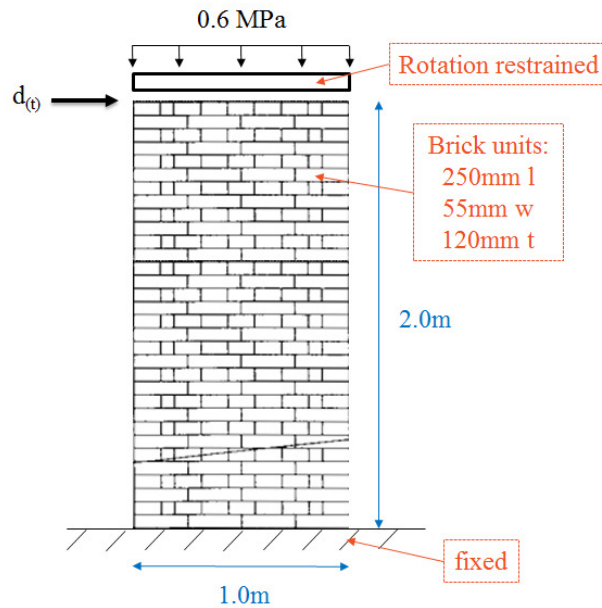
Figure 18 HIGSTA1 – Diagram of test set up (top) and displacement time history (bottom)

The material properties tabulated below are taken from the laboratory material characterization tests.

Table 4 HIGSTA1 Material Properties [2]

Mass density	1652 kg/m^3

Masonry Young's modulus perpendicular to bed joints	1491 MPa
Masonry compressive strength perpendicular to bed joints	6.2 MPa
Tensile strength (flexural bond strength) of mortar joints	0.04 MPa
Initial shear strength of mortar joints	0.23 MPa
Coefficient of friction for sliding of joints	0.58

2.4.2 Test Results

The predominant deformation mode of HIGSTA1 was in-plane rocking with little energy dissipation. Significant loss of stiffness was observed at larger deformation cycles.

Figure 19 HIGSTA1 – Observed crack pattern
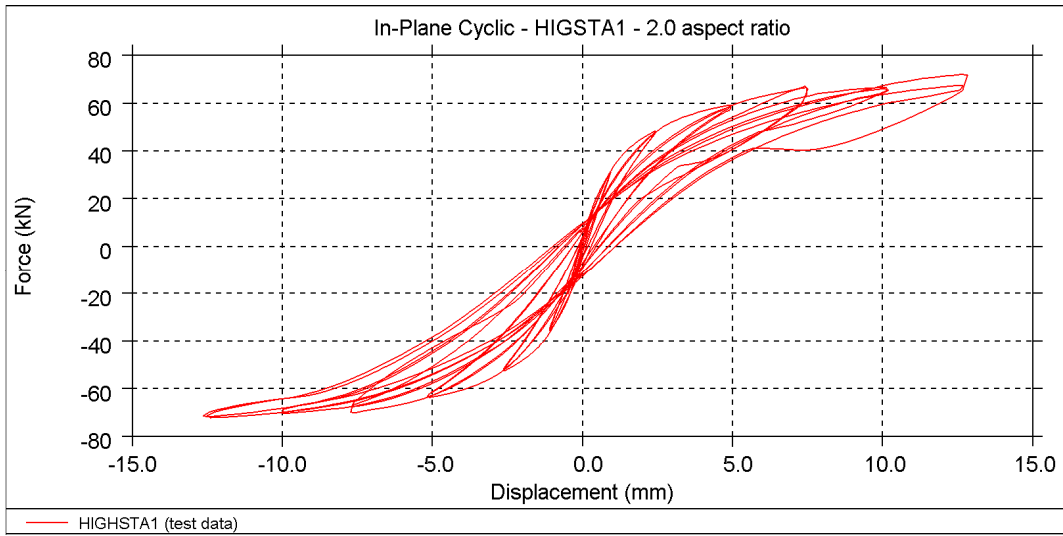
Figure 20 HIGSTA1 – Shear force-displacement plot from test data

2.4.3   LS-DYNA: Model Description
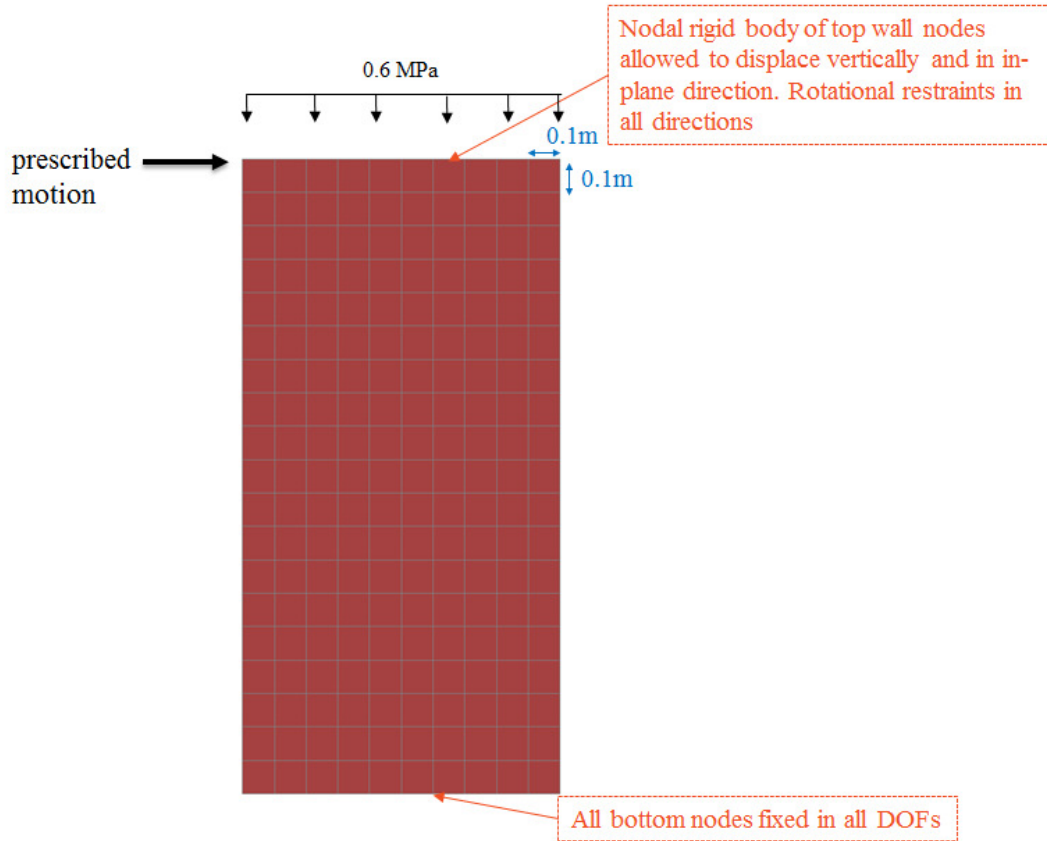
Figure 21 LS-DYNA shell model description

2.4.4   LS-DYNA: Results & Validation

The results presented below were obtained using the 25-May-2016 version of the MAT_SHELL_MASONRY.

Max. displacement in any cracking mode
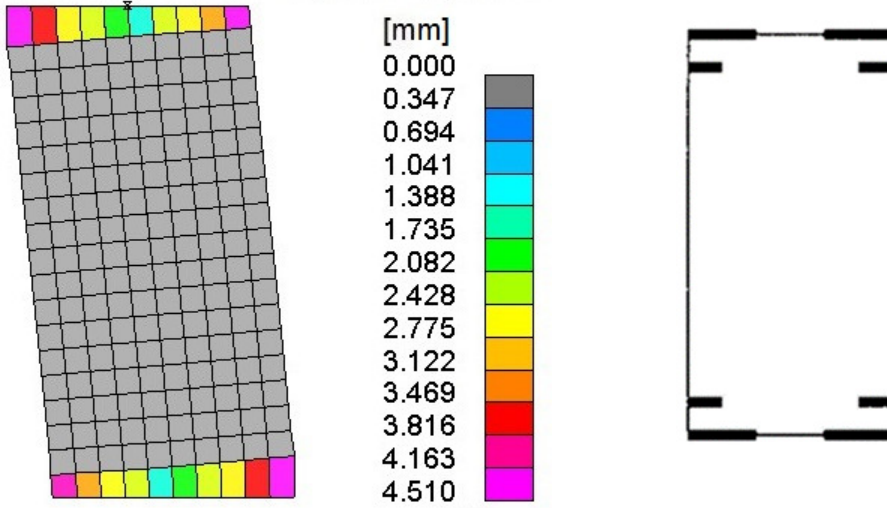
Figure 22 HIGSTA1 – Final crack pattern—comparison between LS-DYNA shell element model (left) and laboratory test (right)

Figure 23 HIGSTA1 – Shear force-displacement comparison plot: test does not reach near collapse conditions, the LS-DYNA simulation did not indicate incipient collapse.

2.4.5   Conclusion

The LS-DYNA results show good correlation to the test in terms of final crack pattern, peak lateral strength, initial stiffness, backbone curve and energy dissipation. However, the observed lateral stiffness degradation was not predicted.

It is not clear how far the test specimen was from collapse under the final loading cycles, and the LS-DYNA simulation did not indicate incipient collapse.

2.5   In-Plane Pier Rocking – Calcium Silicate Brick – EUC-COMP-2

2.5.1   Test Description

EUC-COMP-2 was a quasi-static in-plane cyclic test administered in the Eucentre laboratory at the University of Pavia, Italy. The specimen was a 100 mm thick single-wythe wall with aspect ratio of 2.5 constructed of calcium-silicate brick units. The applied overburden stress was 0.7 MPa. The wall was tested under double clamped boundary conditions [3].
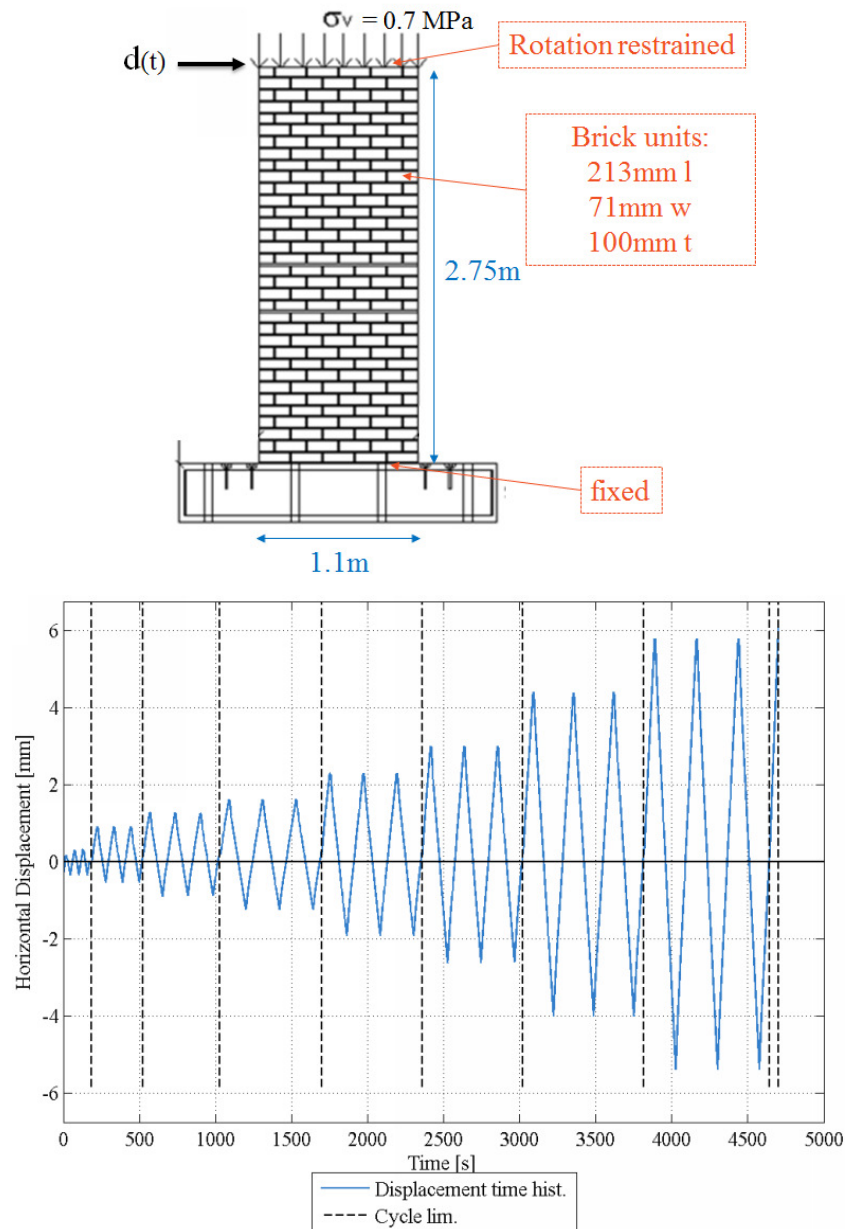
Figure 24 EUC-COMP-2 – Diagram of test set up (top) and displacement time history (bottom)

Table 5 EUC-COMP-2 Material Properties

Mass density	1852 kg/m^3
Masonry Young's modulus perpendicular to bed joints	4182 MPa
Masonry compressive strength perpendicular to bed joints	6.2 MPa
Tensile strength (flexural bond strength) of mortar joints	0.238 MPa
Initial shear strength of mortar joints	0.21 MPa
Coefficient of friction for sliding of joints	0.42

2.5.2　Test Results

The predominant deformation mode of EUC-COMP-2 was in-plane rocking with crushing at the corners.

In the test, the top beam began to rotate at cycles above 0.15% drift (4mm). Since the intended double-clamped boundary conditions were only maintained up to this drift level, the LS-DYNA simulation is only compared with this part of the test.
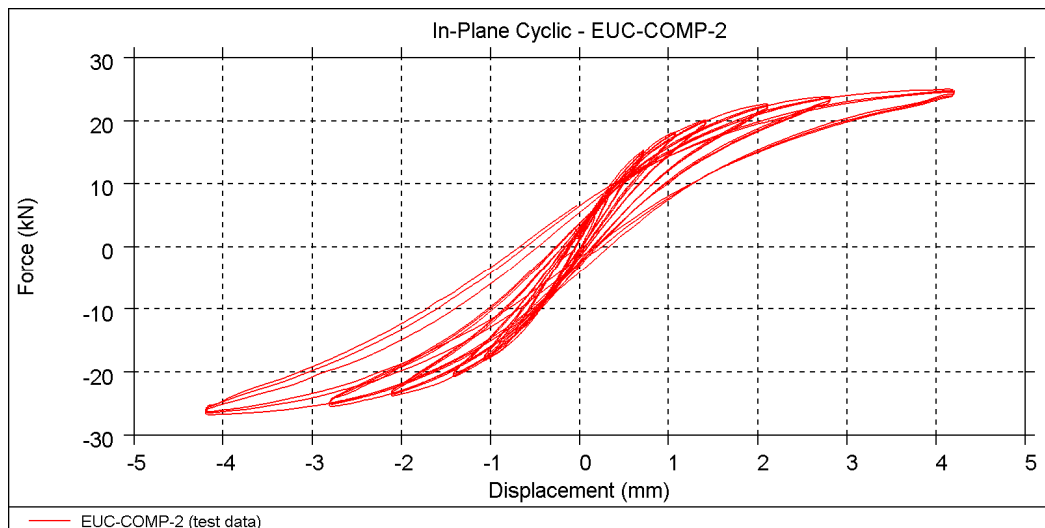
Figure 25 EUC-COMP-2 – Shear force-displacement plot from test data up to 0.15% drift

2.5.3   LS-DYNA: Model Description
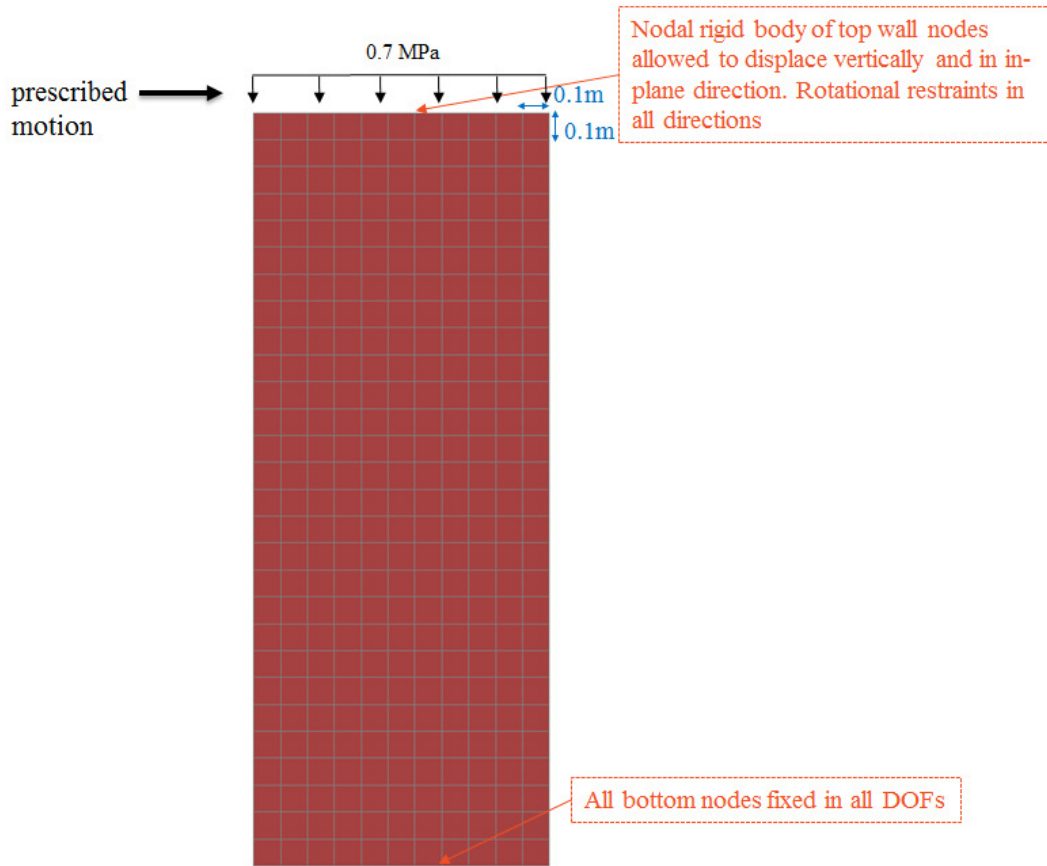
Figure 26 LS-DYNA shell model description

2.5.4   LS-DYNA: Results & Validation

The results presented below were obtained using the 25-May-2016 version of the MAT_SHELL_MASONRY.

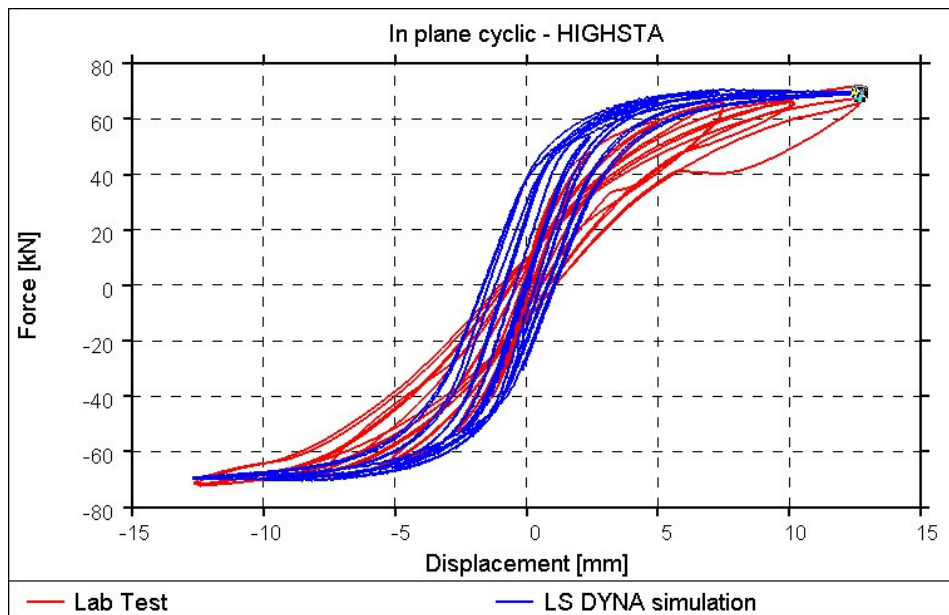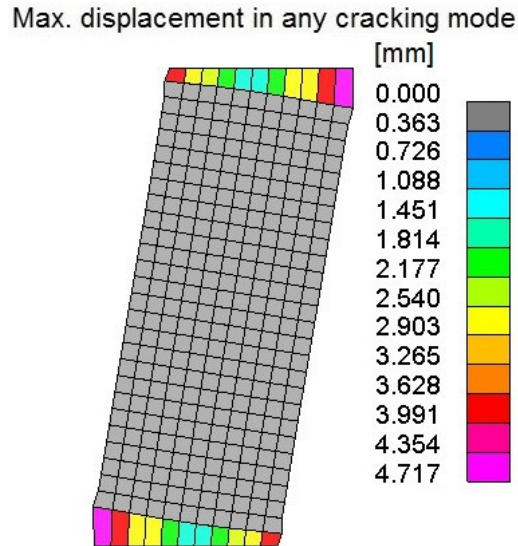Figure 27 EUC-COMP-2 – Final crack pattern of LS-DYNA shell element model
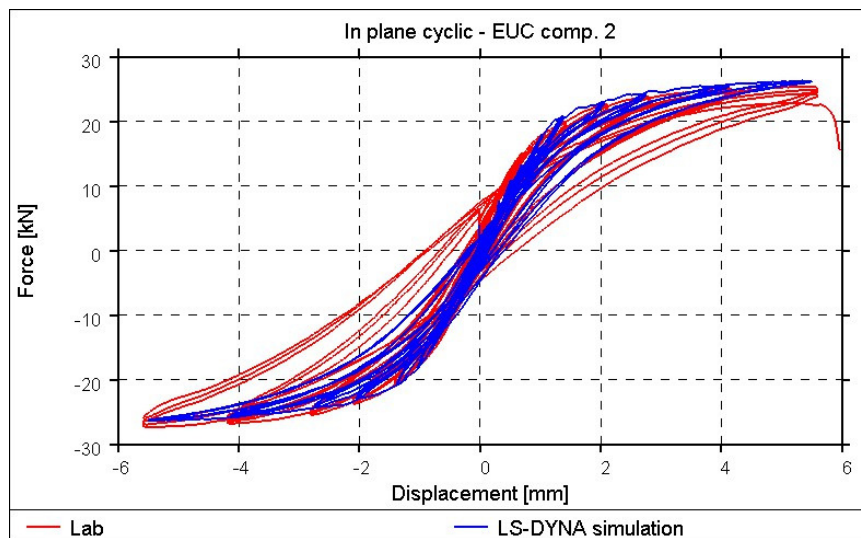
Figure 28 EUC-COMP-2 – Shear force-displacement comparison plot: test does not reach near collapse conditions, the LS-DYNA simulation did not indicate incipient collapse.

2.5.5   Conclusion

The LS-DYNA simulation shows good correlation to the test in terms of final crack pattern, peak lateral strength, initial stiffness and backbone curve. The energy dissipation is well captured at first, but slightly under-predicted at the higher applied deformation cycles. However, the model does not exhibit the

degradation of stiffness observed in higher deformation cycles. Neither the test nor the model exhibited collapse.

2.6 In-Plane Pier Rocking – Calcium Silicate Brick – TUD-COMP-0a

2.6.1 Test Description

TUD-COMP-0a was a quasi-static in-plane cyclic test administered at the Delft University of Technology. With the exception of the measured material properties, this specimen is identical to EUC-COMP-2 (see Section 2.5)

The specimen was a 102 mm thick single-wythe wall with aspect ratio of 2.5 constructed of calcium silicate brick units. The applied overburden stress was 0.7 MPa. The wall was tested under double clamped boundary conditions [5].
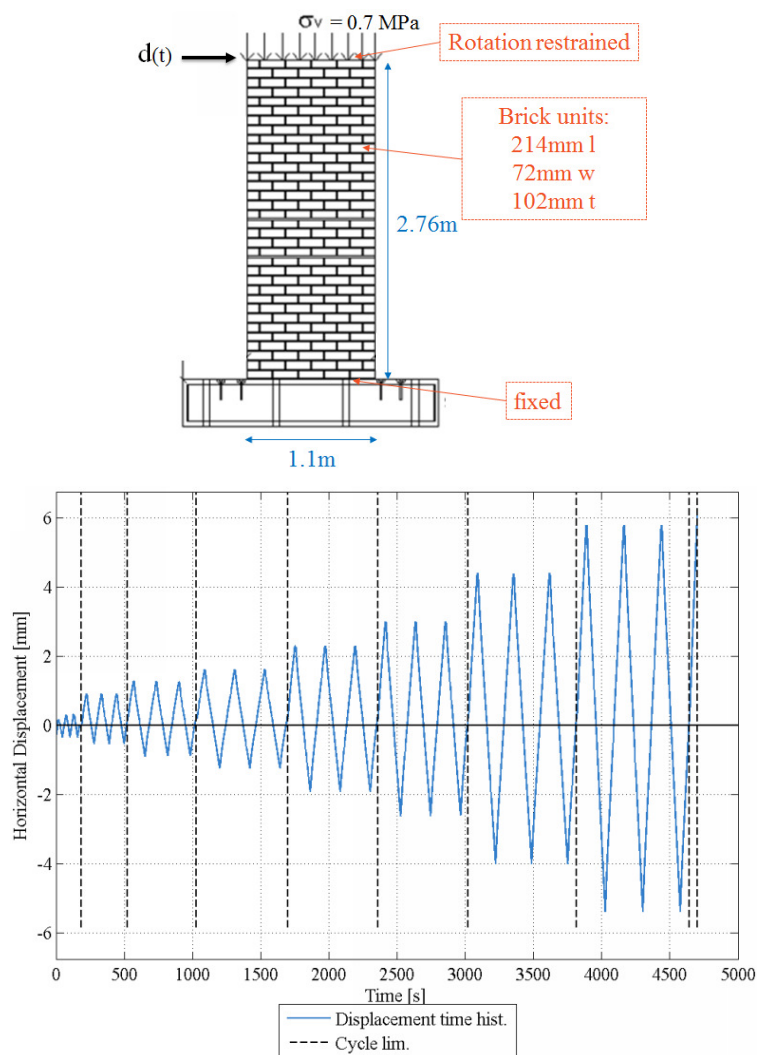
Figure 29 TUD-COMP-0a – Diagram of test set up (top) and displacement time history (bottom)

Table 6 TUD-COMP-0a Material Properties [6]

Mass density	1852 kg/m^3
Masonry Young's modulus perpendicular to bed joints	5091 MPa
Masonry compressive strength perpendicular to bed joints	5.93 MPa
Tensile strength (flexural bond strength) of mortar joints	0.27 MPa
Initial shear strength of mortar joints	0.14 MPa
Coefficient of friction for sliding of joints	0.43

2.6.2   Test Results

The predominant deformation mode of TUD-COMP-0a was in-plane rocking with crushing at the corners.
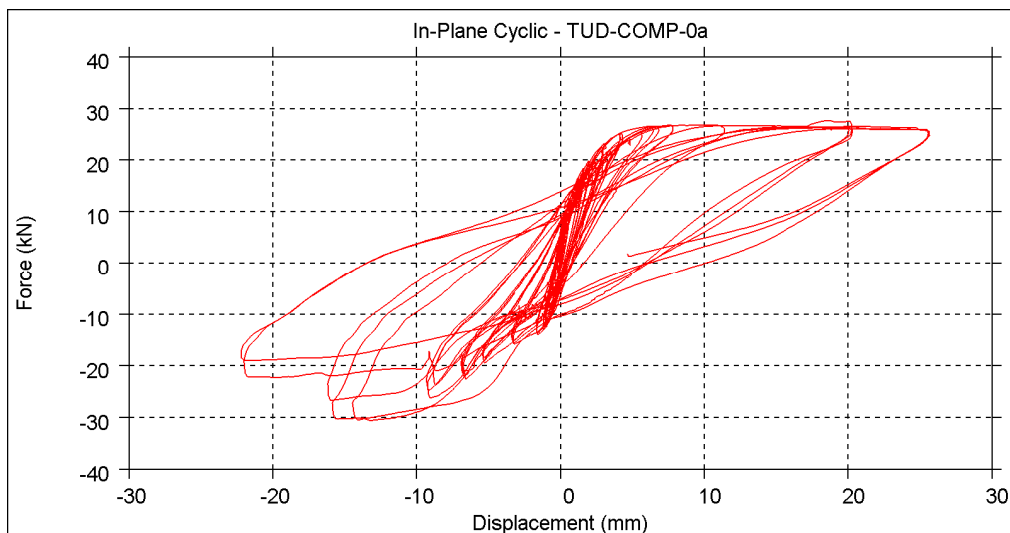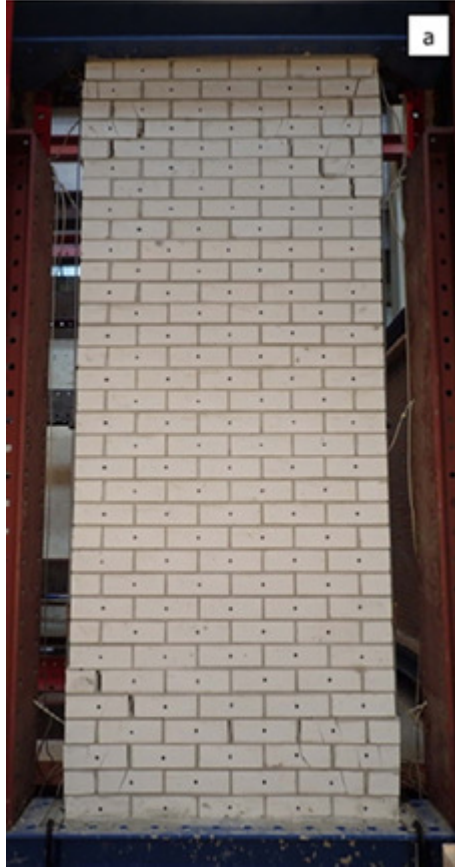
Figure 30 TUD-COMP-0a – Observed crack pattern (top) and shear force-displacement plot from test data (bottom)

Some features of the experimental result are unexpected. For example, the initial lateral resistance is around 26 kN on the "positive" displacement side, but only around 12 kN on the "negative" side. In Figure 31 compares the shear force-displacement plot for TUD-COMP-0a for the initial small cycles (up to 0.12% drift only) with the notionally identical test EUC-COMP-2. Significant differences in the results may be clearly seen. Whether this can be explained by the behaviour of the masonry, or whether it is an artefact of the test equipment and/or measurement system, is not fully understood. However, it is clear that two nearly identical specimens—with the exception of slight differences in the measured material properties (described in

Table 7 below)—tested in different laboratories can produce significantly different behaviours even at low drift levels. Therefore, perfect correlation of numerical models to these tests should not be expected.
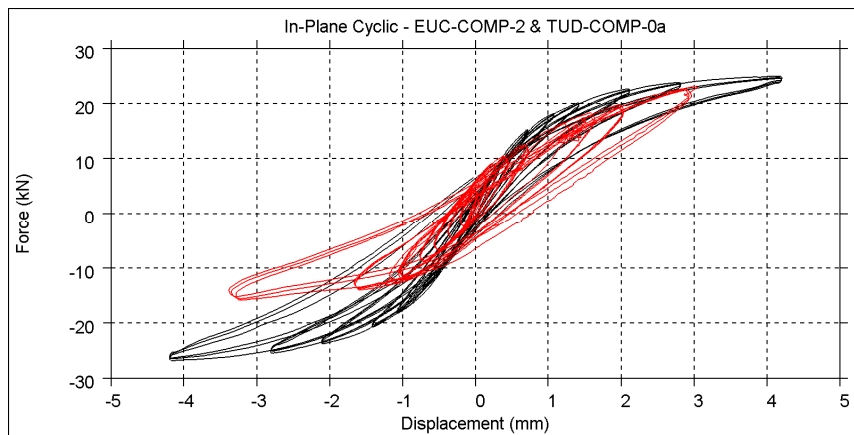
Figure 31 TUD-COMP-0a initial small cycles up to 0.12% drift (red line) compared to test EUC-COMP-2 (black line).

Table 7 TUD-COMP-0a & EUC-COMP-2 material properties

Material property	TUD-COMP-0a	EUC-COMP-2
Masonry Young's modulus perpendicular to bed joints	5.1 GPa	4.2 GPa
Masonry compressive strength perpendicular to bed joints	5.9 MPa	6.2 MPa
Tensile strength (flexural bond strength) of mortar joints	0.27 MPa	0.24 MPa

2.6.3   LS-DYNA: Model Description

Figure 32 LS-DYNA shell model description

2.6.4   LS-DYNA: Results & Validation

The results presented below were obtained using the 25-May-2016 version of the MAT_SHELL_MASONRY.
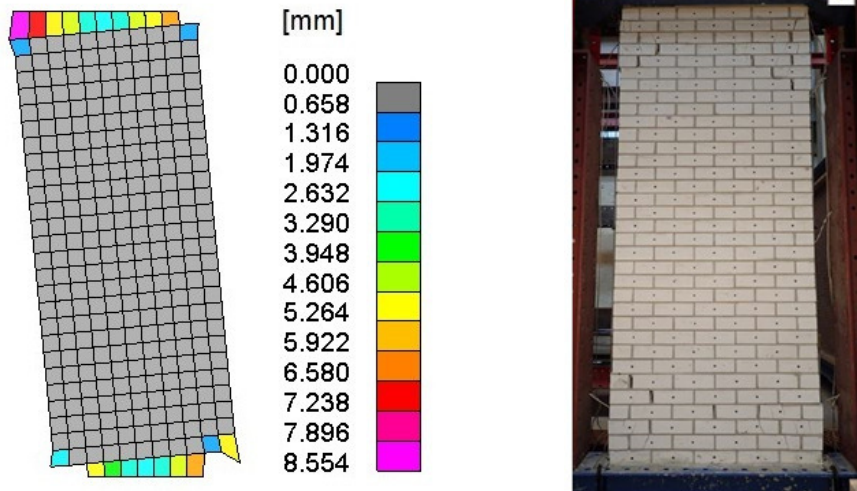
Figure 33 TUD-COMP-0a – Final crack pattern—comparison between LS-DYNA shell element model (left) and laboratory test (right)
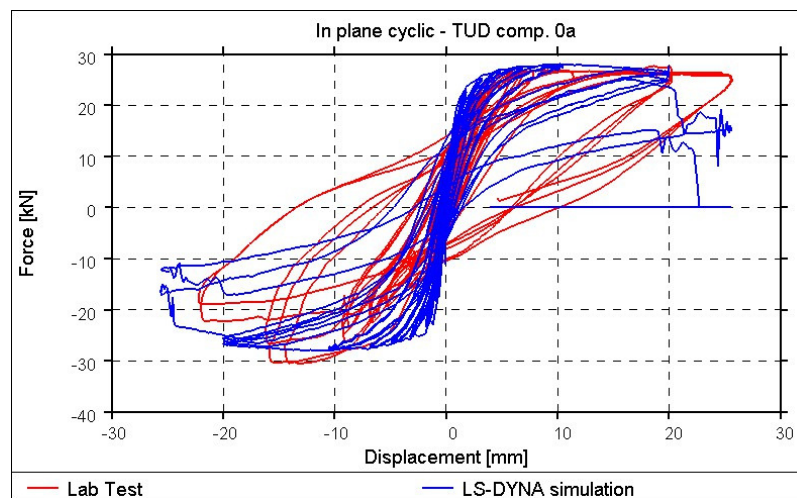
Figure 34 TUD-COMP-0a – Shear force-displacement comparison plot: collapse of the LS-DYNA simulation at 1.0% drift (25mm deflection), lab test near collapse conditions at 1.0 % drift (25mm deflection).

2.6.5   Conclusion

The analysis predicts the ultimate strength well, and indicates collapse at a drift of 1.0% (25mm deflection). The test was interrupted as the specimen could not no longer bear the vertical overburden without significant vertical displacement at a drift of 1.0% (25mm deflection). The analysis predicted less energy absorption than the test specimen, especially during the larger displacement cycles.

2.7 Quasi-Static Out-of-Plane One Way Damage Mode – Clay Brick – Doherty Specimen 8

2.7.1 Test Description

Doherty specimen 8 was a quasi-static out-of-plane pushover test administered at the University of Adelaide in Australia. The specimen was a 110 mm thick single-wythe wall with aspect ratio of 1.58 constructed of clay brick units. The applied overburden stress was 0.15 MPa. The wall was tested under conditions allowing the top and bottom of the wall to rotate [7].
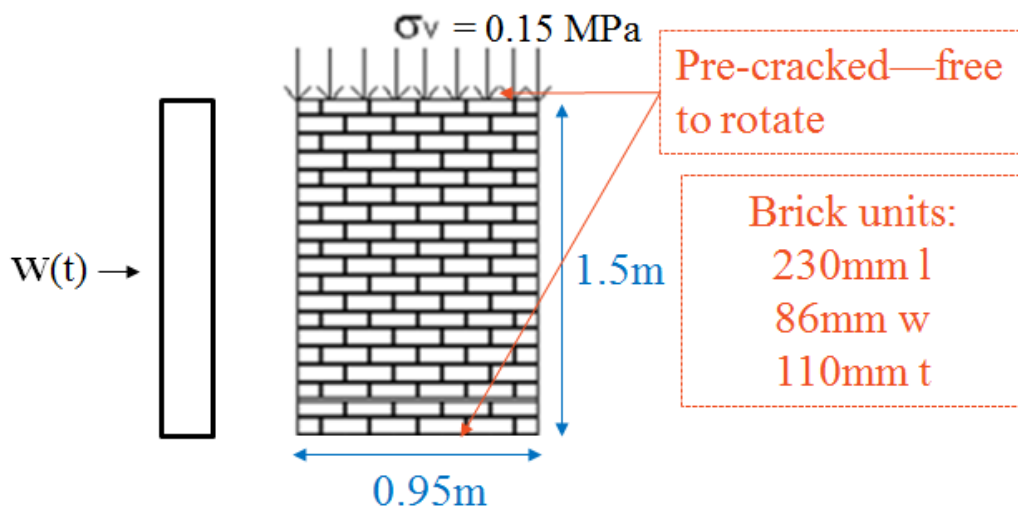
Figure 35 Doherty Specimen 8 – Diagram of test set up

Table 8 Doherty Specimen 8 Material Properties

Mass density	1800 kg/m^3
Masonry Young's modulus perpendicular to bed joints	5400 MPa
Masonry compressive strength perpendicular to bed joints	9.7 MPa
Tensile strength (flexural bond strength) of mortar joints	0.46 MPa
Initial shear strength of mortar joints	---
Coefficient of friction for sliding of joints	---

2.7.2   Test Results

The predominant deformation mode of Doherty specimen 8 was out-of-plane one-way bending with cracks formed at top, bottom and mid-height.
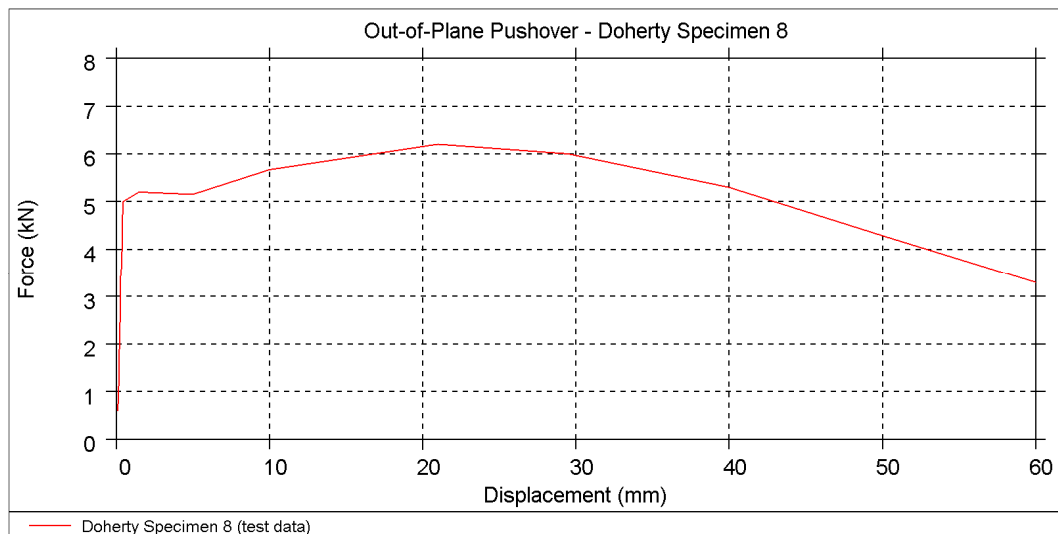
Figure 36 Doherty Specimen 8 – Applied force-mid-height displacement plot from test data

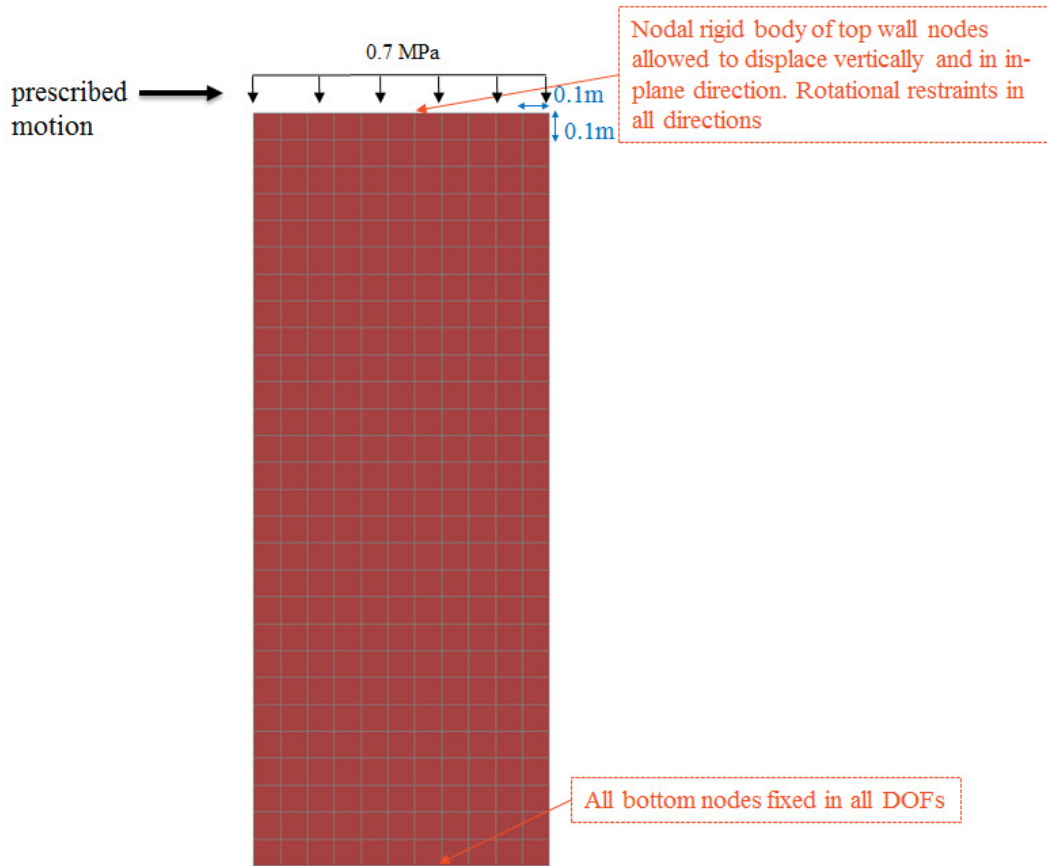## 2.7.3   LS-DYNA: Model Description

Figure 37 LS-DYNA shell model description

2.7.4 LS-DYNA: Results & Validation

The results presented below were obtained using the 25-May-2016 version of the MAT_SHELL_MASONRY.
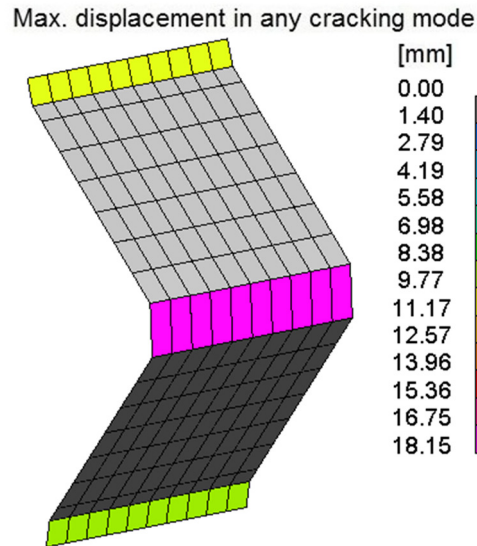
Figure 38 Doherty Specimen 8 – Final crack pattern of LS-DYNA shell element model

Figure 39 Doherty Specimen 8 – Applied force-mid-height displacement comparison plot

2.7.5 Conclusion

The LS-DYNA results show a good correlation to the test in terms of overall response. The predicted peak strength before the formation of the mid-height crack is higher than observed in the test. This will be sensitive to the tensile strength and toughness of the joints.

2.8 Quasi-Static Out-of-Plane One Way Damage Mode – Calcium Silicate Brick – TUD-COMP-7

2.8.1 Test Description

TUD-COMP-7 was a quasi-static one-way out-of-plane test administered at the Delft University of Technology. This specimen was a 102 mm thick single-wythe wall with aspect ratio of 0.51 constructed of calcium silicate brick units. The applied overburden stress was 0.2MPa. The wall was tested under double clamped boundary conditions [8].
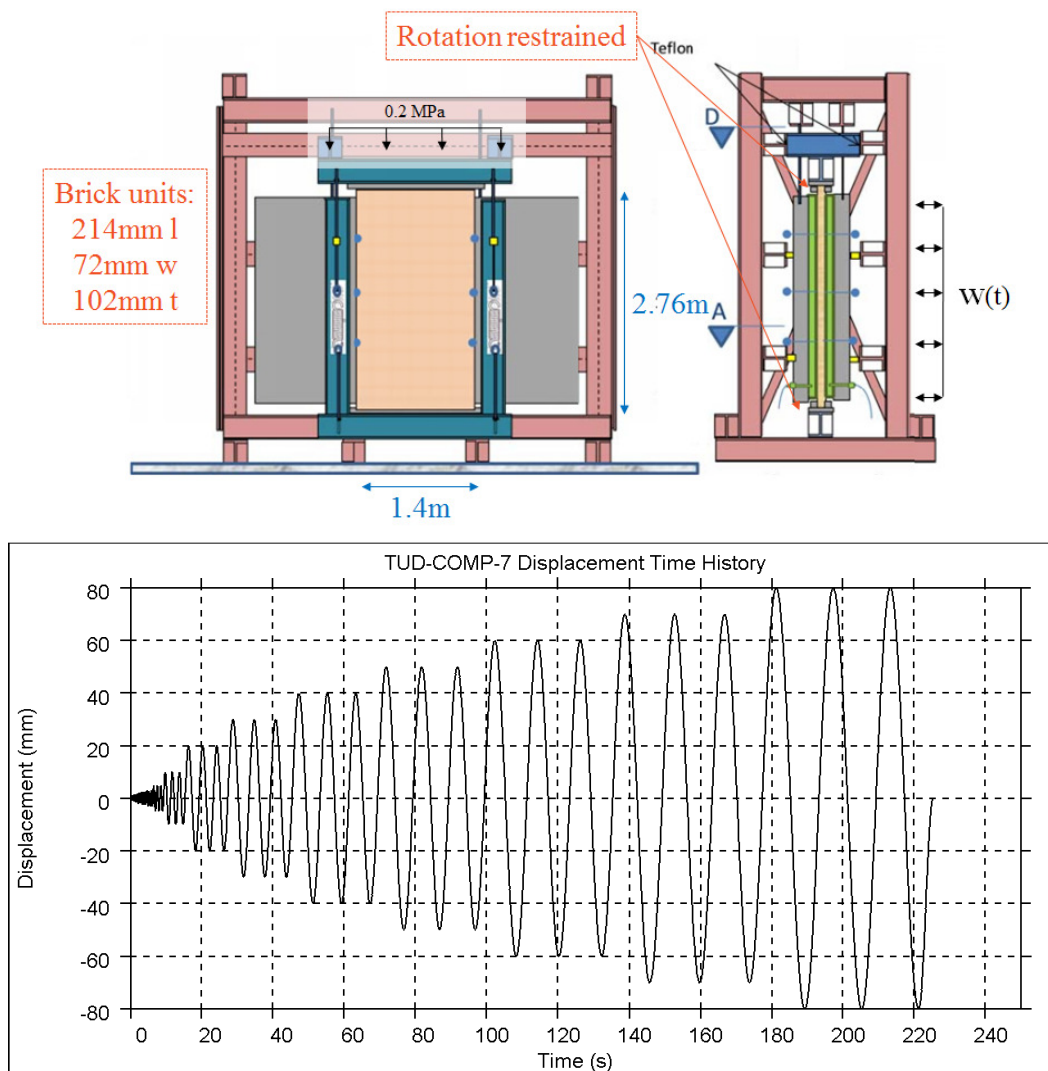
Figure 40 TUD-COMP-7 – Diagram of test set up (top) and displacement time history (bottom)

Table 9 TUD-COMP-7 Material Properties [6]

Mass density	1852 kg/m^3
Masonry Young's modulus perpendicular to bed joints	5091 MPa
Masonry compressive strength perpendicular to bed joints	5.93 MPa
Tensile strength (flexural bond strength) of mortar joints	0.27 MPa
Initial shear strength of mortar joints	0.14 MPa
Coefficient of friction for sliding of joints	0.43

2.8.2 Test Results

The predominant deformation mode of TUD-COMP-7 was out-of-plane one-way rocking with bed-joint opening at top, bottom and mid-height.
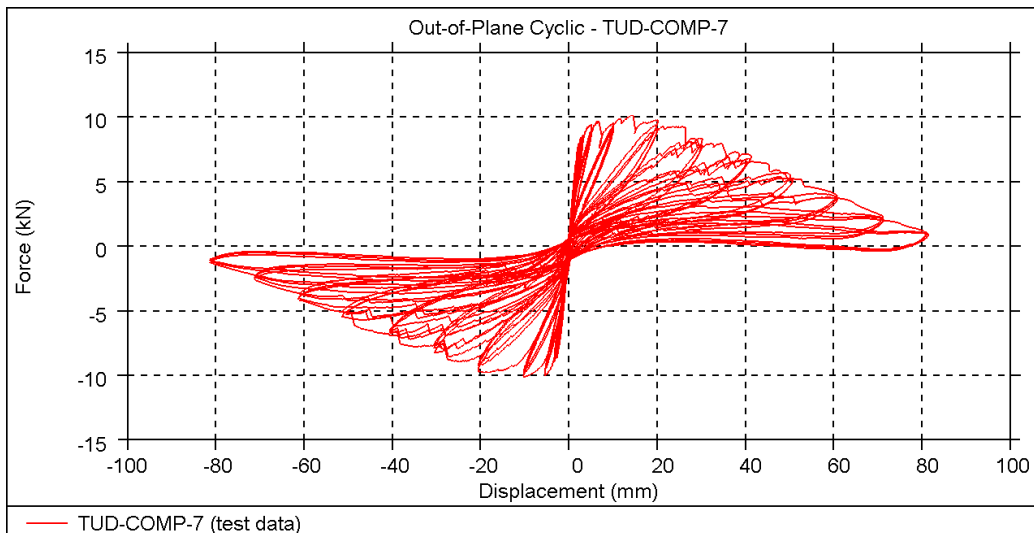
Figure 41 TUD-COMP-7 – Observed damage (top) and applied force-mid-height displacement plot from test data (bottom)

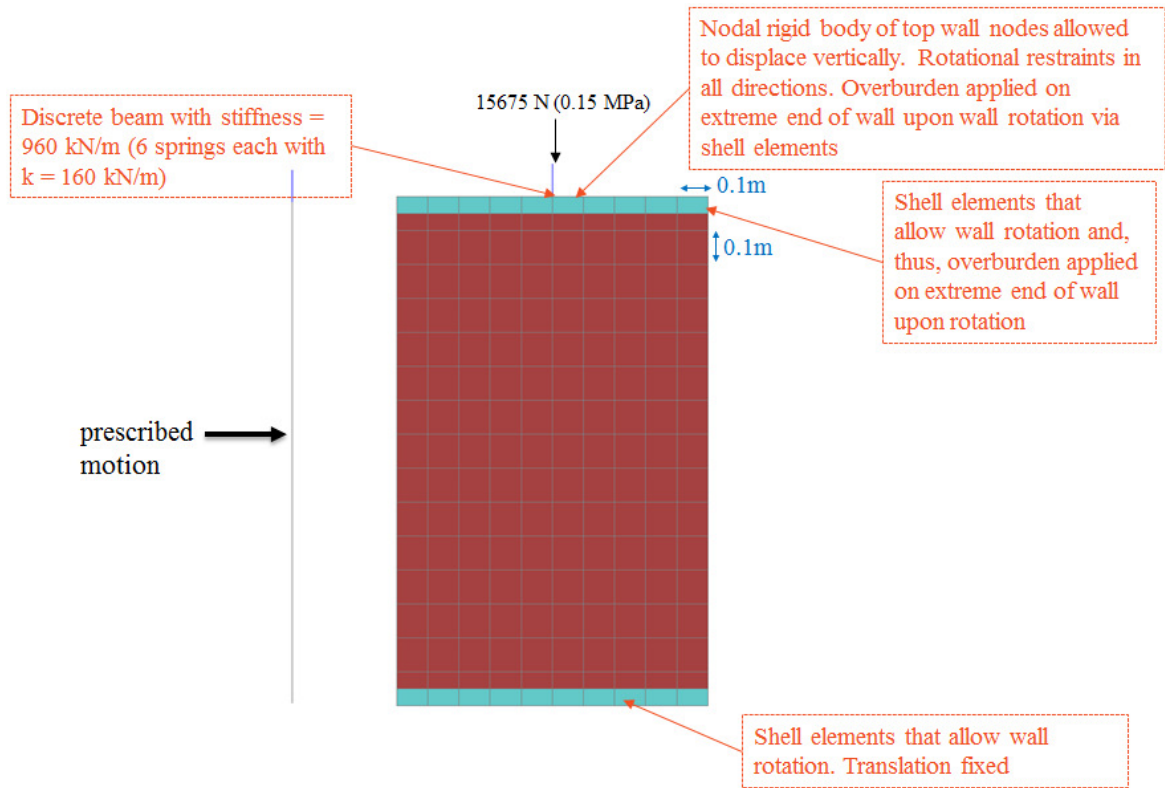## 2.8.3   LS-DYNA: Model Description

Figure 42 LS-DYNA shell model description

2.8.4   LS-DYNA: Results & Validation

The results presented below were obtained using the 25-May-2016 version of the
MAT_SHELL_MASONRY.
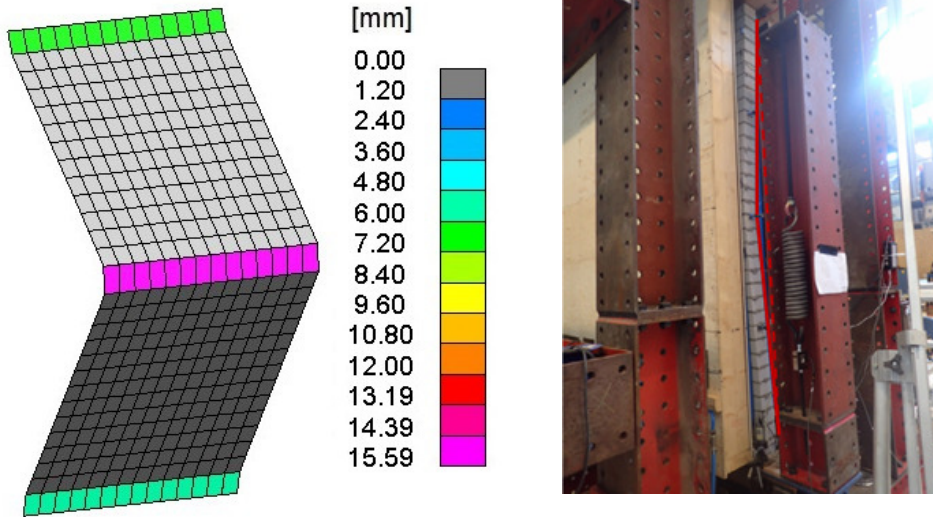
Figure 43 TUD-COMP-7 – Final crack pattern—comparison between LS-DYNA shell
element model (left) and laboratory test (right)
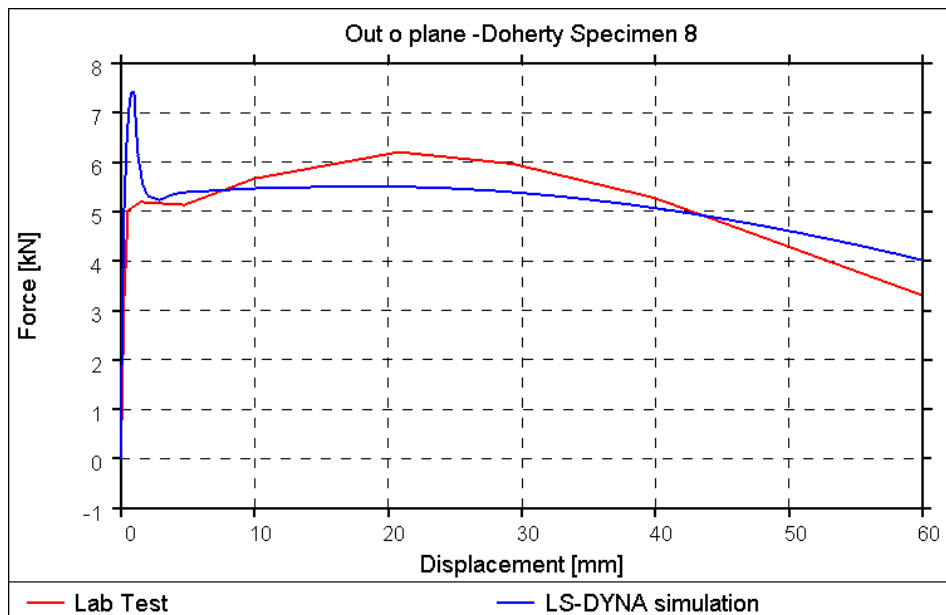

Figure 44 TUD-COMP-7 – Applied force-mid-height displacement comparison plot

2.8.5   Conclusion

The LS-DYNA results show good correlation to the test in terms of final crack
pattern. The initial stiffness and backbone curve are well predicted, but the peak
lateral strength is slightly over-predicted. In addition, the model under-predicts the

energy dissipation. The model response nearly follows the backbone curve with little energy dissipation (as expected for rigid body rocking mode), while the test specimen degrades in stiffness and in strength with increasing deformation cycles, dissipating a significant amount of energy.

2.9 Quasi-Static Out-of-Plane Two Way Damage Mode – Calcium Silicate Brick – TUD-COMP-12

2.9.1 Test Description

TUD-COMP-12 was a quasi-static two-way out-of-plane test administered at the Delft University of Technology. This specimen was a 102 mm thick single-wythe wall with aspect ratio of 1.45 constructed of calcium silicate brick units, and contained a large opening. The applied overburden stress was 50 kPa. The wall was tested under double clamped boundary conditions in which rotation was fully fixed at the top and bottom but the wall was free to rotate in the out-of-plane direction along the vertical edges [8]. The specimen is loaded cyclically by means of four airbags. These are placed on the both sides of the specimen on either side of the opening as shown in green in Figure 46. During the cycles, the airbag at the positive side was kept at a constant pressure of 35 millibar. The desired positive or negative displacements were then achieved by increasing or decreasing the pressure of the negative side

Figure 45 TUD-COMP-12 – Diagram of test set up

Figure 46 TUD-COMP-12 – Displacement time history

Table 10 TUD-COMP-12 Material Properties [6]

Mass density	1852 kg/m^3
Masonry Young's modulus perpendicular to bed joints	5091 MPa
Masonry compressive strength perpendicular to bed joints	5.93 MPa
Tensile strength (flexural bond strength) of mortar joints	0.27 MPa
Initial shear strength of mortar joints	0.14 MPa
Coefficient of friction for sliding of joints	0.43

2.9.2   Test Results

The predominant deformation mode of TUD-COMP-12 was two-way out-of-plane damage characterized by diagonal cracking.
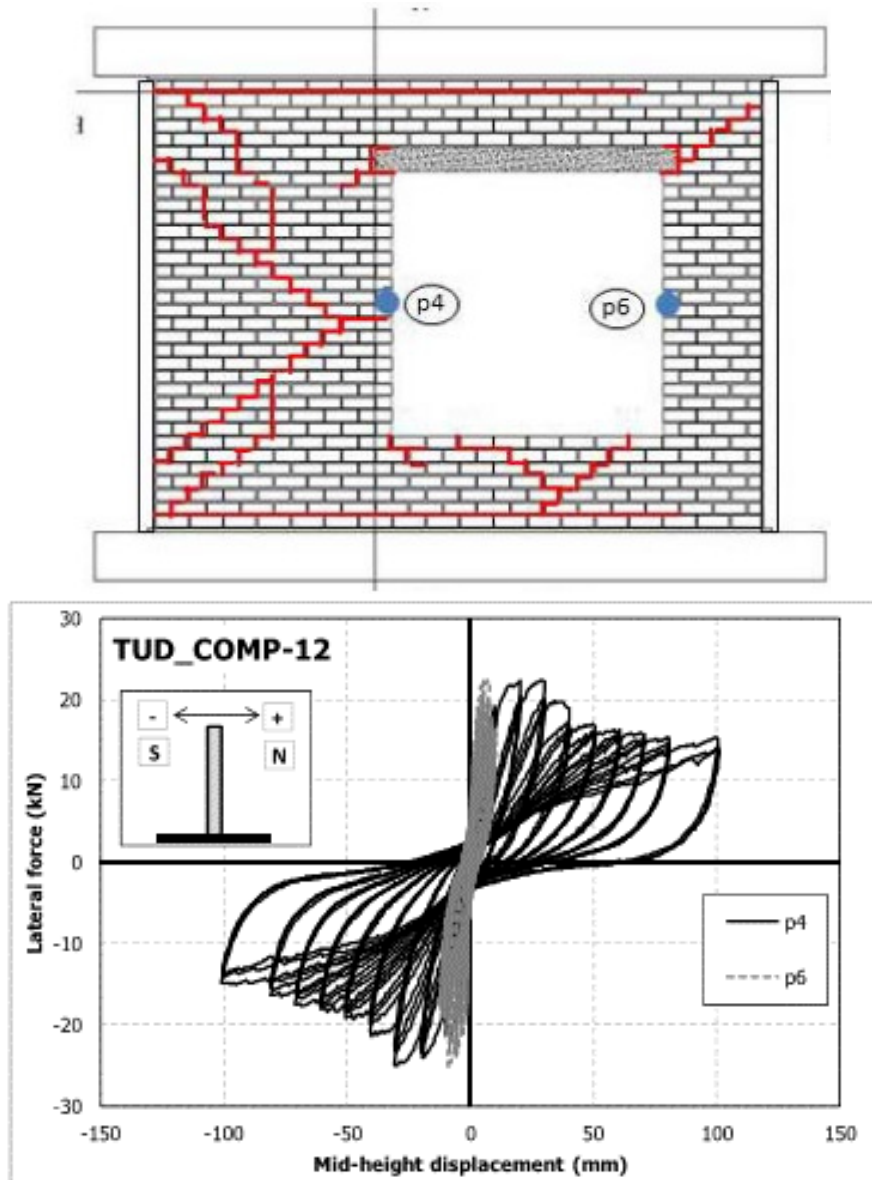
Figure 47 TUD-COMP-12 – Observed damage (top) and applied force-mid-height displacement plot from test data (bottom)
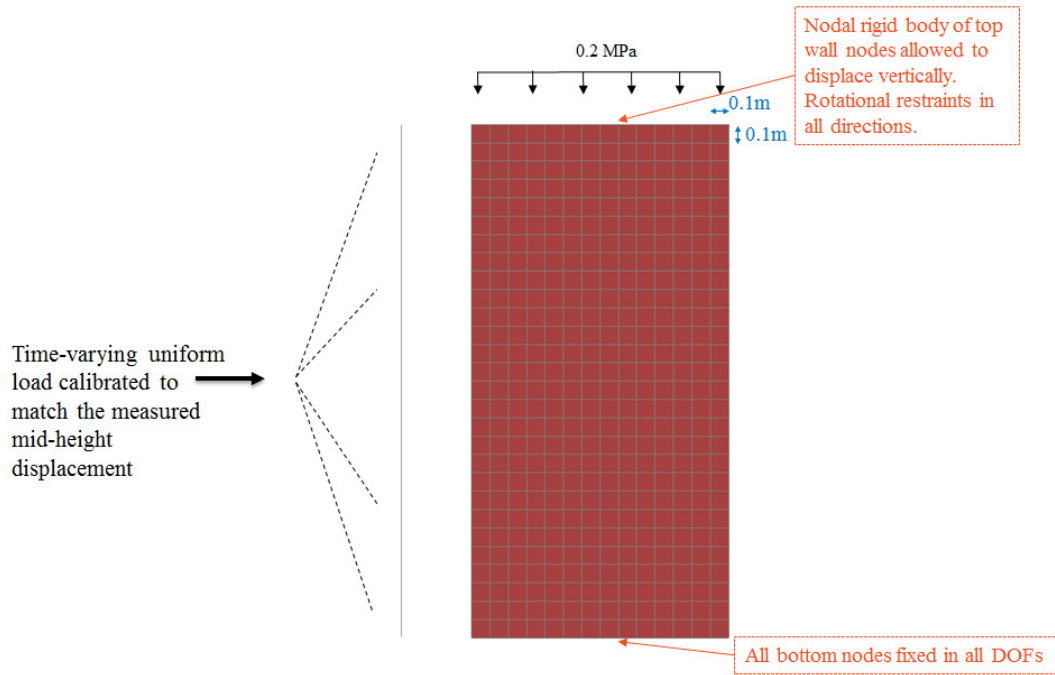
2.9.3 LS-DYNA: Model Description
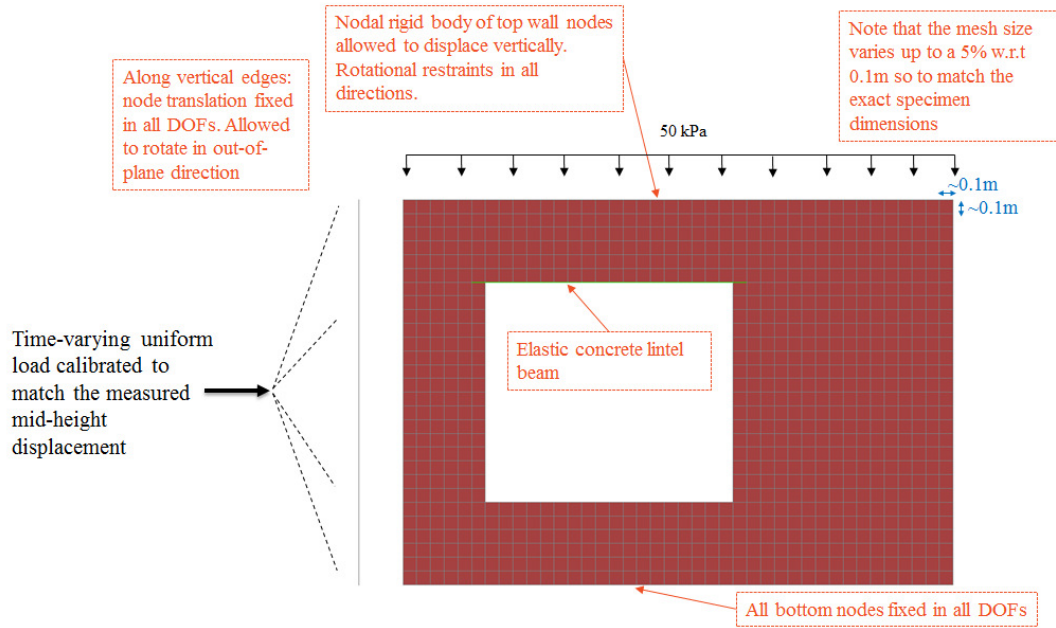
Figure 48 LS-DYNA shell model description

2.9.4   LS-DYNA: Results & Validation

The results presented below were obtained using the 25-May-2016 version of the MAT_SHELL_MASONRY.
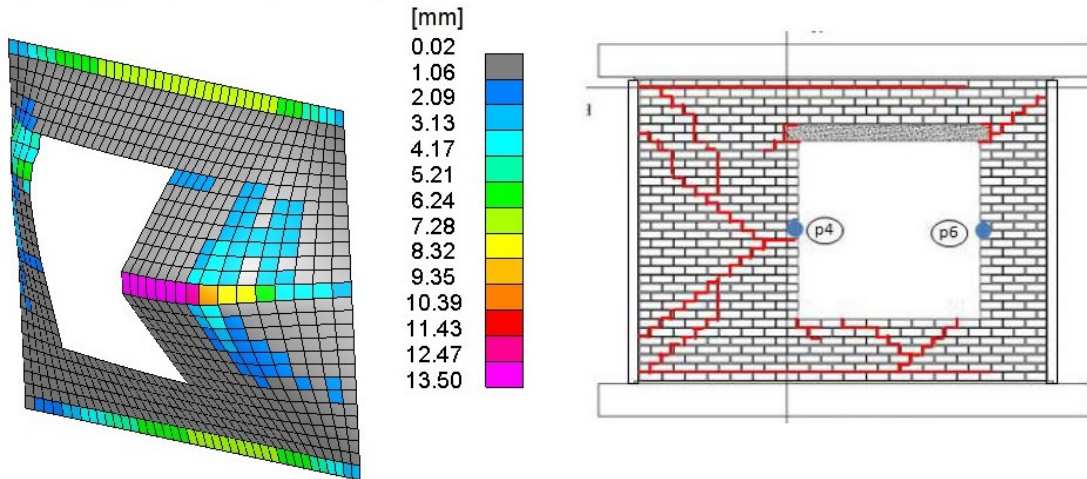
Figure 49 TUD-COMP-12 – Final crack pattern—comparison between LS-DYNA shell element model (left) and laboratory test (right)
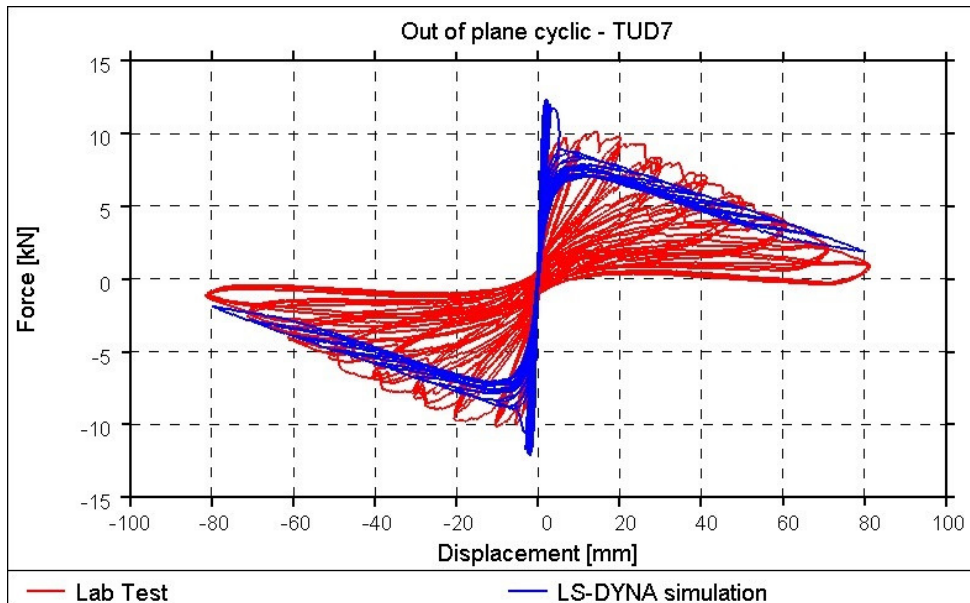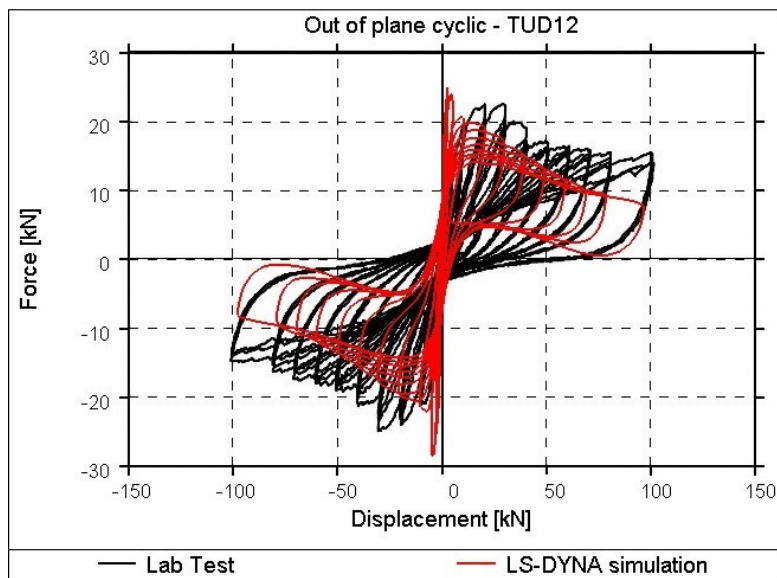

Figure 50 TUD-COMP-12 – Applied force-mid-height displacement comparison plot

2.9.5   Conclusion

The crack pattern of the LS-DYNA simulation does not match that of the test specimen exactly, but the correct failure mechanism (two-way bending failure in both piers) is observed. The initial stiffness and peak lateral strength are generally well predicted. The strength degradation for larger amplitude cycles is overestimated by the simulation. The model somewhat under-predicts the stiffness degradation and associated energy dissipation.

2.10 Dynamic Out-of-Plane Damage Mode – Calcium Silicate Brick – EUC-COMP-4

2.10.1 Test Description

EUC-COMP-4 was a dynamic out-of-plane test administered in the Eucentre laboratory at the University of Pavia, Italy. The specimen was a 100 mm thick single-wythe wall with aspect ratio of 2.0 constructed of calcium-silicate brick units. The applied overburden stress was 0.3 MPa for test phases 1 and 2, reducing to 0.1 MPa for phases 3 4 and 5. The wall was tested under double clamped boundary conditions [3].

Figure 51 EUC-COMP-4 – Diagram of test set up (top) and Gr_1 acceleration time history (bottom)
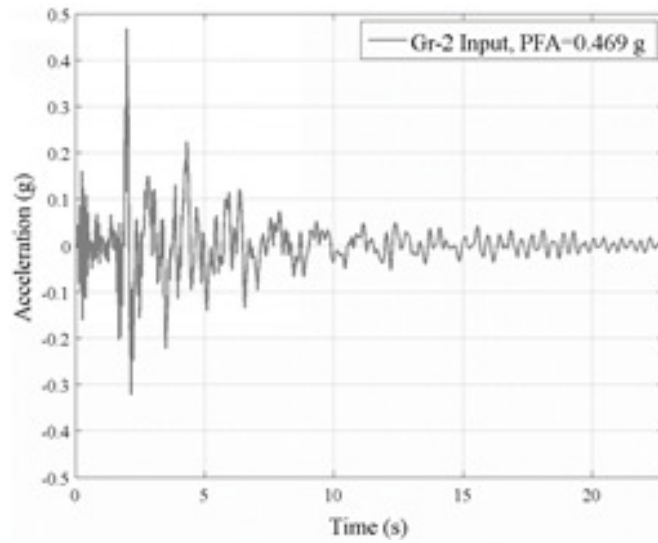
Figure 52 EUC-COMP-4 –Gr_2 acceleration time history

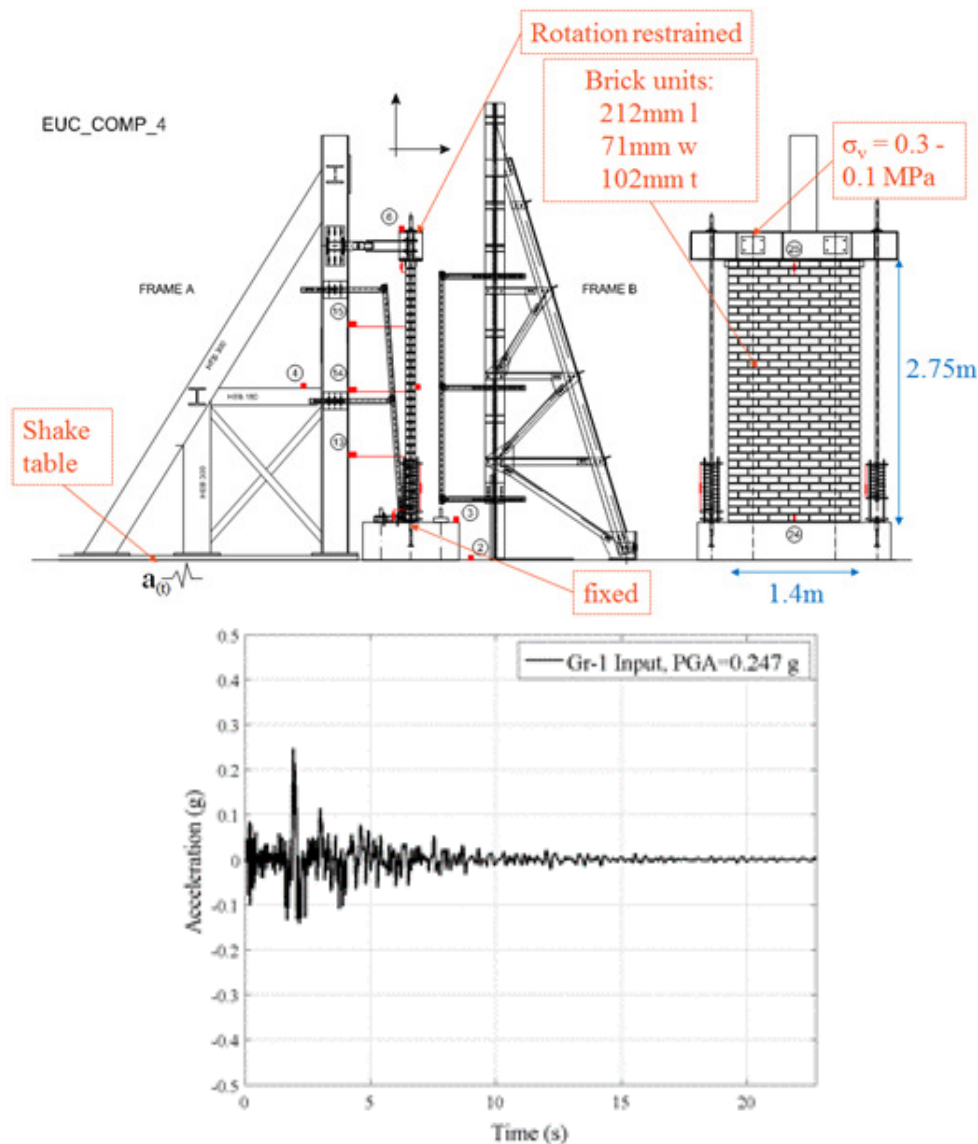| Phase #	Test #	N #	Dynamic Input	Input Scaling	PGA [g]	Max CS ½ H Disp. [mm]
Imposed Overburden Pressure: 0.3 MPa
1	1.1	1	Gr_1	20%	+0.04	+0
	1.2	2	Gr_1	40%	+0.09	+0.12
	1.3	3	Gr_1	80%	+0.16	+0.37
	1.4	4	Gr_1	100%	+0.20	+0.57
	1.5	5	Gr_1	160%	+0.32	+0.93
	1.6	6	Gr_1	200%	+0.42	+1.21
	1.7	7	Gr_1	250%	+0.53	+1.41
	1.8	8	Gr_1	350%	+0.74	+1.69
	1.9	9	Gr_1	450%	+0.96	+4.91
2	2.1	1	RWA 2Hz	-	-1.11	-1,97
	2.2	2	RWA 2Hz	-	-1.63	-9,62
	2.3	3	RWA 2Hz	-	-1.04	-2,68
	2.4	4	RWA 2Hz	-	-1.88	-14,09
Imposed Overburden Pressure: 0.1 MPa
3	3.1	1	Gr_1	40%	+0.08	-0,35
	3.2	2	Gr_1	80%	+0.17	-0,73
	3.3	3	Gr_1	100%	+0.21	-0,92
	3.4	4	Gr_1	160%	+0.34	-1,29
	3.5	5	Gr_1	200%	+0.41	1,94
	3.6	6	Gr_1	250%	+0.51	-7,42
	3.7	7	Gr_1	300%	+0.60	-14,42
	3.8	8	Gr_1	350%	+0.73	-16,61
4	4.1	1	RWA 2Hz	-	-0.25	-0,38
	4.2	2	RWA 2Hz	-	-0.48	-1,92
	4.3	3	RWA 2Hz	-	-0.72	-16,05
	4.4	4	RWA 2Hz	-	-0.96	-52,99
5	5.1	1	Gr_2	100%	+0.44	2,88
	5.2	2	Gr_2	150%	+0.64	-9,87
	5.3	3	Gr_2	200%	+0.85	-failure

Figure 53 EUC-COMP-4 – Load protocol

Table 11 EUC-COMP-4 Material Properties

Mass density	1835 kg/m^3
Masonry Young's modulus perpendicular to bed joints	4182 MPa
Masonry compressive strength perpendicular to bed joints	6.2 MPa
Tensile strength (flexural bond strength) of mortar joints	0.238 MPa
Initial shear strength of mortar joints	0.21 MPa
Coefficient of friction for sliding of joints	0.42

2.10.2   Test Results
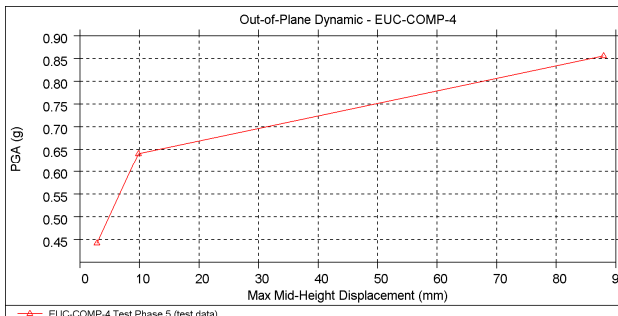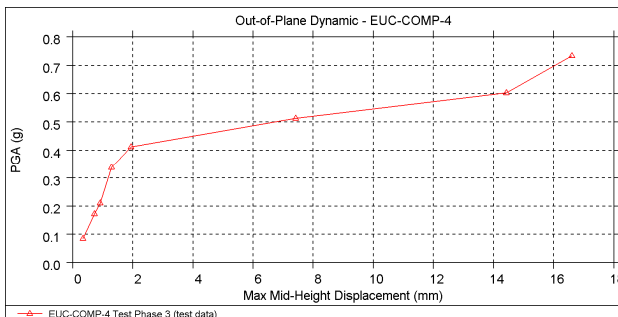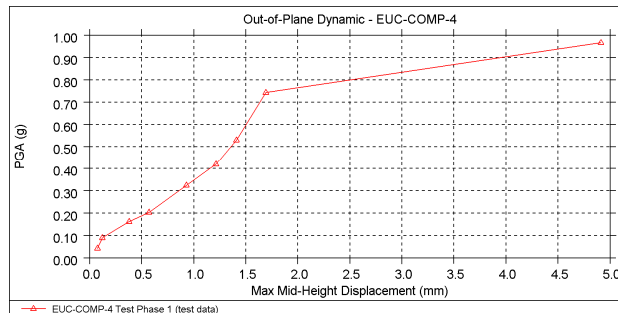
Figure 54 EUC-COMP-4 – Observed crack pattern (top) and maximum mid-height displacement vs PGA plots from test phases 1, 3 and 5 (bottom three)

Global instability occurred when the applied motion was scaled to 0.85g.

2.10.3   LS-DYNA: Model Description
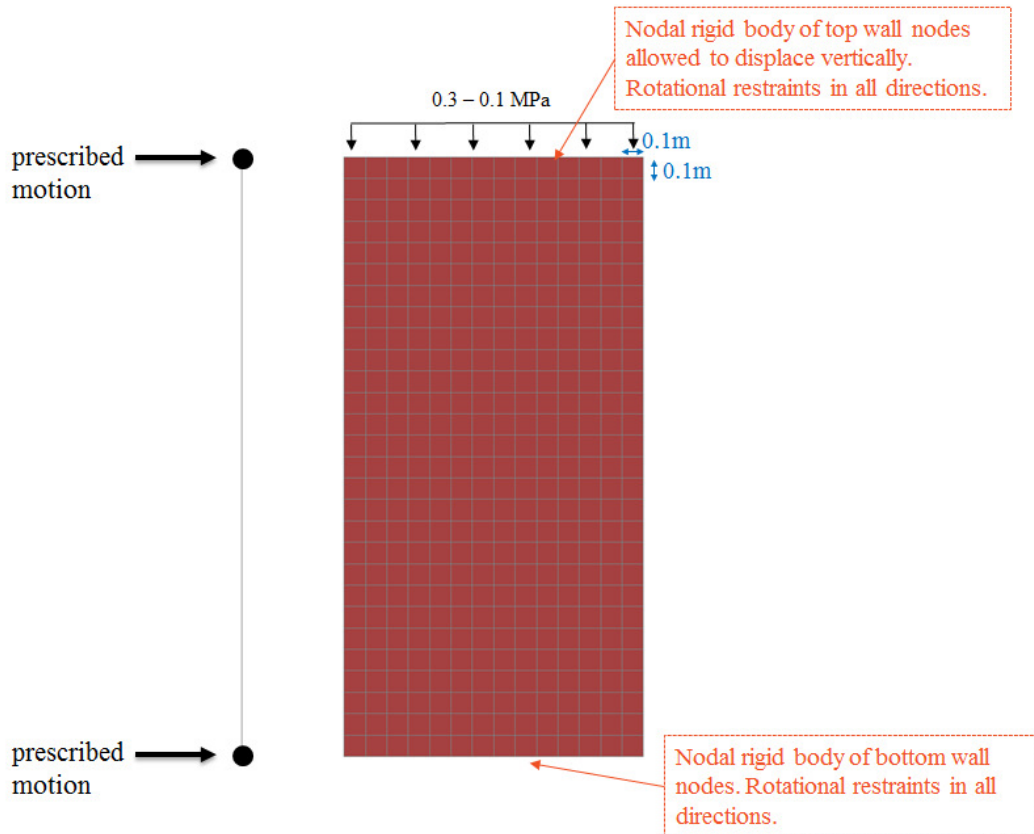
Figure 55 LS-DYNA shell model description

In the test EUC-COMP-4 the specimen was subjected to ground motion Phases 1, 3 and 5 (see Figure 53). Phases 2 and 4, consisting of the calibration Ricker Wave Acceleration signal, were not modelled.

2.10.4   LS-DYNA: Results & Validation

The results presented below were obtained using the 25-May-2016 version of the MAT_SHELL_MASONRY. The following figures compare the predicted maximum lateral displacements of the mid-height of the wall with those measured in the experiment as a function of the ground motion scaling (PGA).
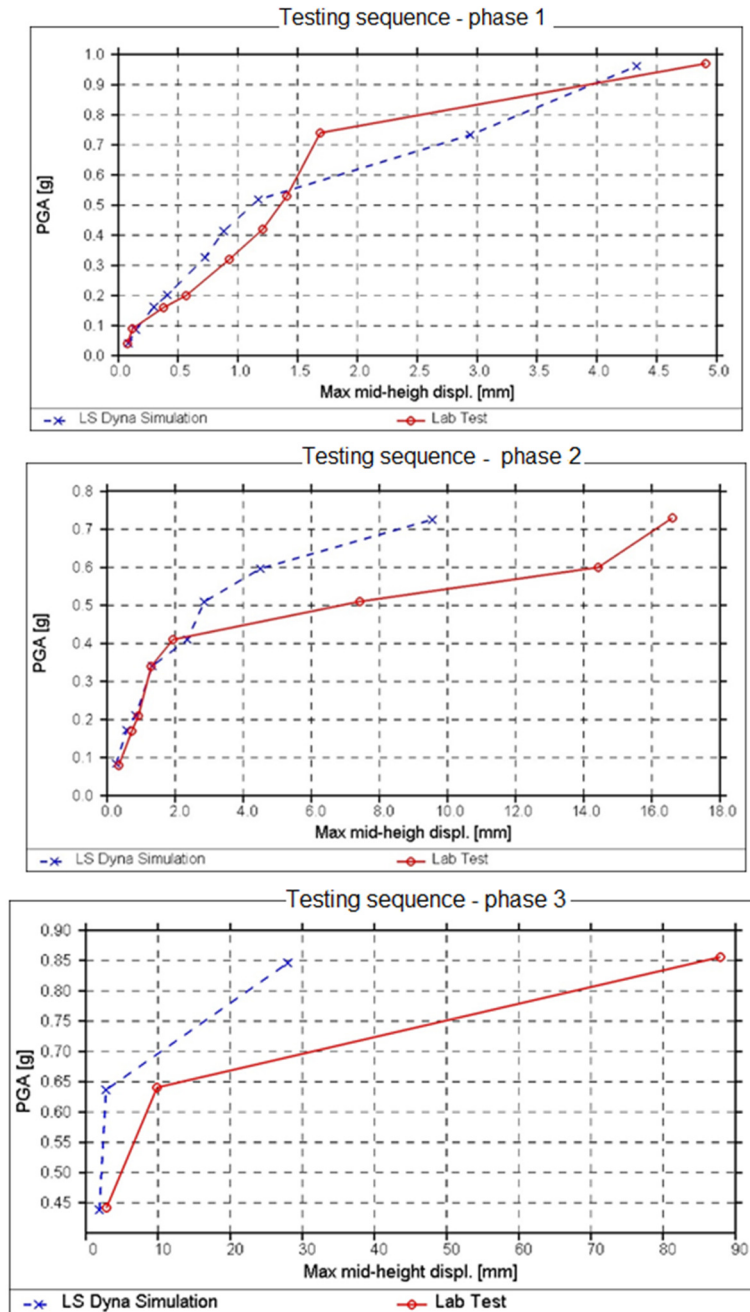
Figure 56 LS-DYNA results for EUC-COMP-4: 0.3 MPa overburden, ground motion Gr_1 (top); 0.1 MPa overburden, Gr_1 (middle); 0.1 MPa overburden, Gr_2 (bottom)

Although global instability was not predicted in the LS-DYNA simulation during application of Gr_2 scaled to max PGA of 0.85g, the displacements became relatively large and it is expected that collapse would arise under slightly higher scaling.

2.10.5   Conclusion

The analysis results match the lab tests quite well. For the highly nonlinear responses (displacements above, say, 5-10mm) there is likely to be significant random variation of the peak displacement response, so an exact match with experiment is not expected. Of more importance is the prediction of the transition between small, quasi-linear response and larger nonlinear response. These transitions are fairly well predicted. However, collapse was not predicted at the same motion scaling as in the lab.

2.11 Dynamic Out-of-Plane Damage Mode – Cavity Wall – EUC-COMP-5

2.11.1 Test Description

EUC-COMP-5 was a dynamic out-of-plane test administered in the Eucentre laboratory at the University of Pavia, Italy. The specimen was a cavity wall. The inner (structural) leaf was a 102 mm thick single-wythe wall with aspect ratio of 2.0 constructed of calcium-silicate brick units. The outer leaf was a 100 mm thick single-wythe wall constructed of clay brick units. The applied overburden stress was 0.1 MPa and applied on the inner leaf only. The inner leaf was set up under double clamped boundary conditions and the outer leaf, cantilever boundary conditions [3].
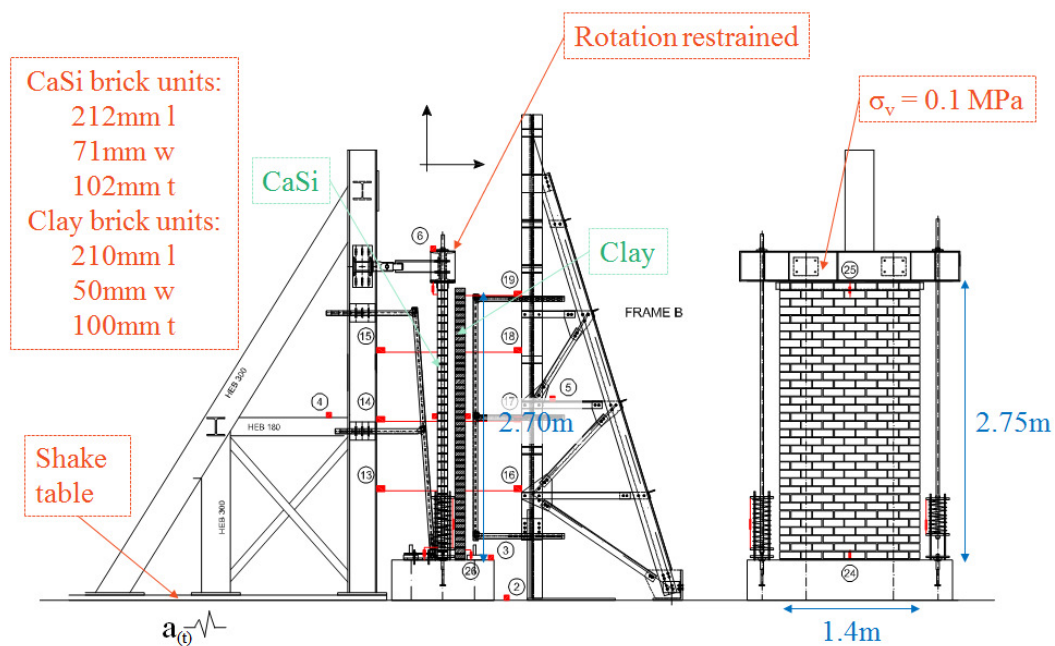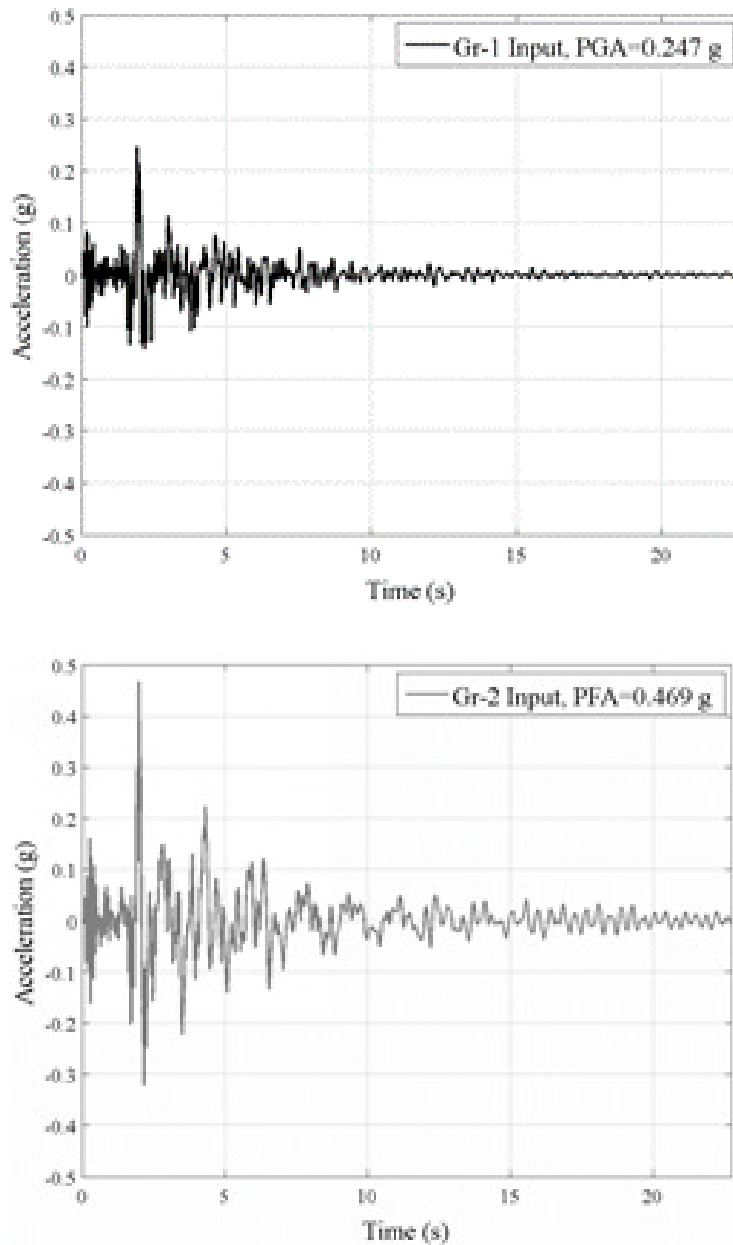

Figure 57 EUC-COMP-5 – Diagram of test set up

Figure 58 EUC-COMP-5 –Gr_1 acceleration time history (top) and Gr_2 acceleration time history (bottom)
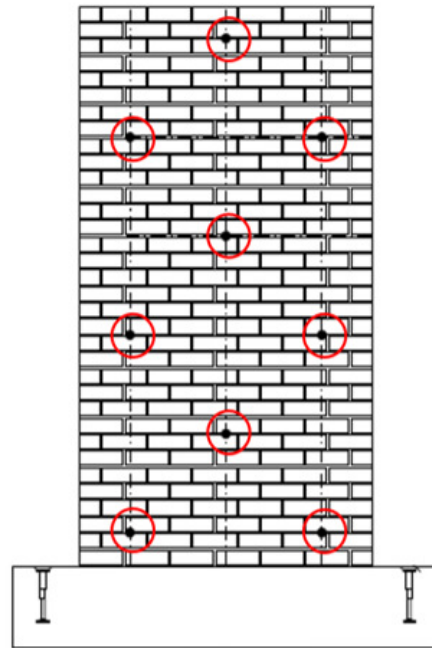
Figure 59: EUC comp. 5 ties arrangement for an overall density of 2 ties /m^2

Specimen	Phase #	Test #	Dynamic Input	Input Scaling	PGA [g]	File Name
EC_COMP_5	0	0.1	Hammering	-	-	-
EC_COMP_5	0	0.2	White Noise	-	0.1	-
EC_COMP_5	1	1.1	Gr_1	+20%	+0.04	-
EC_COMP_5	1	1.2	Gr_1	+40%	+0.09	-
EC_COMP_5	1	1.3	Gr_1	-40%	-0.09	-
EC_COMP_5	1	1.4	Gr_1	+60%	+0.12	-
EC_COMP_5	1	1.5	Gr_1	+80%	+0.17	-
EC_COMP_5	1	1.6	Gr_1	+100%	+0.21	-
EC_COMP_5	1	1.7	Gr_1	-60%	-0.13	-
EC_COMP_5	1	1.8	Gr_1	-80%	-0.17	-
EC_COMP_5	1	1.9	Gr_1	-100%	-0.23	-
EC_COMP_5	2	2.1	RWA	-	-0.22	-
EC_COMP_5	2	2.2	RWA	-	-0.30	-
EC_COMP_5	3	3.1	Gr_2	+70%	+0.31	-
EC_COMP_5	3	3.2	Gr_2	+100%	+0.49	-
EC_COMP_5	3	3.3	Gr_2	+150%	+0.66	-
EC_COMP_5	4	4.1	Gr_1	+300%	+0.60	-
EC_COMP_5	5	5.1	RWA	-	-0.30	-
EC_COMP_5	5	5.2	RWA	-	-0.49	-
EC_COMP_5	6	6.1	Gr_2	+150%	+0.65	-

Figure 60: EUC-COMP-5 – Load protocol

Table 12 EUC-COMP-5 Material Properties

|		CaSi	Clay
Mass density		1835 kg/m^3	1905 kg/m^3
Masonry Young's modulus perpendicular to bed joints		4182 MPa	6033 MPa
Masonry compressive strength perpendicular to bed joints		6.2 MPa	11.32 MPa
Tensile strength (flexural bond strength) of mortar joints		0.238 MPa	0.158 MPa
Initial shear strength of mortar joints		0.21 MPa	0.15 MPa
Coefficient of friction for sliding of joints		0.42	0.87
Wall tie strength	Tension	1.02 kN	3.03 kN
	Compression	0.40 kN	1.42 kN

2.11.2 Test Results
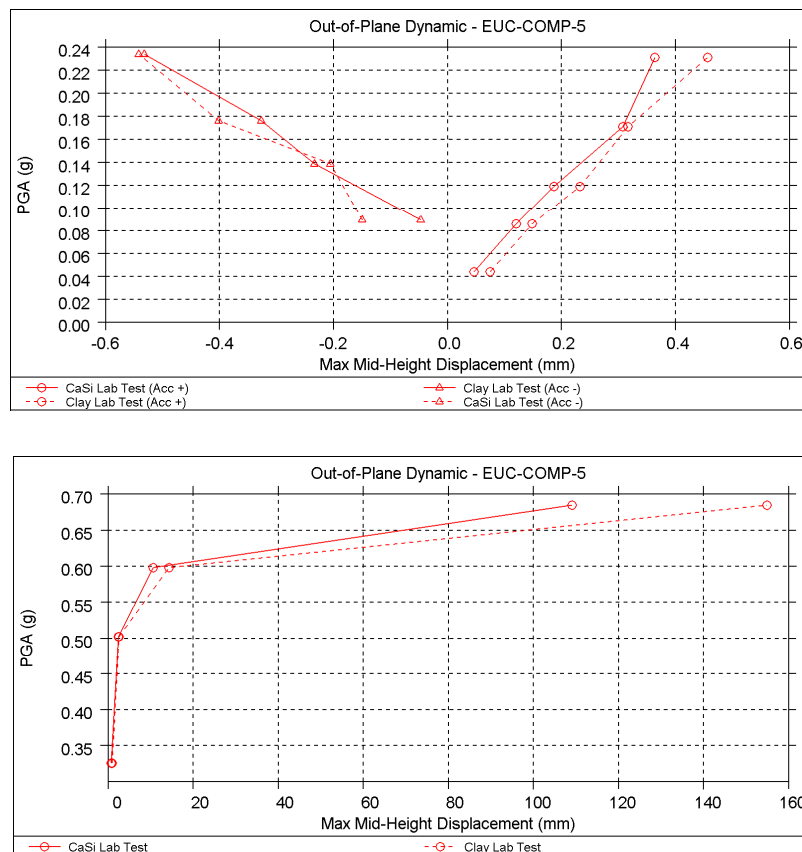
Figure 61 EUC-COMP-5 – Observed crack pattern (top) and maximum mid-height displacement vs PGA plots from test data—application of Phase 1(top) and Phases 3, 4, and 6 (bottom). Continuous lines show displacements of calcium silicate leaf; dashed lines show displacements of clay leaf.
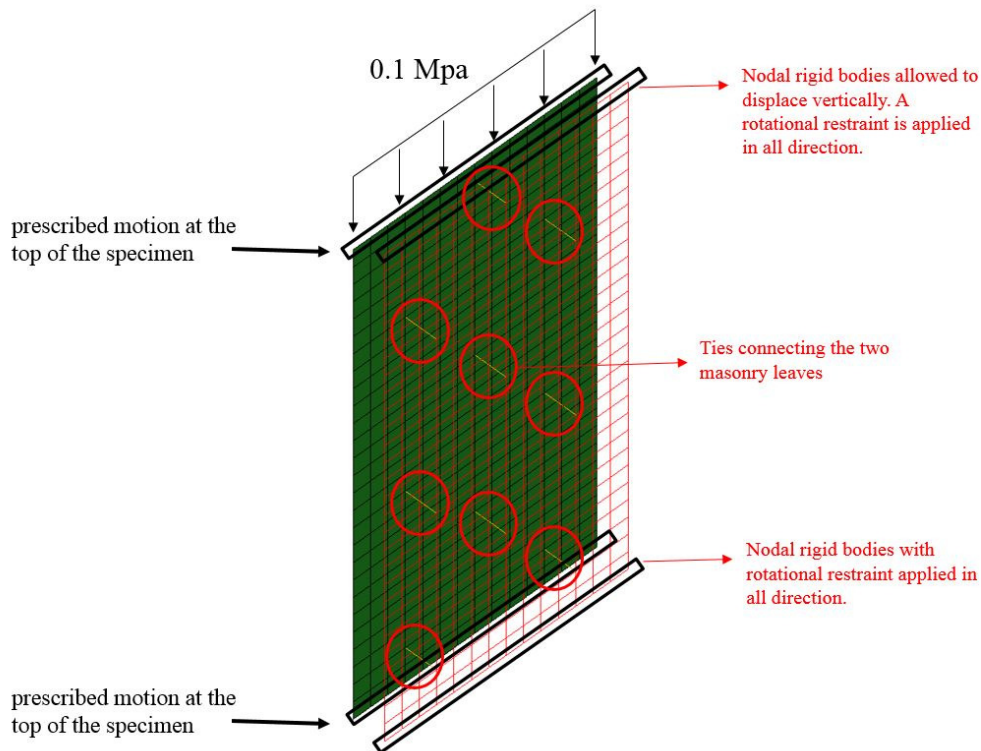
2.11.3   LS-DYNA: Model Description

Figure 62 LS-DYNA shell model description

The two leaves were modelled as separate planes of shell elements. As in the experiment, the overburden and top edge restraint were applied to the Calcium Silicate leaf only, while the clay leaf is free at the top. The same motion time-history was applied to the bottom of both leaves and to the top of the Calcium Silicate leaf. Thus, it was assumed that dynamic distortion of the testing frame was negligible.

The simulated performance was found to be sensitive to the assumed wall tie strength. The baseline results presented in the following section correspond to a tensile wall tie strength of 1kN. The force-deflection curve was taken from quasi-static cyclic tests on wall ties [10]. It is noted that during this dynamic test the ties undergo bending and shear loading as well as axial, which is different to the simpler regime in the TU Delft lab pull-out test, and which may enhance friction or other resistance mechanisms. Given the lack of certainty surrounding the wall tie behaviour under such conditions, further analyses were undertaken with the wall tie force-displacement curve scaled by different factors.

In the LS-DYNA analysis of test EUC-COMP-5 the specimen was subjected to ground motion Phases 1, 3, 4 and 6 (see Figure 53). Phases 2 and 5, consisting of the calibration Ricker Wave Acceleration signal, were not modelled.

2.11.4   LS-DYNA: Results & Validation

The results presented below were obtained using the 25-May-2016 version of the MAT_SHELL_MASONRY.
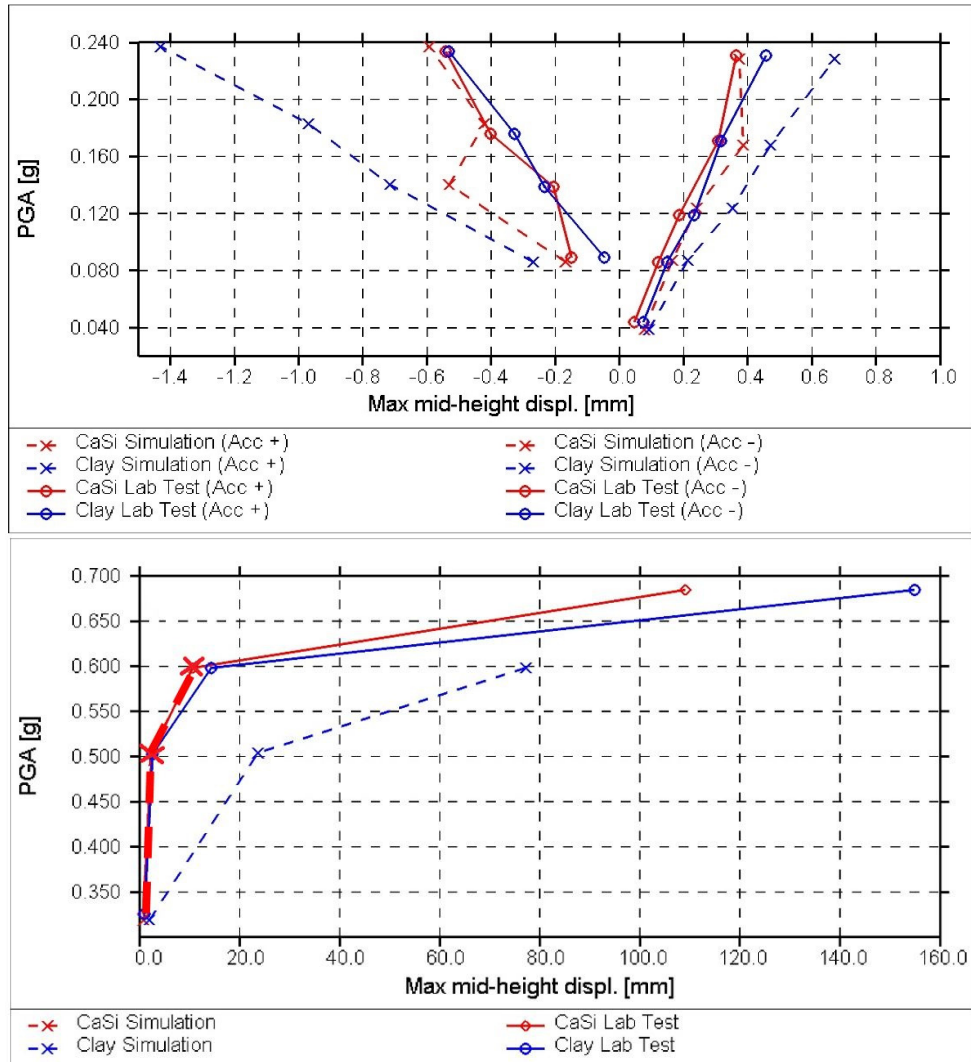

Figure 63 LS-DYNA results for EUC-COMP-5: application of Phase 1(top) and Phases 3, 4, and 6 (bottom)

2.11.5   Conclusion

The simulation shows large displacements starting from 0.5g PGA and collapse at a PGA of 0.60g (limited by wall tie failure leading to collapse of the clay leaf). In the lab, the specimen showed large displacement starting at 0.6g PGA and reached a PGA of 0.68g before collapse. In overall terms, this is good agreement.

A sensitivity study (Figure 64) demonstrated better correlation to the strong motion phase of the EUC-COMP-5 test results when the input force-deflection curve for the wall ties was scaled by 1.5. Meanwhile, if the wall ties were treated as elastic, the possibility for collapse due to wall tie pull-out is eliminated, and therefore the capacity is limited only by the total strength of the two walls. In that

case, the capacity exceeds 0.68g. Thus, results are very sensitive to the assumed characteristics of the wall ties.
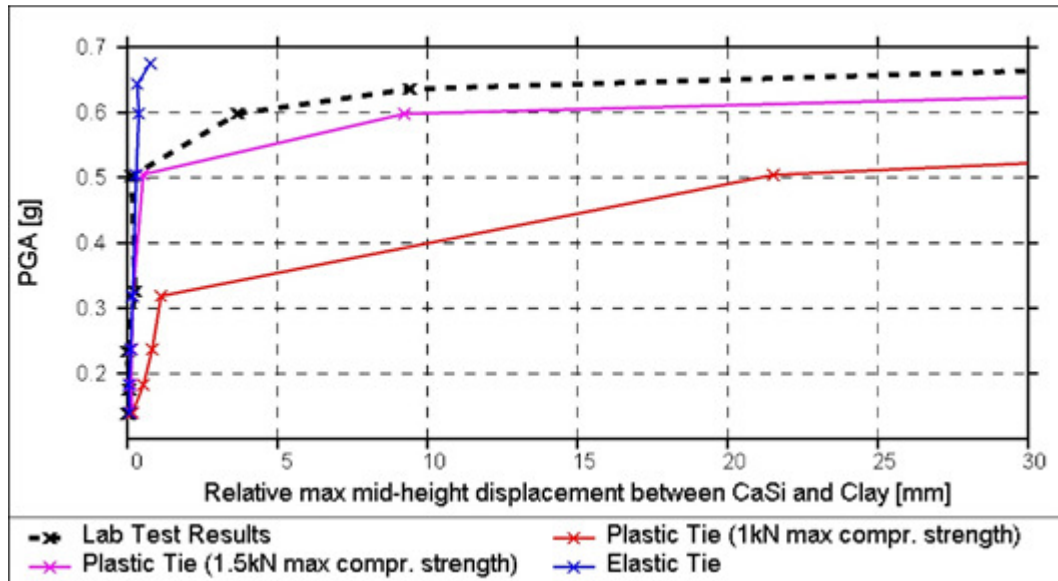

Figure 64: EUC-COMP-5: Effect of wall tie input data on LS-DYNA simulation –test phases #3, 4 & 6. Red curve: using result measured in cyclic wall tie test; Pink curve: using measured result scaled by 1.5; Blue curve: stiff elastic wall tie (no pull-out).

Note that, as well as the tensile response of the wall ties (pull-out), the results are sensitive to the compressive part of the assumed force-deflection curve. This corresponds to the tie being pushed into the mortar as the distance between the two leaves reduces. The resistance in this mode may be influenced by several factors, for example, the mortar may be damaged by the wall's response to the previous ground motion; the ties may have been bent by the previous relative movement of the two leaves and may therefore buckle more easily; or the bent portion may exhibit more resistance to being pushed into the mortar. Thus, conditions experienced by the wall ties in this dynamic test may be quite different from the pull-out tests from which the wall tie force-deflection curve was derived. In the light of these uncertainties, an exact match to the lab tests is not expected. Further laboratory testing of wall ties under a wider range of conditions, including tri-axial conditions, is recommended.

In real buildings there is the added possibility of corrosion, or that the ties may not have been straight when initially installed. Therefore, for purposes of modelling existing buildings, conservative characteristics for wall tie behaviour should be adopted.

2.12 Pseudo-Dynamic Full Scale Building – Pavia

2.12.1 Test Description

The Pavia full scale building was a pseudo-dynamic uni-directional cyclic test administered at the University of Pavia, Italy. The structure was constructed of single-wythe walls of clay brick units. The applied overburden was 265 kN on the first floor and 265 kN on the second floor [9].
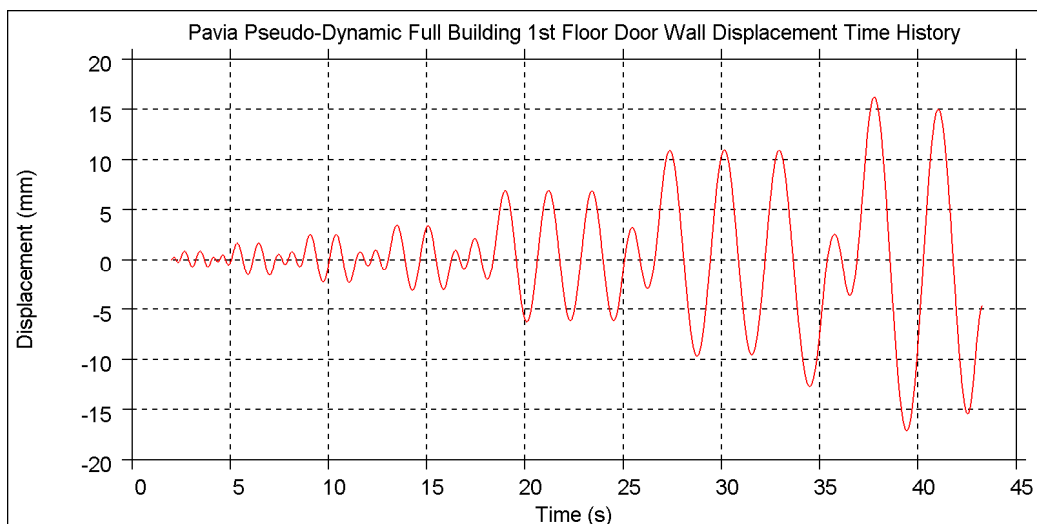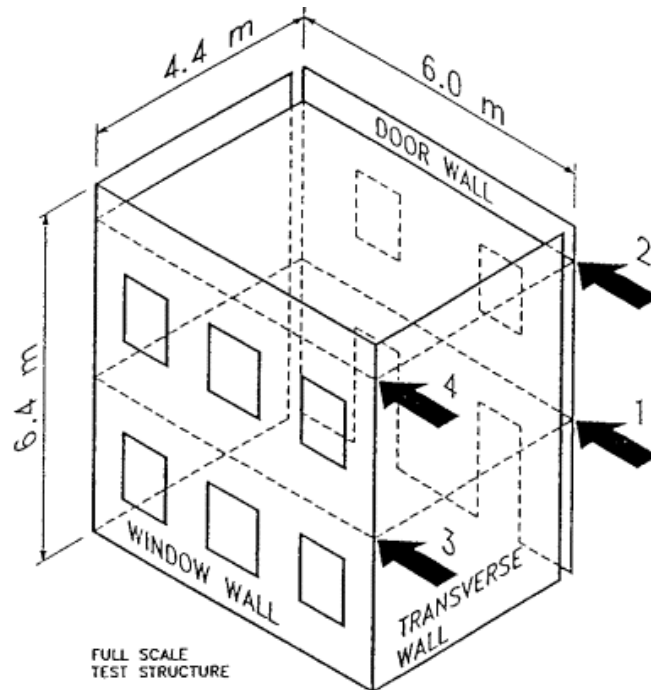

Figure 65 Pavia Pseudo-Dynamic Full Building – Diagram of test set up (top) and displacement time history (bottom)

Table 13 Pavia Pseudo-Dynamic Full Building Material Properties [2]

Mass density	1652 kg/m^3
Masonry Young's modulus perpendicular to bed joints	1491 MPa
Masonry compressive strength perpendicular to bed joints	6.2 MPa
Tensile strength (flexural bond strength) of mortar joints	0.04 MPa
Initial shear strength of mortar joints	0.23 MPa
Coefficient of friction for sliding of joints	0.58

2.12.2   Test Results
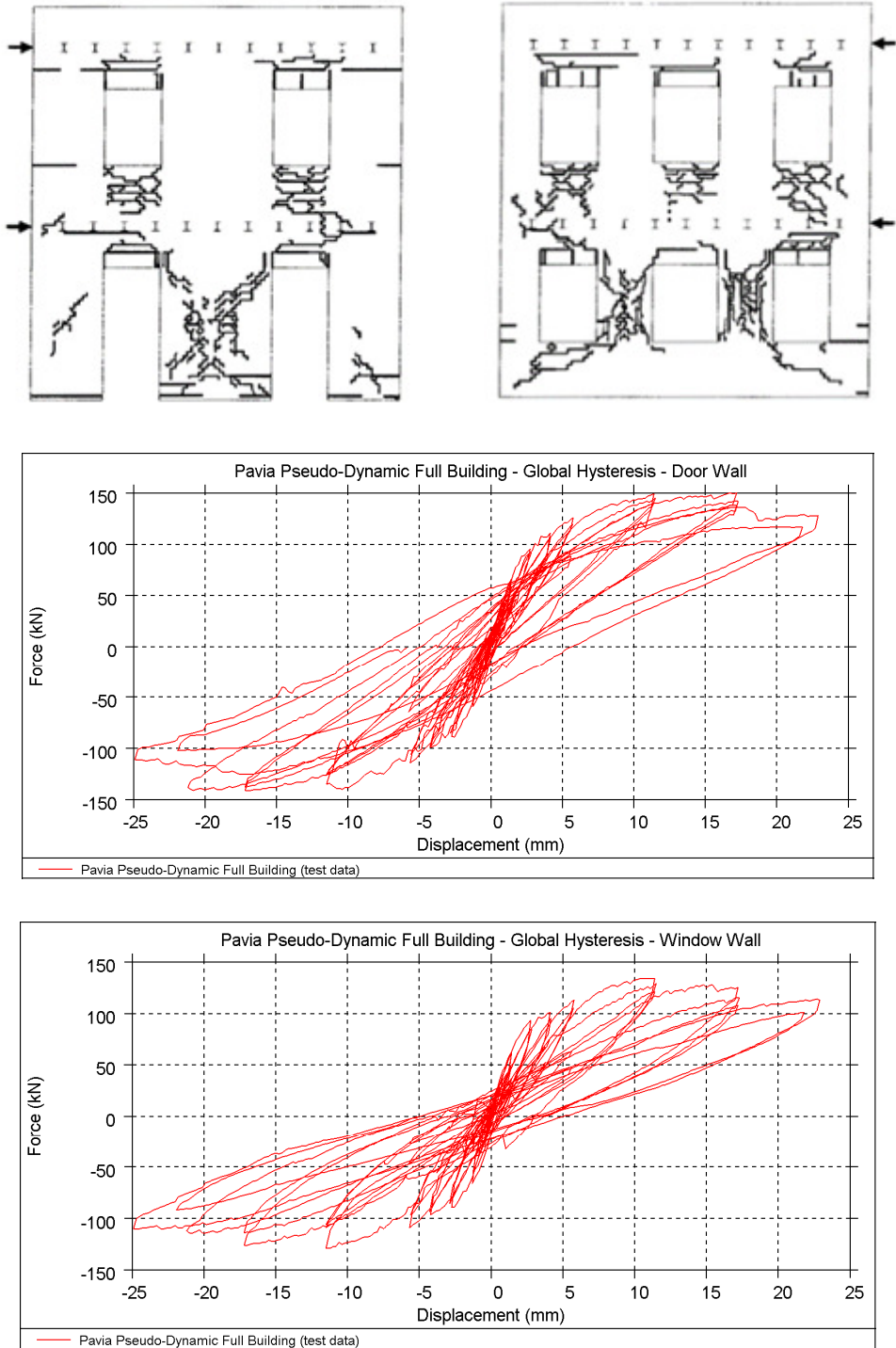

Figure 66 Pavia Pseudo-Dynamic Full Building – Observed crack pattern for final run (top) and shear force-displacement plots from test data—Door Wall (middle) and Window Wall (bottom).

2.12.3 LS-DYNA: Model Description
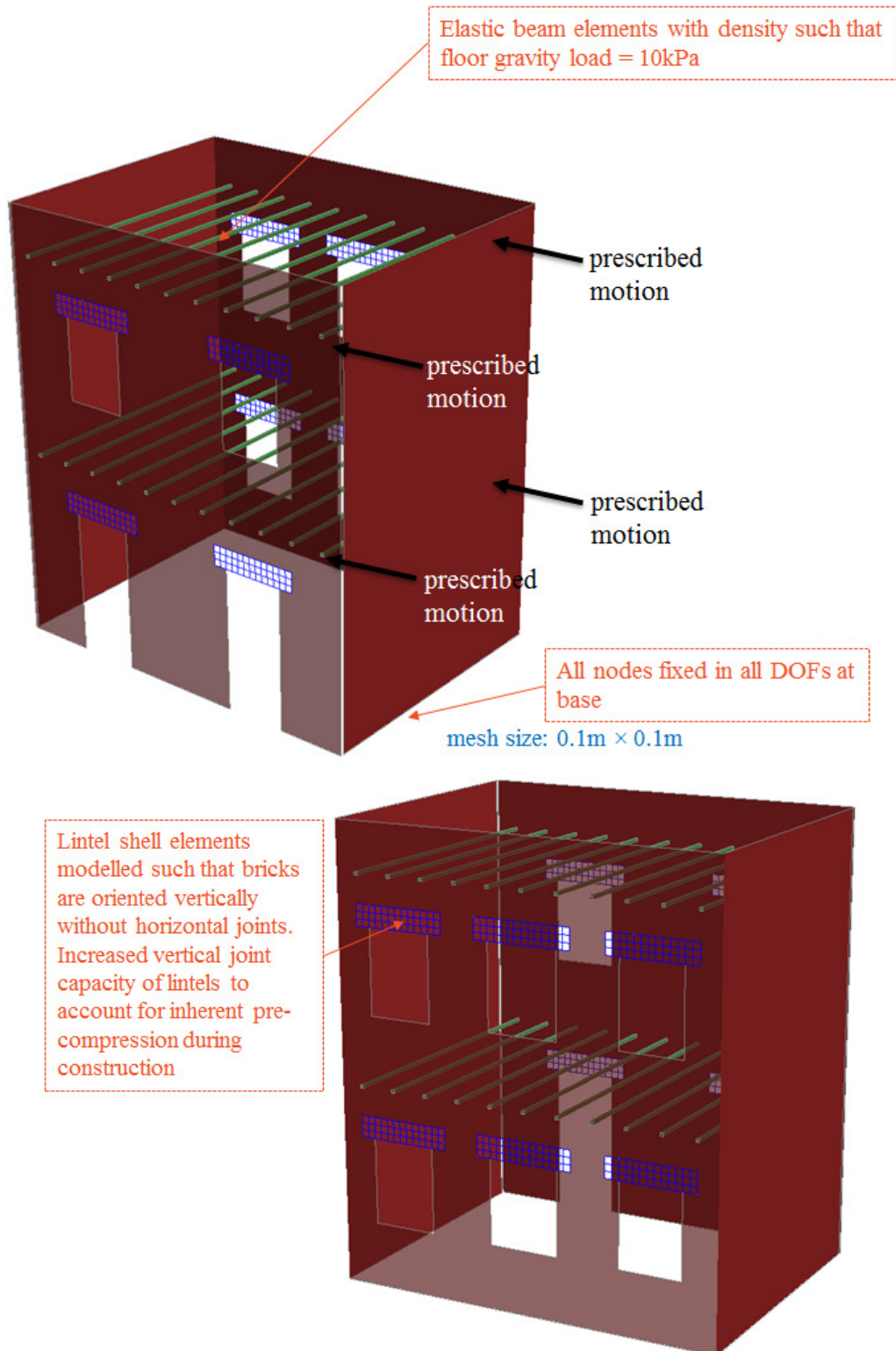
Figure 67 LS-DYNA shell model: door wall (top) and window wall (bottom)

2.12.4 LS-DYNA: Results & Validation

The results presented below were obtained using the 25-May-2016 version of the MAT_SHELL_MASONRY.

Figure 68: Pavia Pseudo-Dynamic Full Building – Crack pattern after Run 5— comparison between LS-DYNA shell element model (left) and laboratory test (right)
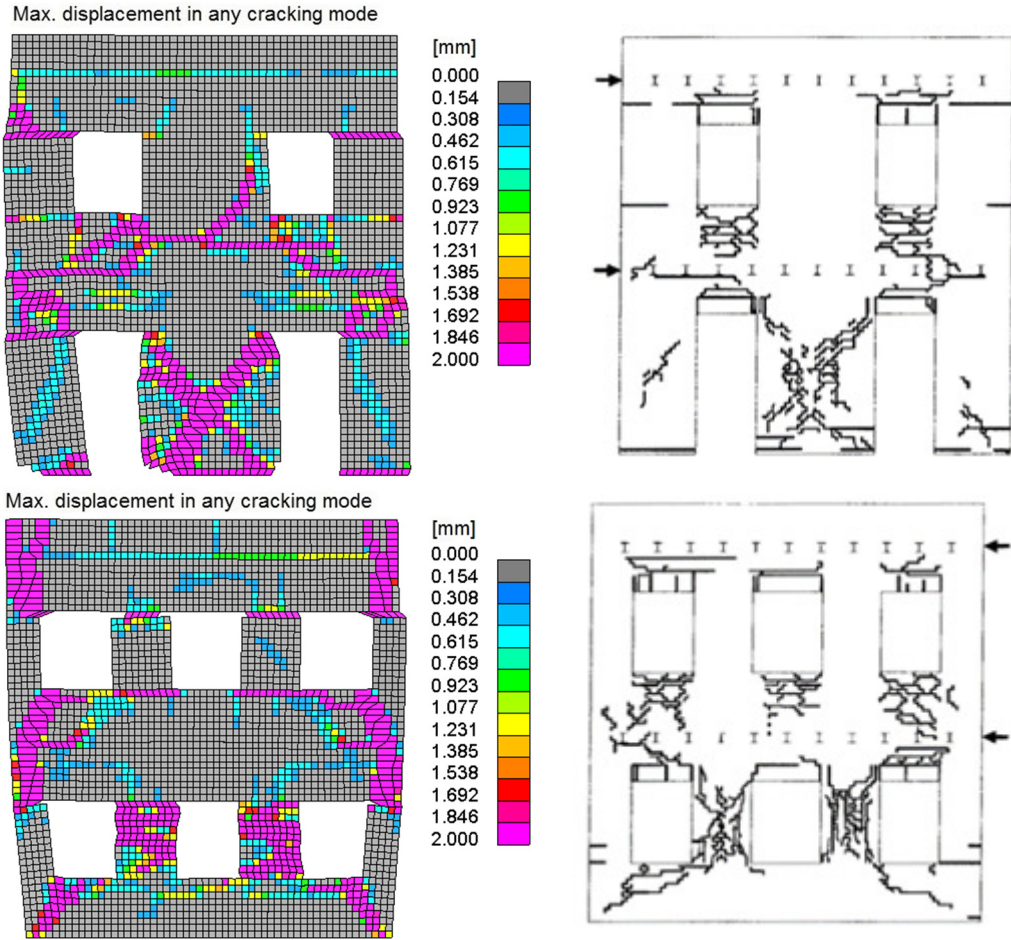
Figure 69 Pavia Pseudo-Dynamic Full Building – Crack pattern after final run (Run 7)—comparison between LS-DYNA shell element model (left) and laboratory test (right)
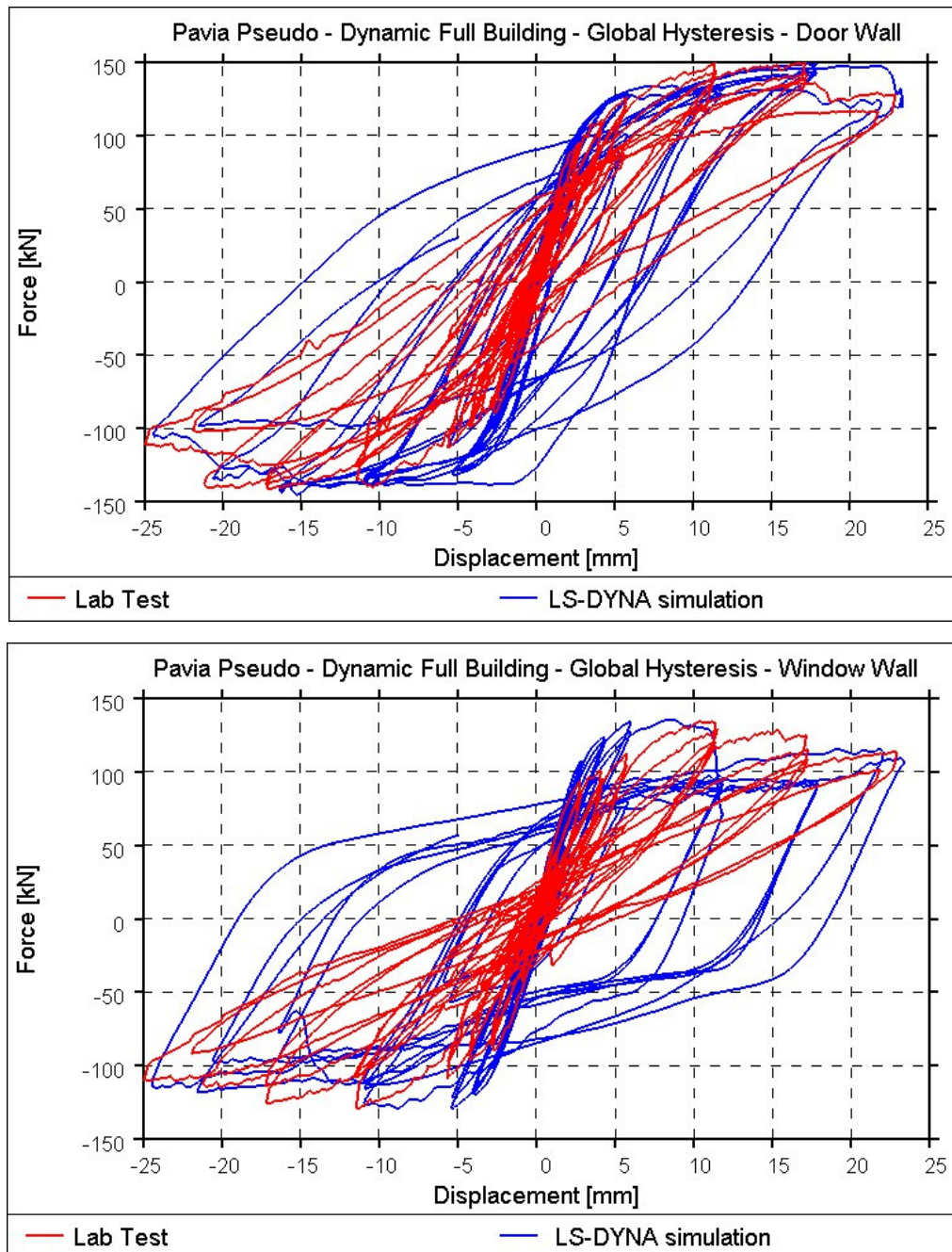
Figure 70 Pavia Pseudo-Dynamic Full Building – Shear force-displacement comparison plots

2.12.5   Conclusion
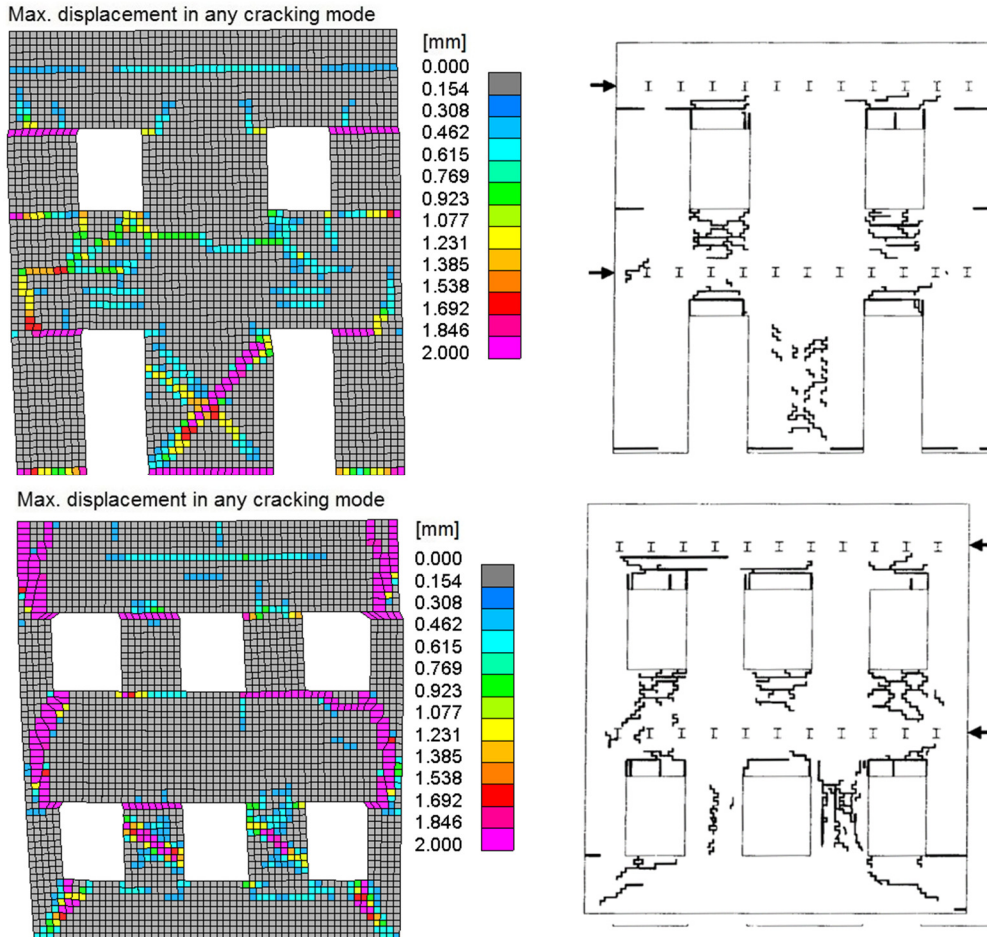
The LS-DYNA simulation exhibits damage generally in the same locations as the laboratory specimen, although there is more damage on the sides of the window wall due to the flange walls bowing out during the analysis. The global shear force versus displacement relationships for the Door Wall and Window Wall are fairly well predicted by the model, although the window wall exhibits more shear damage (and more energy dissipation) than was observed during the test.

The test was not taken to collapse, and it is not clear how much further deformation of the test specimen, or the LS-DYNA model, would be required to cause collapse.

2.13 Dynamic Full Scale Building – Eucentre Full Scale Building Shake Table Test

2.13.1 Test Description

EUC BUILD 1 was a full scale building shake table test administered in the Eucentre laboratory at the University of Pavia, Italy. The purpose of this test was to investigate the seismic behaviour of a terraced house that embodies typical modern Dutch residential construction. The building comprised two-story masonry cavity walls with reinforced concrete floor slabs and a timber roof. The inner leaf of the cavity wall was constructed of calcium silicate units 102 mm thick. The outer leaf of the cavity wall, which was located along the East, North, and West walls only, was constructed of clay units 100 mm thick. Wall ties were provided across the 80mm cavity. The building was 5.82 m long in the north-south direction, 5.46 m in the east-west direction and 7.76 m high. The base of the building was fixed to shake table [3].
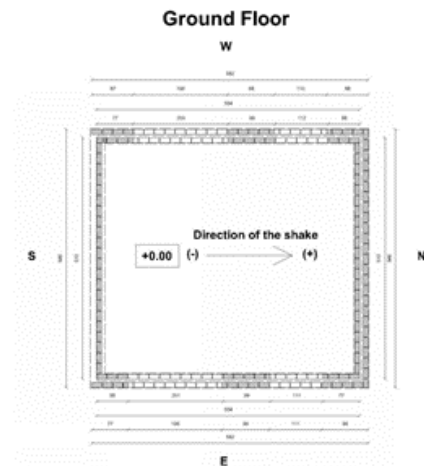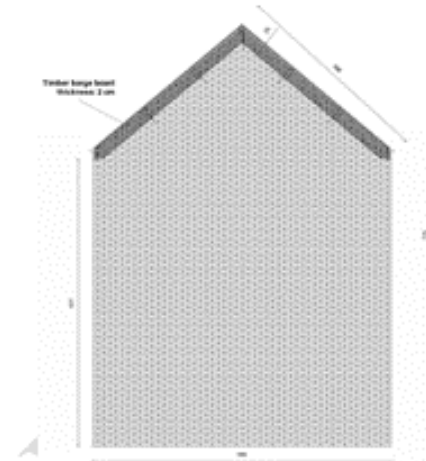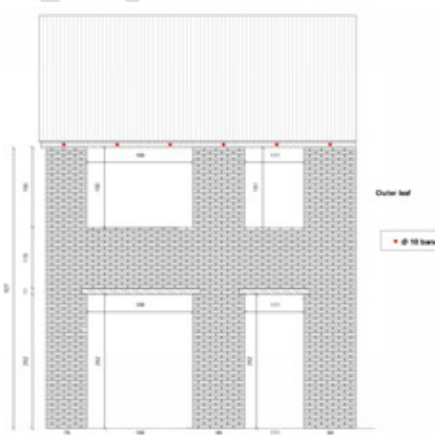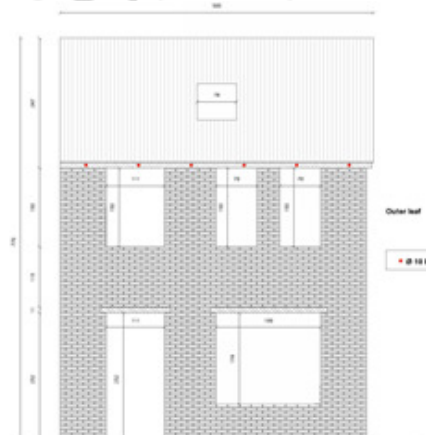
Figure 71 Eucentre Full Scale Building – Diagram of test set up
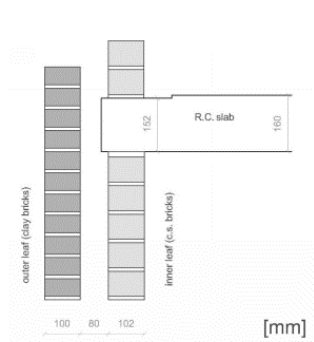
Figure 276. Detail of the connection between the r.c. slab of the first an and the inner leaf (c.s. walls) - South side.
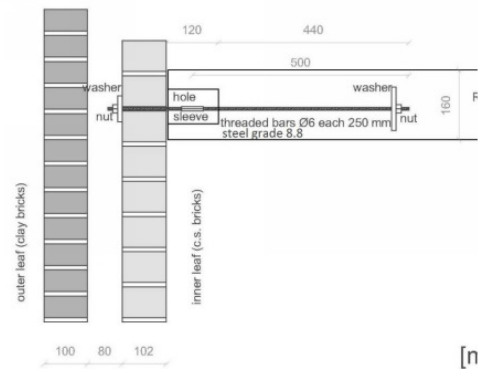
Figure 277. Detail of the connection between the r.c. slab of the first inner leaf (c.s. walls) - East and West side.
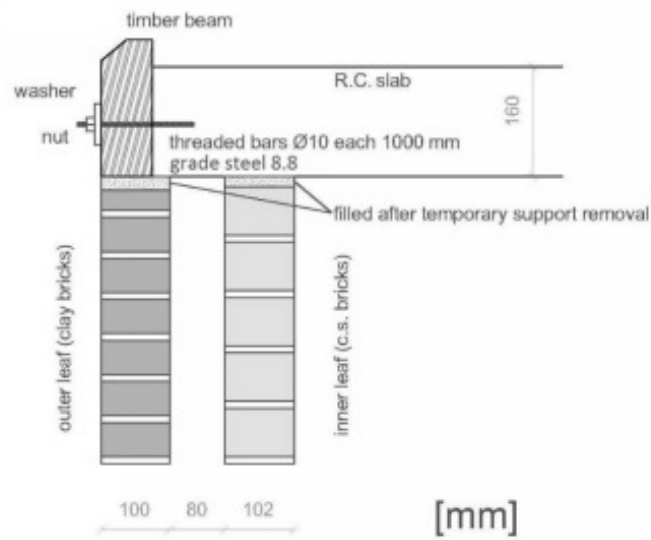
Figure 280. Detail of the connection between the r.c. slab of the second fl inner leaf (c.s. walls) - East and West side.

Figure 72 Eucentre Full Scale Building –Connection details

Uni-directional ground motion signals were applied in the longitudinal direction of the building only. Two sets of signals were applied at various scaling levels in an extended sequence shown in Figure 65 below.
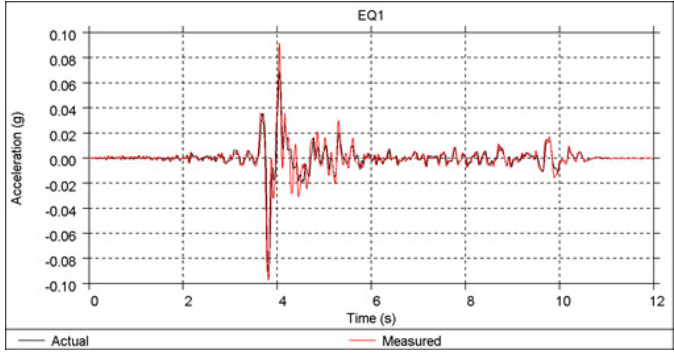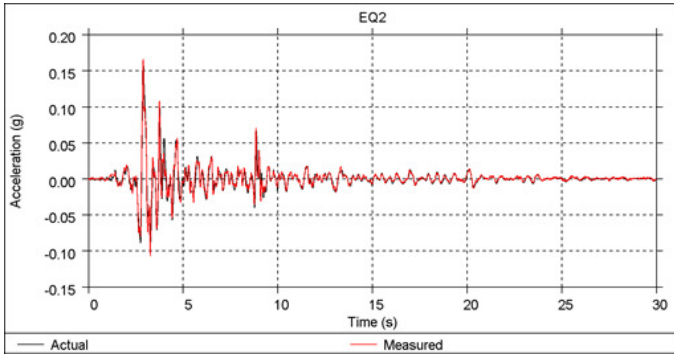
Earthquake	Graph	Protocol
EQ1		EQ1 @ 50%
		EQ1 @ 100%
		EQ1 @ 150%
EQ2		EQ2 @ 100%
		EQ2 @ 150%
		EQ2 @ 200%

Figure 73 Eucentre Full Scale Building: Loading protocol

Table 14 Eucentre Full Scale Building Material Properties

Calcium Silicate Masonry	
Mass density	1835 kg/m^3
Masonry Young's modulus perpendicular to bed joints	2132 MPa
Masonry compressive strength perpendicular to bed joints	5.49 MPa
Tensile strength (flexural bond strength) of mortar joints	0.056 MPa
Initial shear strength of mortar joints	0.035 MPa
Coefficient of friction for sliding of joints	0.5
Clay Masonry	
Mass density	1905 kg/m^3
Masonry Young's modulus perpendicular to bed joints	3926 MPa
Masonry compressive strength perpendicular to bed joints	12.72 MPa
Tensile strength (flexural bond strength) of mortar joints	0.152 MPa
Initial shear strength of mortar joints	0.15 MPa
Coefficient of friction for sliding of joints	0.7

2.13.2   Test Results

The following figures describe the damage state after application of the final motion (EQ2 scaled to 200%).
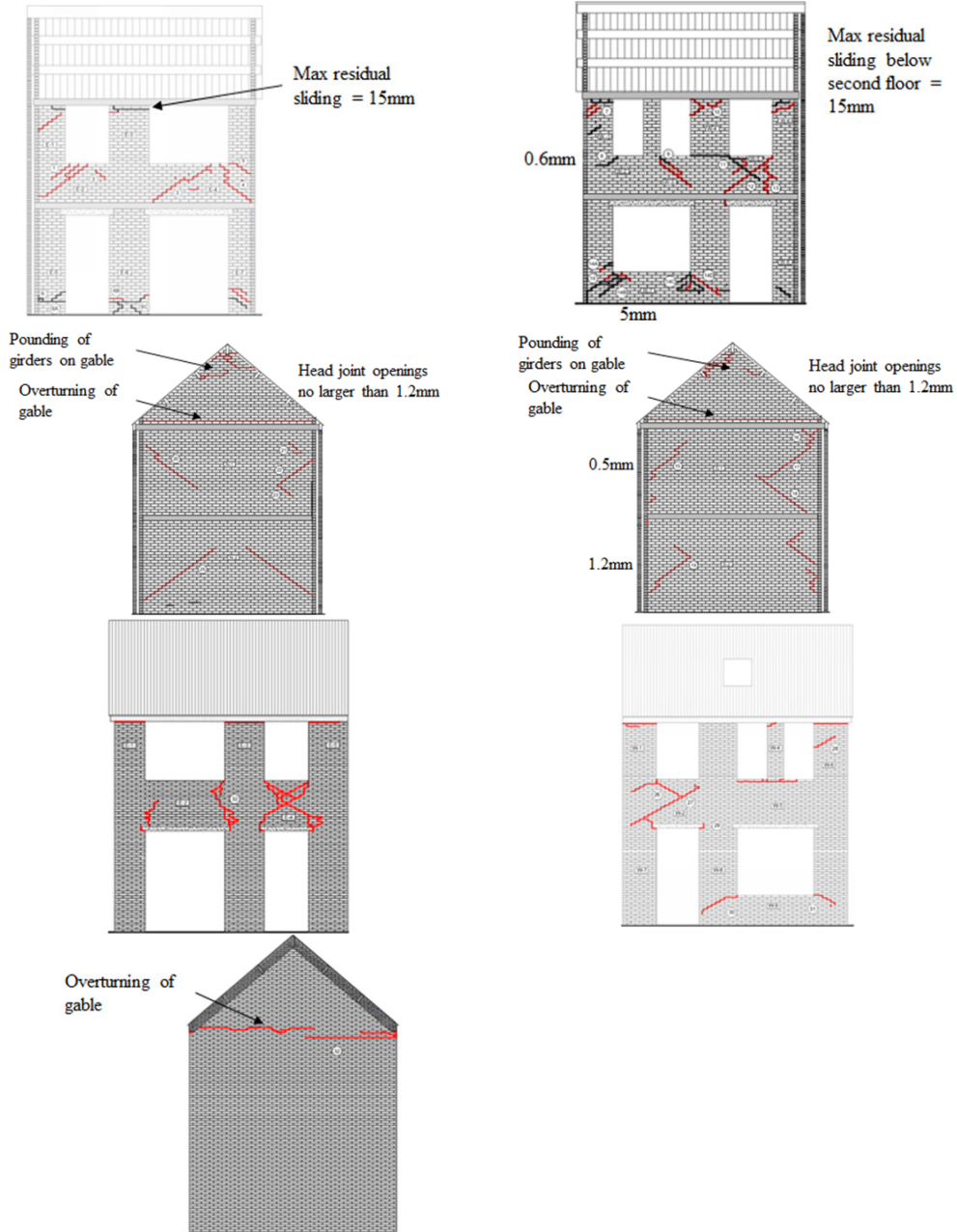
Figure 74 Eucentre Full Scale Building: Observed crack patterns at the end of the final run. From left to right, top to bottom: inner leaf – east side, inner leaf – west side, inner leaf – north side, inner leaf – south side, outer leaf - east side, outer leaf - west side and outer leaf – north side

The following figures illustrate the measured hysteresis of base shear vs displacement of roof.
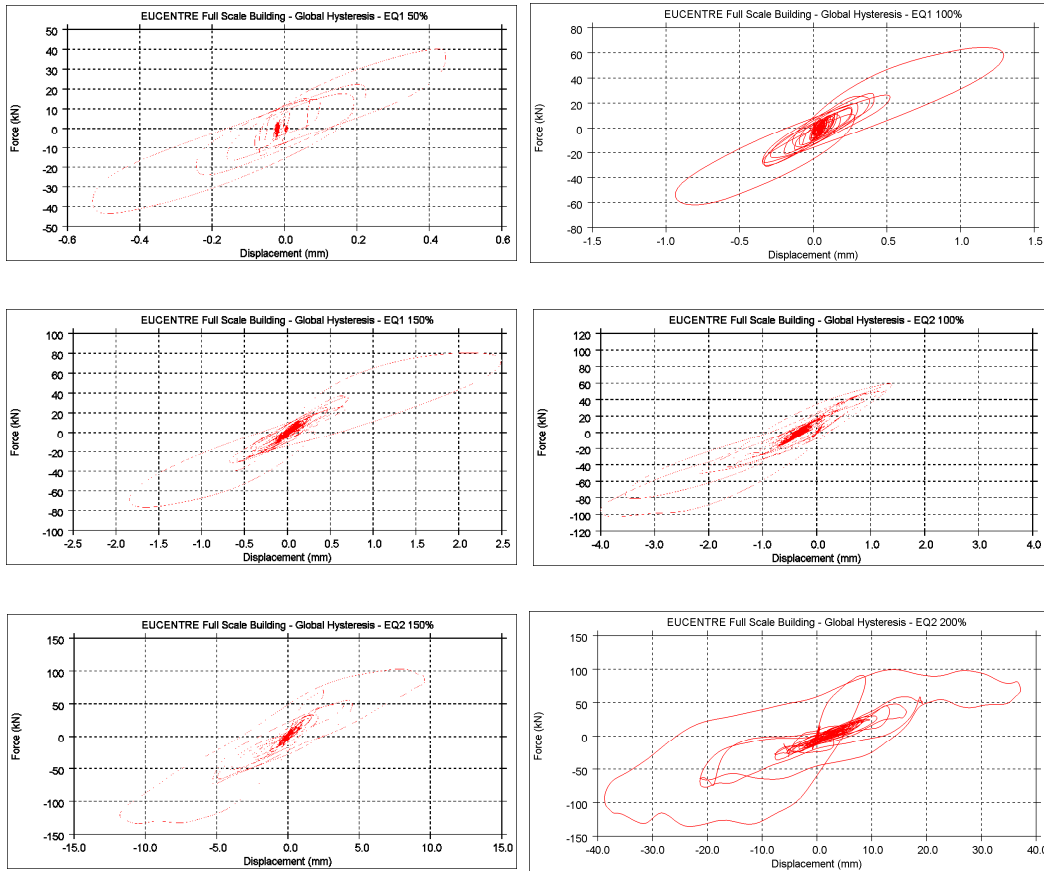
Figure 75 Eucentre Full Scale Building: shear force-displacement plot after each run. Note that the scales vary.

At the end of the test the building had suffered moderate damage, but did not appear to be at a near collapse state.

2.13.3   LS-DYNA: Model Description
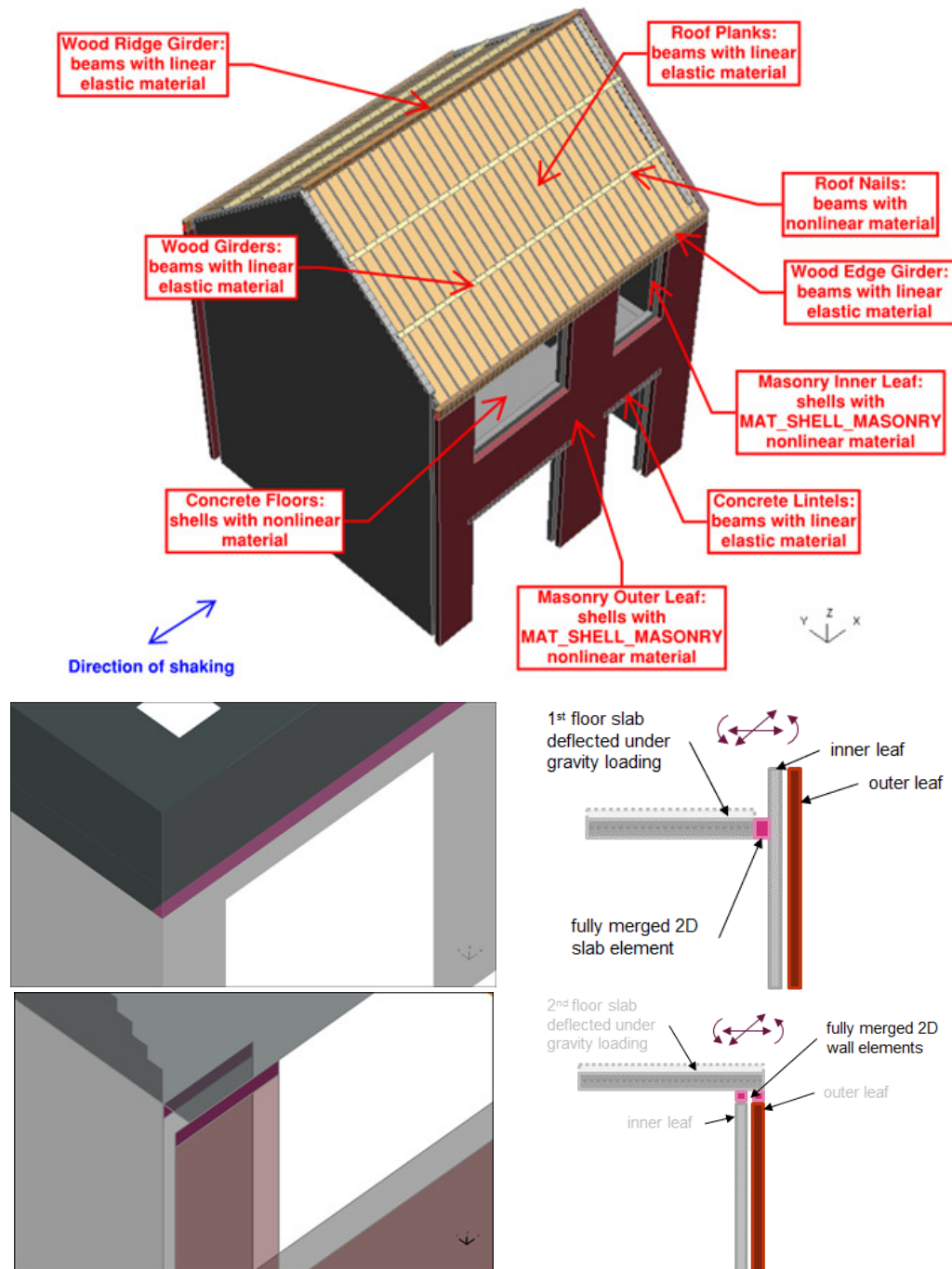
Figure 76 LS-DYNA shell model description

In the simulation the building is modelled in two stages. During the first stage all elements are erected except for the connections to the two façades parallel to the direction of ground shaking. In this way the two façades resisting the in plane ground motion are supporting only their self-weight whereas the slabs and the roof are supported by the out-of-plane walls and gables.

2.13.4 LS-DYNA: Results & Validation

The results presented below were obtained using the 25-May-2016 version of the MAT_SHELL_MASONRY.
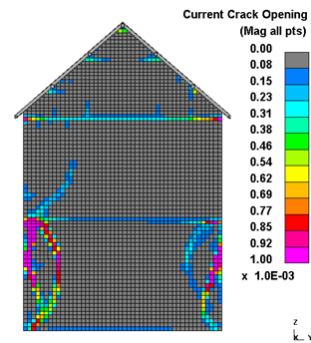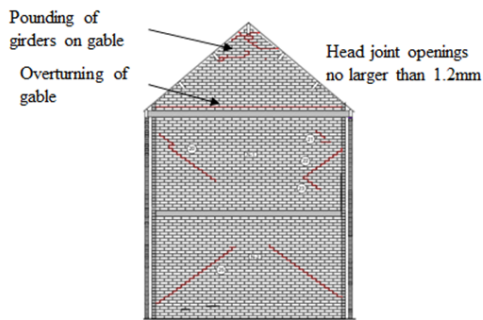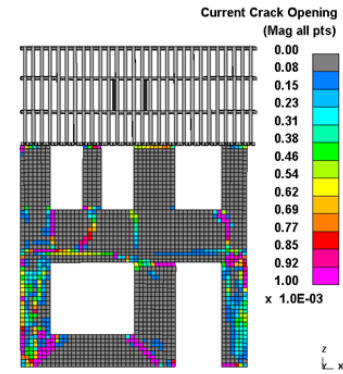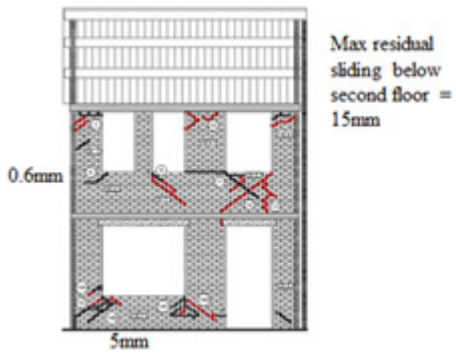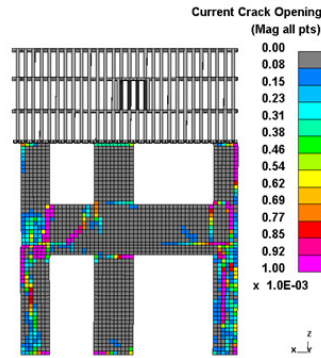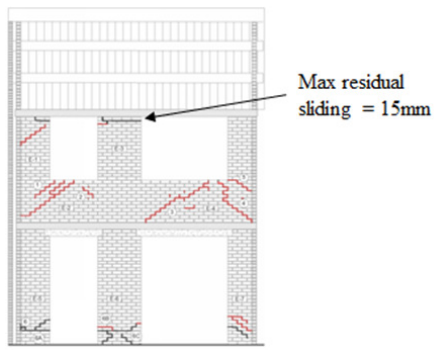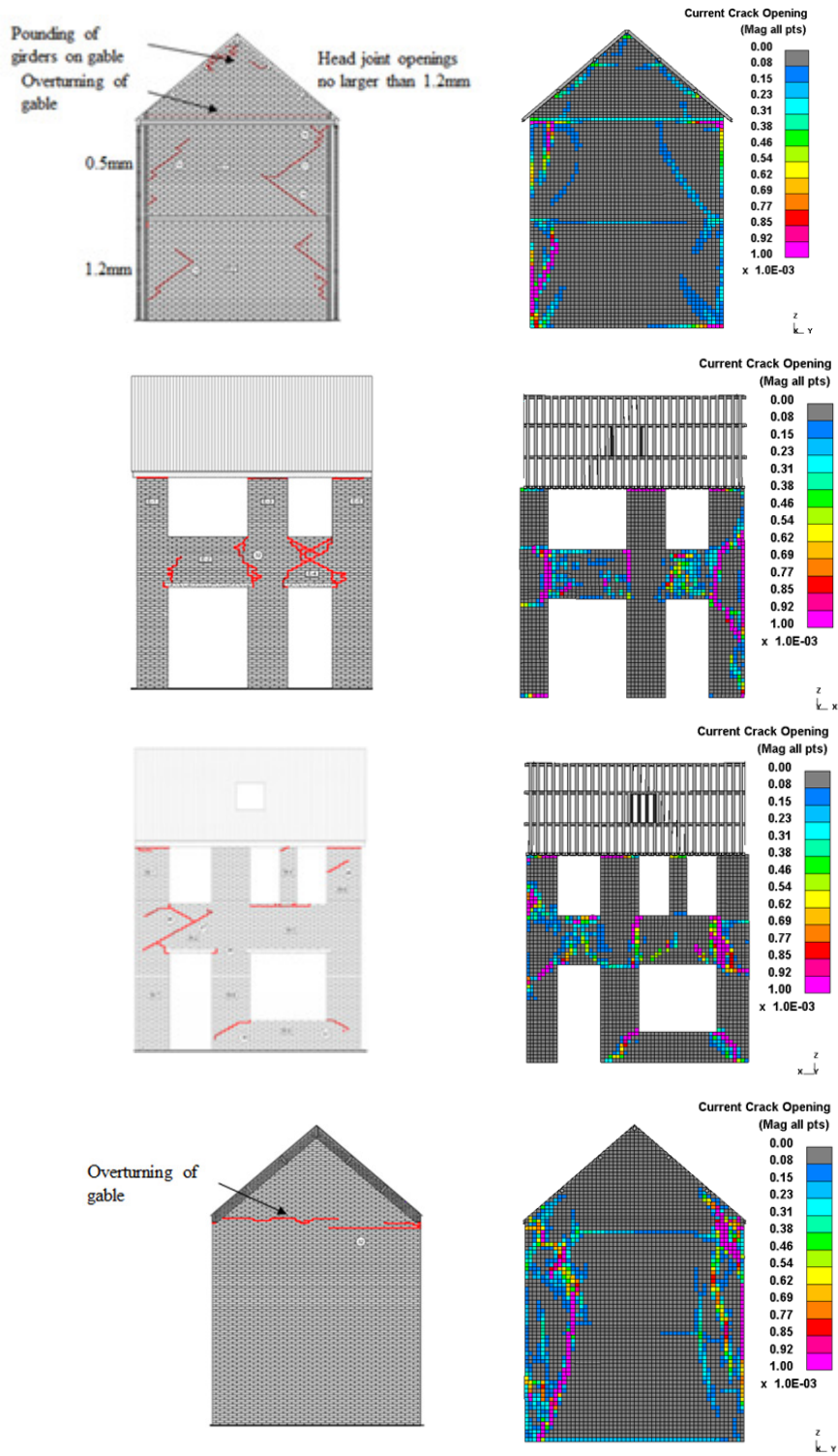
Figure 77 EUC-COMP-2 – Final crack pattern—comparison between laboratory test
(left) and LS-DYNA shell element model (right)

The observed and predicted hysteresis of base shear vs roof displacement are compared below.
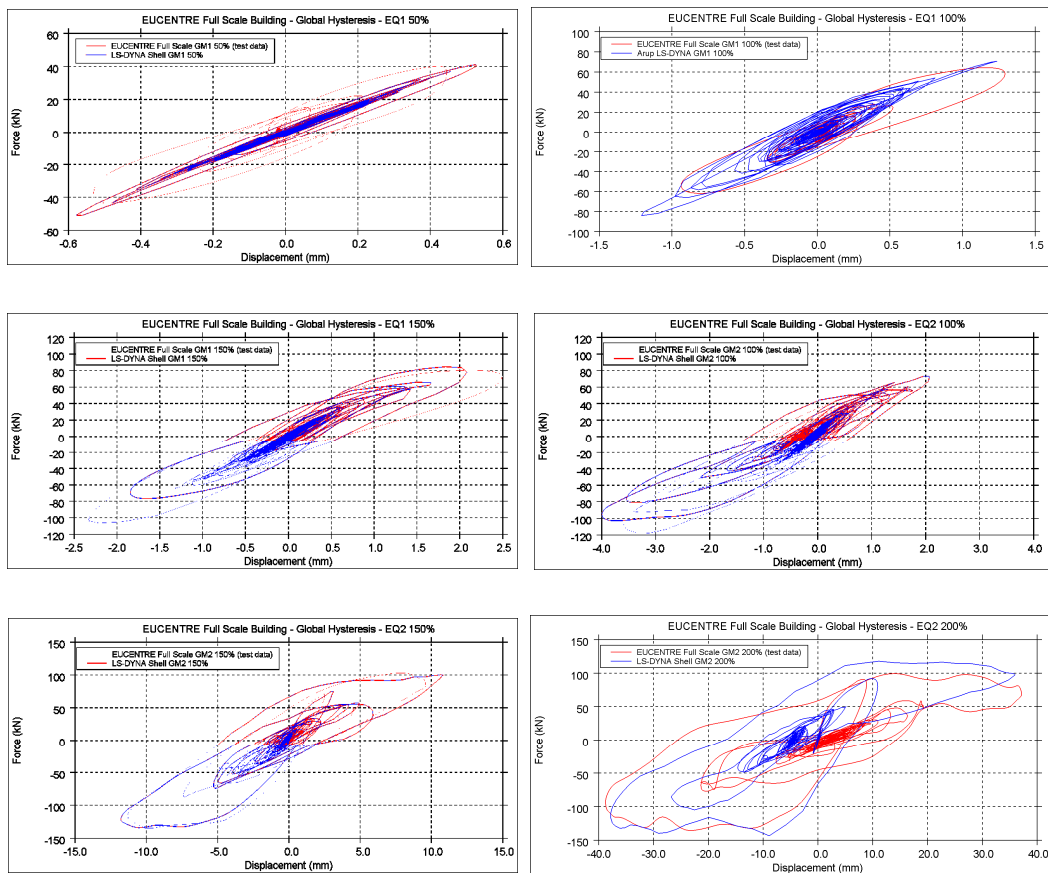
Figure 78: Full Scale Building – Shear force-displacement comparison plots for the six ground motions. Note: different scales are used on each of the six graphs to suit the responses to the six ground motions.

2.13.5   Conclusion

The LS-DYNA model of the full scale shake table building offers a generally realistic simulation of the behaviour observed in the laboratory.

The hysteresis loops shows that the model predicts well the building stiffness, strength and energy dissipation.

The deformation patterns predicted by the LS-DYNA model compare reasonably well to those observed in the lab test. The observed diagonal crack patterns extending from the corners of the openings and the damage to the spandrels are well captured in the LS- DYNA simulation. However the crack patterns in the out-of-plane walls are less realistic, showing more vertical cracking than was observed in the laboratory.

The building test was not taken to collapse, and therefore the accuracy of collapse prediction by LS-DYNA could not be assessed.

2.14   References

[1]   Anthoine A., Magonette G., Magenes G., (1995) "Shear compression testing and analysis of brick masonry walls", Proc. 10th European conference on earthquake engineering, Vienna.

[2]   Magenes G., Calvi G.M., (1997) "In-plane seismic response of brick masonry walls", Earthquake Engineering & Structural Dynamics, 26, 1091-1112.

[3]   Eucentre, "Experimental campaign on cavity walls systems representative of the Groningen building stock", November 2015

[4]   Lozincă, E., Popa, V., Coțofană, D. & Cheșcă, A. . B., 2015. *Unidirectional cyclic behavior of old masonry walls in Romania,* Bucharest: (unpublished, direct contact).

[5]   TU-Delft, "Preliminary test reports for in-plane tests on masonry walls at TU-Delft", October 2015

[6]   TU-Delft, "Tests for the characterisation of replicated masonry", October 2015

[7]   Doherty K, (2000) "An investigation of the weak links in the seismic load path of unreinforced masonry buildings", University of Adelaide, Australia

[8]   TU-Delft, "Preliminary test reports for out-of-plane tests on masonry walls at TU-Delft", January 2016

[9]   Magenes G., Calvi G.M., Kingsley G.R., (1995) "Seismic Testing of a Full-Scale, Two-Story Masonry Building: Test Procedure and Measured Experimental Response", University of Pavia, Italy.

[10]   Francesco Messali, Rita Esposito, Matteo Maragna (2015), "Pull-Out Strength Of Wall Ties". Delft University of Technology

3 Reinforced Concrete Modelled with *MAT_CONCRETE_EC2 and *MAT_HYSTERETIC_REINFORCEMENT

This section describes validations of the predicted performance of reinforced concrete structures composed of walls and slabs modelled using the MAT_CONCRETE_EC2 and MAT_HYSTERETIC_REINFORCEMENT features in LS-DYNA.

3.1 One Way Spanning Concrete Slab

3.1.1 Theoretical Test Description

A one way spanning fixed ended slab of 4.5m length, 2m width and 0.145m thickness is modelled. The assumed reinforcement is shown in Figure 79.
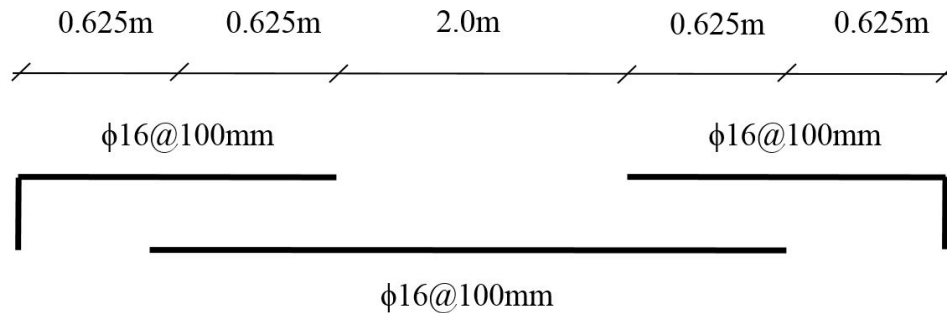
Figure 79 One way spanning slab - reinforcement distribution

The slab is built-in at both ends and is subjected to a linearly increasing uniform pressure up to when its ultimate capacity is reached.

The material properties in Table 15 are used in the simulation with *MAT_CONCRETE_EC2.

Table 15 Assumed concrete and reinforcement material properties in the simulation.

Concrete mass density	2400 kg/m^3
Concrete compressive strength	20.0 MPa
Concrete tensile strength	2 MPa
Reinforcement Young modulus	200 GPa
Reinforcement ultimate strength	235 MPa

3.1.2   LS-DYNA: Model Description
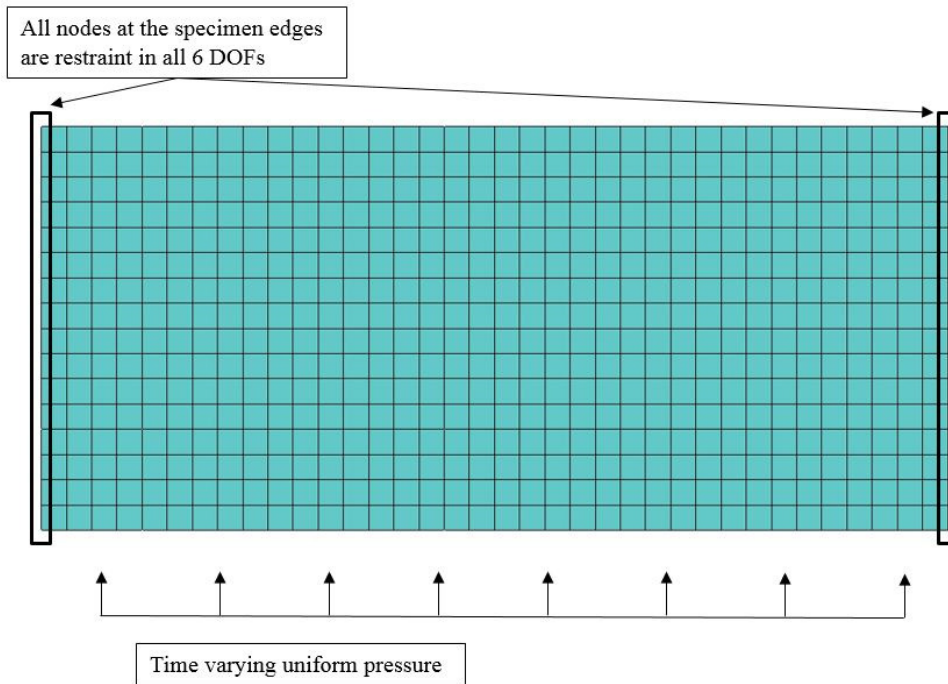
Figure 80 One way spanning concrete slab.

The elements are square with 0.125m side length. Fully integrated element formulation is used and different material properties are assigned to the various layers through thickness in order to match the concrete and reinforcement distribution. All degrees of freedom are fixed at the two short slab edges.

The model is subjected to a spatially-uniform pressure increasing monotonically with time, applied by a displacement-controlled method to prevent a sudden failure after the slab capacity is reached. The loading leads to the formation of two plastic hinges at the short edges, and then the formation of a plastic hinge in the middle of the specimen to form a mechanism.

3.1.3 LS-DYNA: Results & Validation

The slab response is validated by comparing the LS-DYNA simulation with the theoretical results which can be calculated from an equivalent double clamped beam subjected to a distributed load.

The bending moment distribution of a double clamped beam with a symmetrical stiffness distribution and subjected to uniform loading is parabolic. The maximum bending moment is reached at the two supports: $\frac{pl^2}{12}$, whereas the moment at mid-span is equal to : $\frac{pl^2}{24}$.

The bending moment capacity of the section (equal for support and span moments) is computed assuming the EC2 stress block distribution of concrete (EN 1992-1-1:2004, section 3.1.7, clause (3)), and assuming the steel under tension to be yielded.

The neutral axis position at the section capacity is computed out of the translational equilibrium equation:

$$x = \frac{f_y \; x \; A_s}{0.8 \; x \; f_c \; x \; b} = \frac{235 \; x \; 10^6 x \; 0.004}{0.8 \; x \; (20 \; x \; 10^6) \; x \; 2} = 0.029 \; m$$

with:

x = neutral axis position

f_y = yielding stress of steel

A_s = steel area per meter length

f_c = concrete capacity

b = considered section width

The moment capacity is:

$$M_{resistant} = \left(f_y \; x \; A_s\right) x \; (d - 0.4x) = (235 \; x \; 10^6 \; x \; 0.004) \; x \; (0.13 - 0.4 \; x \; 0.029 \;) = 111 \; kNm$$

with

d = cross section effective height

The magnitude for the distributed load at the formation of the first plastic hinge is estimated imposing the bending moment at the supports out of equilibrium consideration to be equal to the cross section capacity:

$$\frac{p \; x \; l^2}{12} = 111 \quad => \quad P_{first \; plastic \; hinge} = 66 \, kN/m$$

After the plastic hinges at the support form, the mid-span moment can increase up to the cross sectional capacity. Figure 81 shows the deformed shape and the top rebar stresses after the formation of the first plastic hinges. The ultimate pressure

which the slab can support before the formation of a third plastic hinge can be accordingly computed:

$$\frac{p \; x \; l^2}{24} + \frac{\Delta p \; x \; l^2}{8} = 111 \quad => \quad \Delta p = \frac{22kN}{m} \quad =>$$

$$P_{ultimate} = 66 + 22 = 88kN/m$$

Figure 82 shows the stresses distribution on the bottom reinforcement and the deformed shape after a mechanism has formed with the third plastic hinge at mid-span.

Table 16: Comparison of the simulation results to the theoretical solution

	Load per meter length at formation of the 1st plastic hinge [kN/m]	Ultimate load at formation of a mechanism [kN/m]
Theoretical value	66	88
LS-DYNA simulation	66.9	87.9
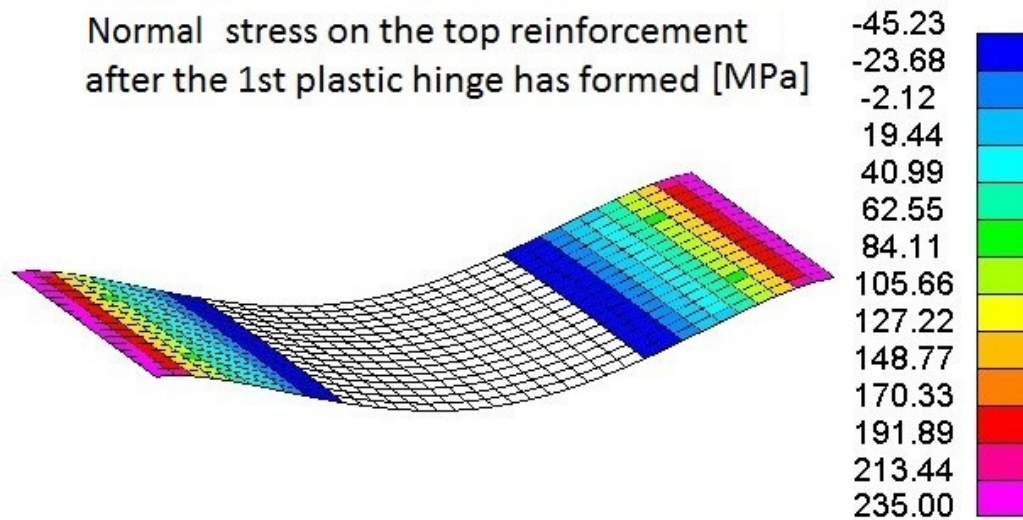
Figure 81 Deformed shape after the formation of the first two plastic hinges at the two supports. The contour describe the stress distribution on the top rebars.
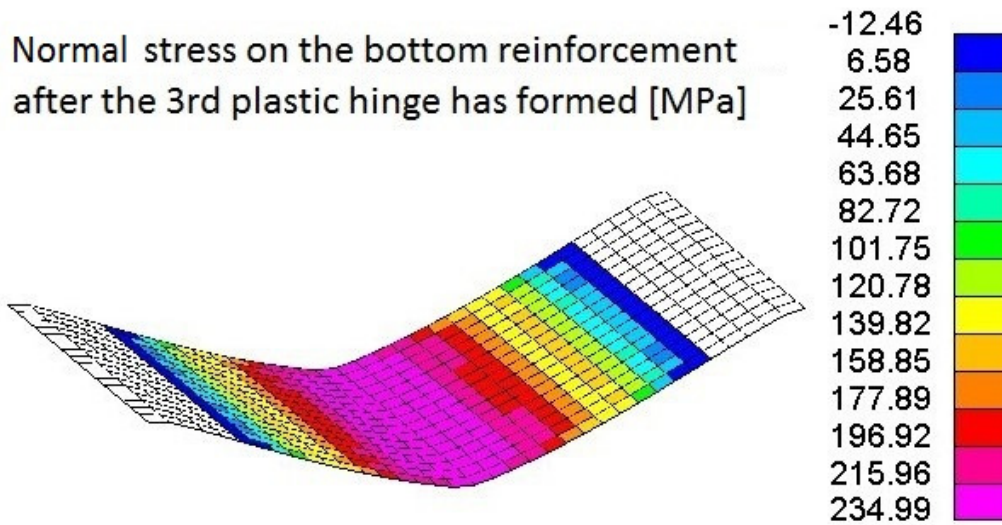
Figure 82 Deformed shape after the formation of the third plastic hinge at mid-span. The contour describe the stress distribution on the bottom rebars.

Both the ultimate load and the load at formation of the first plastic hinges are confirmed by the LS-DYNA curve for the pressure variation as shown on Figure 83.
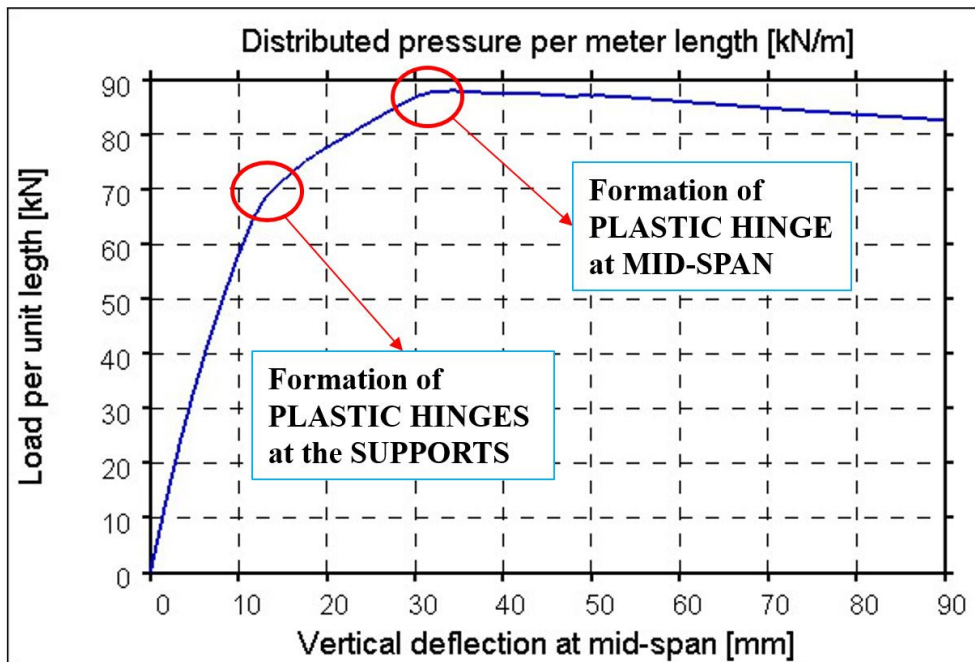
Figure 83 Pressure variation with respect to the mid-span displacement.

The vertical deflection at formation of the three plastic hinges and the cross sectional moment capacity are confirmed by the moment diagrams shown on Figure 84.
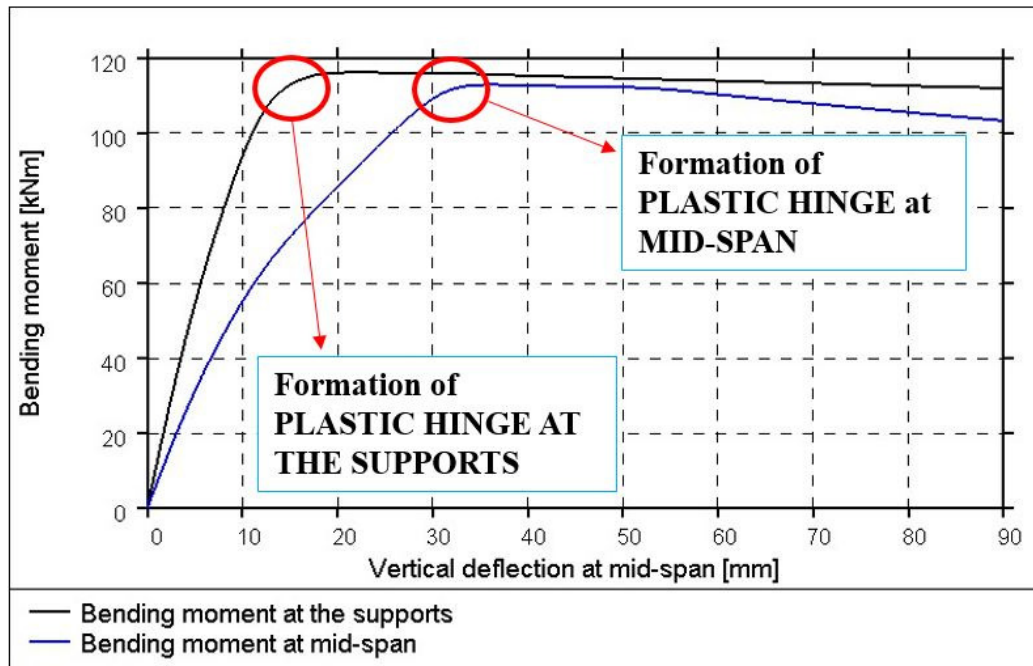
Figure 84 Bending moment at supports and pressure load variation with the increasing mid-span displacement.

3.1.4   Conclusion

The LS-DYNA simulation provides a good match to the computed theoretical value for the cross section bending moment capacity, for the load at first yielding and ultimate load.

3.2   In Plane Cyclic – Quasi Static – RW2 Test

This test validates the ability of LS-DYNA to model reinforced concrete walls subject to cyclic in-plane shear. The confined concrete within the reinforcement cage is given different properties from the cover concrete, based on equations developed by Mander (1988) and implemented in LS-DYNA's *MAT_CONCRETE_EC2. The reinforcement is modelled using *MAT_HYSTERETIC_REINFORCEMENT which includes Bauschinger effect, bar buckling, and dowel action in shear.

3.2.1   Test Description

The RW2 in plane cyclic test is part of a series of tests performed by Thomsen and Wallace (1995, 2003) in the Structural Engineering Research Laboratory (SERL) at Clarkson University. The test consists of a rectangular wall 3.66m tall, 102mm thick and with a width of 1.22m as shown in Figure 87. Details of the reinforcement arrangement are reported in Figure 87.

The specimen is embedded in a concrete block at the bottom whereas at the top a steel load transfer assembly is connected to the specimen. The steel assembly is pinned to an actuator responsible for the imposed horizontal displacement in the plane of the wall. Support is provided at the top of the specimen to prevent possible out of plane instabilities.
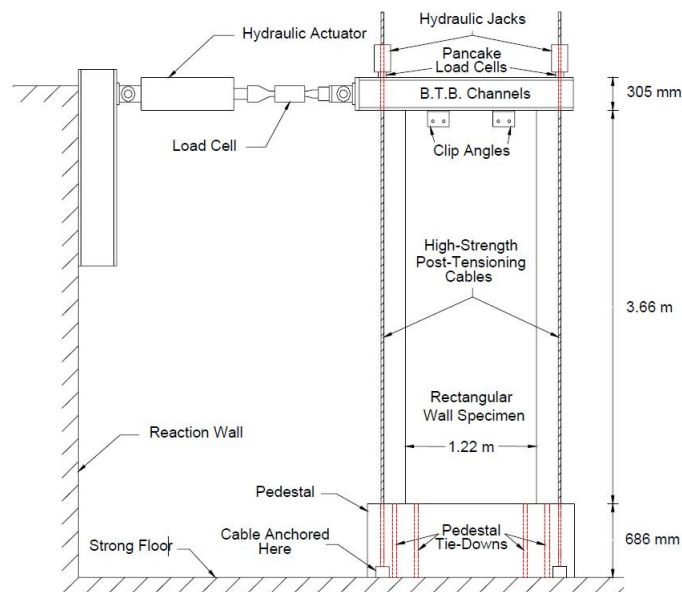
Figure 85 RW2-Schematic of test setup (Thomsen and Wallace, 1995)

A vertical overburden of 378kN is applied throughout the whole duration of the test by means of a series of post-tensioned strands. Holes on the specimen pedestal are present to enable the strands to be anchored to the lab floor. The other end of the cables is anchored to the load transfer assembly at the top of the specimen. The load transfer assembly redistributes the overburden force applied by the cables to the specimen.
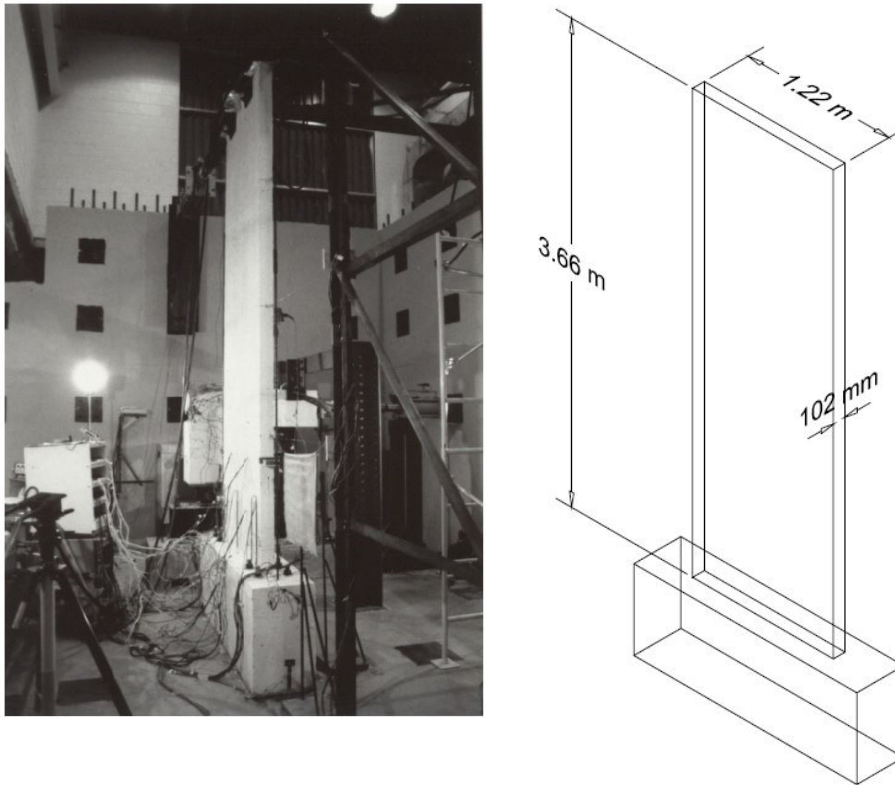
Figure 86 RW2-On the left a photograph of test setup (Kutay Orakcal, Leonardo M. Massone, and John W. Wallace 2006), on the right the dimensions of RW2 specimen.
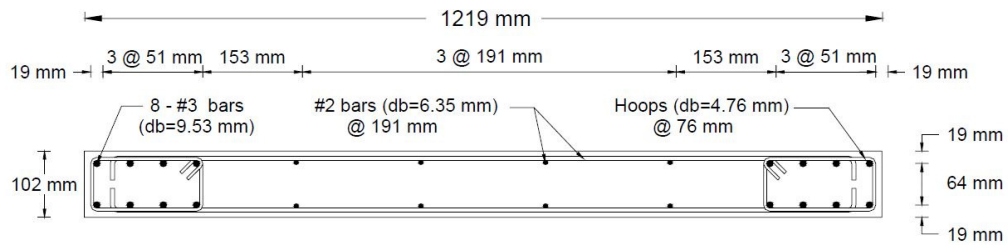
Figure 87 RW2 reinforcement arrangement.

A series of cyclic displacements is prescribed at the top of the specimen by the hydraulic actuator following the protocol in Figure 88. Both ends of the actuator are pinned in the plane of the wall but they can restrain any out of plane displacements of the wall.
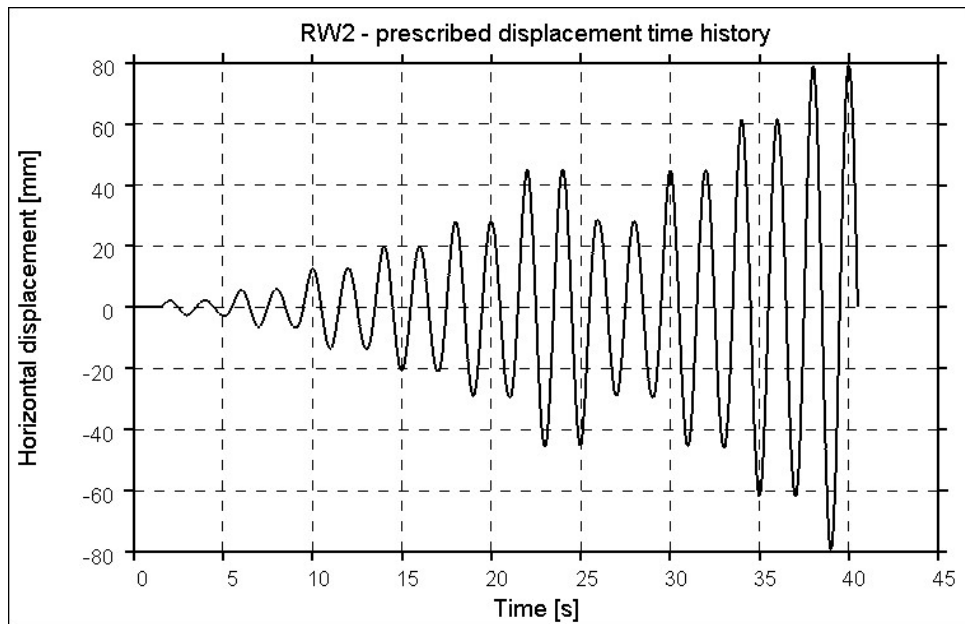
Figure 88 RW2-Measured time history of the horizontal displacement prescribed by the actuator to the top of the specimen.

The unconfined concrete properties measured through a cylindrical specimen test are reported on Table 17. Three types of grade 60 reinforcement bars are used: the type 3 bars (d_b=9.53mm) have the typical grade 60 material properties with a yield strength of 414 MPa, the type 2 bars (d_b=6.35mm) and the 4.76 mm diameter wire exhibited a yield stress of 448 MPa.

Table 17 RW2-Unconfined wall concrete properties as measured on a cylinder compression test.

Mass density	2400 kg/m^3
Young's modulus	26.8 GPa
Compressive strength	42.8 MPa
Tensile strength (assumed)	3.86 MPa
Poisson's ratio	0.2
Strain at peak compressive stress	0.002
Failure strain (assumed)	0.0035
Aggregate type	Crushed gravel
Aggregate size (assumed)	10 mm

3.2.2   Test Results

Figure 89 RW2-Crack pattern upon completion of testing (Thomsen and Wallace, 1995)
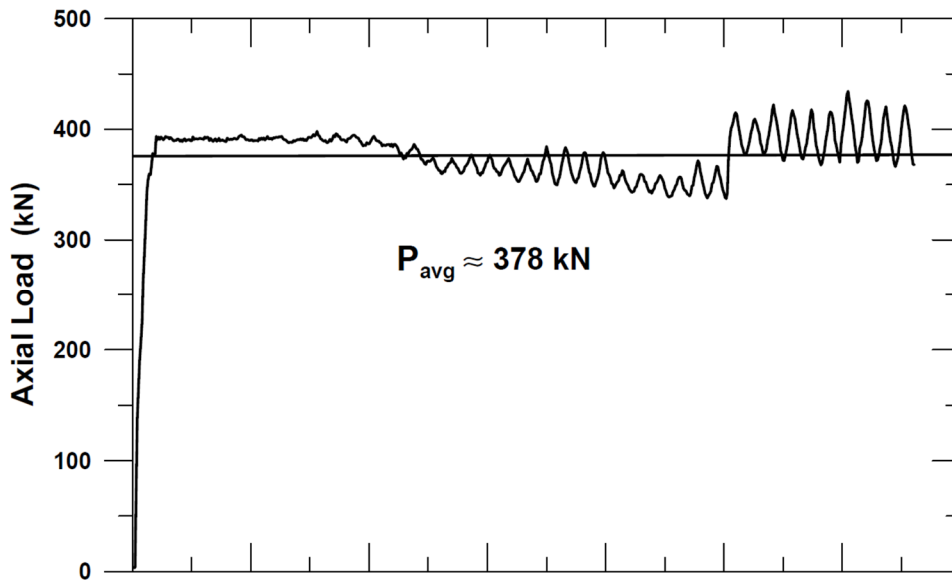
Figure 90 RW2-measured overburden time history during testing
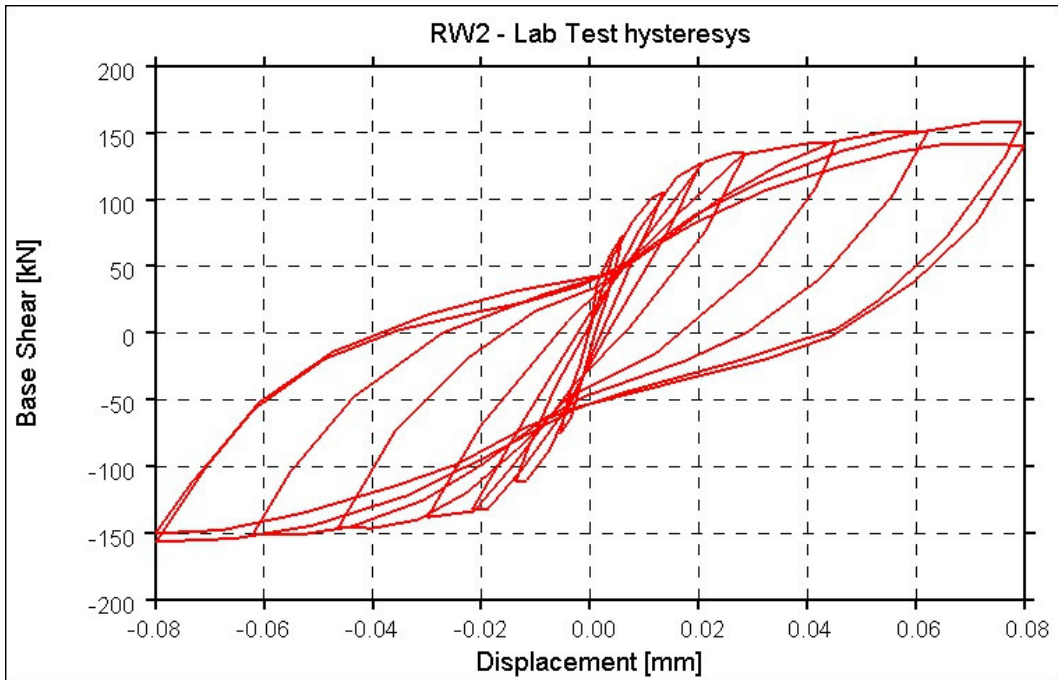
Figure 91 RW2-Hysteresis loop from lab test

3.2.3   LS-DYNA: Model Description
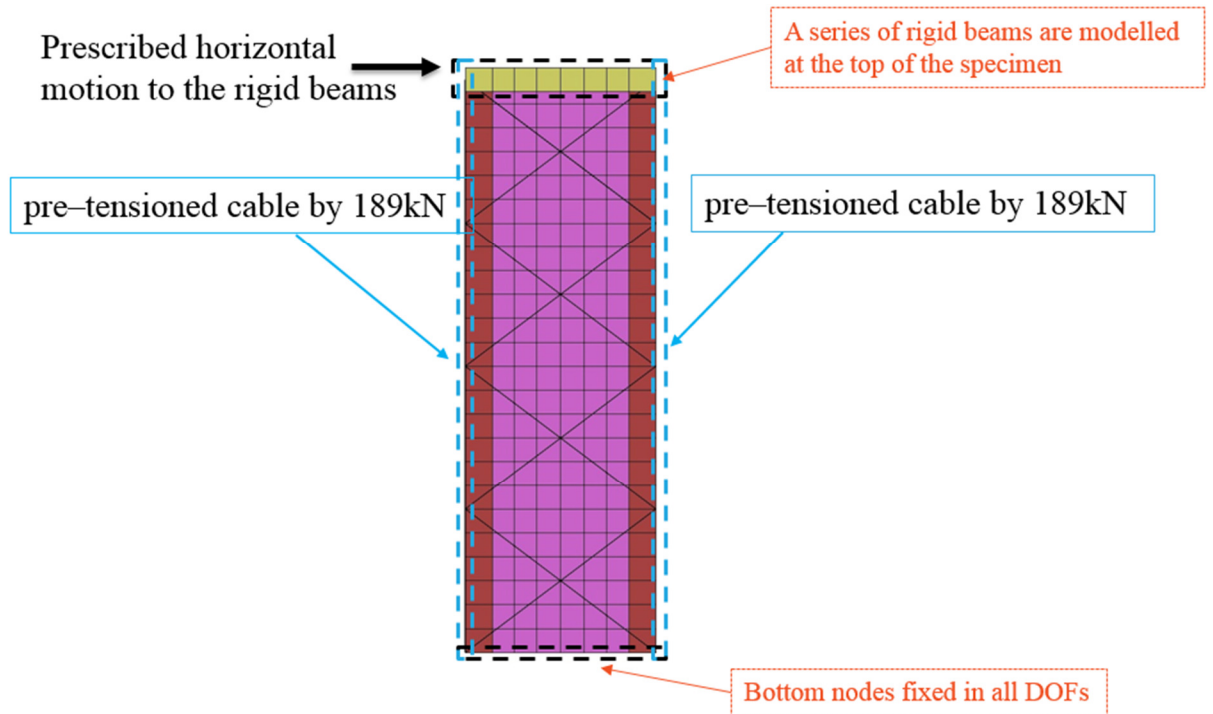
Figure 92   RW2-LS-DYNA model

Separate material properties are assigned to layers through the thickness of the model representing unconfined (cover) concrete, reinforcement, and confined concrete.

As previously described, the vertical overburden was applied by strands at the sides of the specimen. The horizontal displacement of the top anchorage of the strands led to a series of small variation of the vertical resultant applied to the wall. The measured value of the vertical overburden is shown in Figure 90.

The cable stiffness in the simulation is calibrated to approximately match the measured oscillations of the vertical overburden.

Figure 93 shows the vertical overburden out of the LS-DYNA simulation.
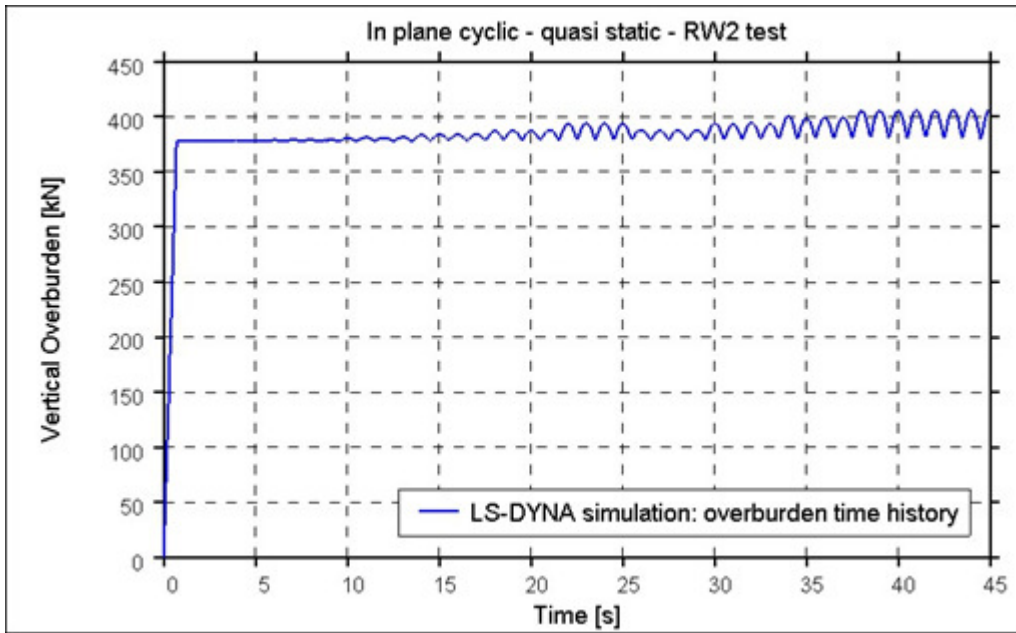
Figure 93 RW2-Simulation vertical load time history

3.2.4 LS-DYNA: Results & Validation

Results obtained using the version of LS-DYNA dated 25-May-2016 are given below.
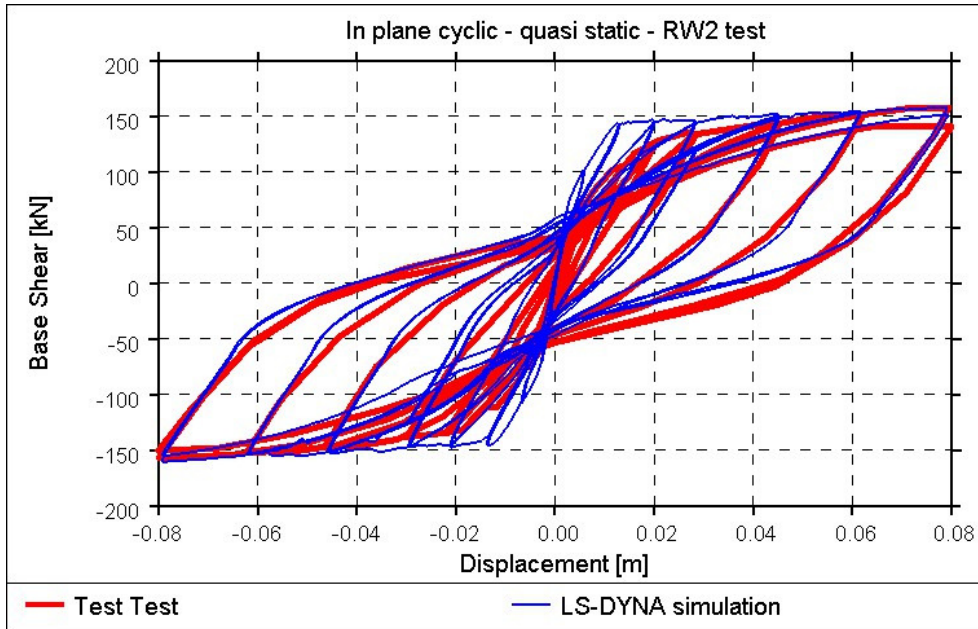
Figure 94 RW2-Hysteresis loop comparison: in red the Lab test results, in blue the LS-DYNA simulation
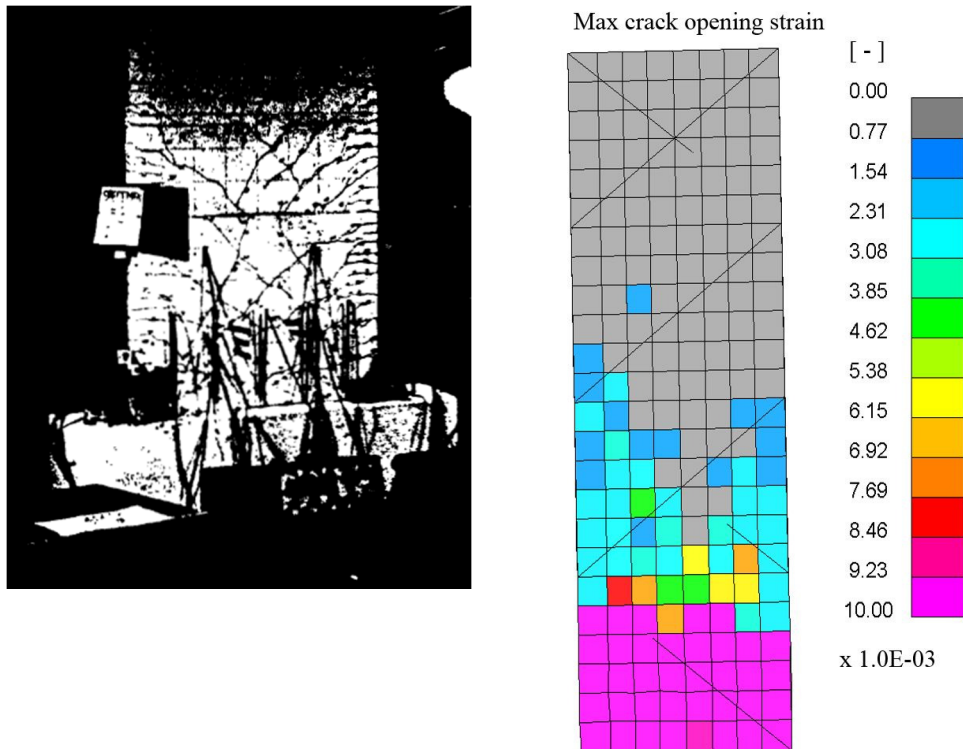
Figure 95 RW2 - Comparison of the cracks pattern and width in the lab test and LS-DYNA simulation. The photo from the lab test shows the crack pattern of the bottom quarter of the specimen. The LS-DYNA plot on the right shows the maximum crack opening strain of the specimen in its full height.

3.2.5   Conclusion

The LS-DYNA simulation provides a good match to experimental data. The hysteretic behaviour closely matches and the degree of cracking also agrees closely.

The wall was not taken to collapse in the laboratory, and therefore the accuracy of collapse prediction by LS-DYNA could not be accessed.

3.2.6 References

[1] Kutay Orakcal, Leonardo M. Massone and John W. Wallace. "Analytical Modelling of Reinforced Concrete Walls for Predicting Flexural and Coupled– Shear-Flexural Responses". PEER Report 2006/07, University of California, Berkeley, October 2006

[2] Mander, J.B., Priestley, M.J.N., Park, R. "Theoretical stress-strain model for confined concrete." J. Struct. Engin., ASCE 1998; 114(8): 1804-26

[3] John H. Thomsen, John W. Wallace. "Displacement-Based Design of reinforced Concrete Structural Walls: An Experimental Investigation of walls with rectangular and T-shaped Cross sections". Report No. CU/CEE-95-06, Clarkson University, June 1995

[4] Thomsen, J., IV and Wallace, J. (2004). "Displacement-Based Design of Slender Reinforced Concrete Structural Walls-experimental Verification." J. Struct. Eng., 10.1061/(ASCE)0733-9445(2004)130:4(618), 618-630

3.3 Dynamic Unidirectional Full Scale Building – UCSD 7-Story Shake Table Test

3.3.1 Test Description

The UCSD 7-Story Shake Table Test was performed in 2006-07 at the Large High-Performance Outdoor Shake Table at the University of California, San Diego (UCSD). The structure consisted of reinforced concrete walls and slabs, with pin-ended concrete-filled steel tubes for gravity columns. The shear wall from levels 2-6 had one layer of vertical rebar in the middle, while the level 1 and 7 shear wall had two layers of vertical rebar (one on each face) in the boundary zones.
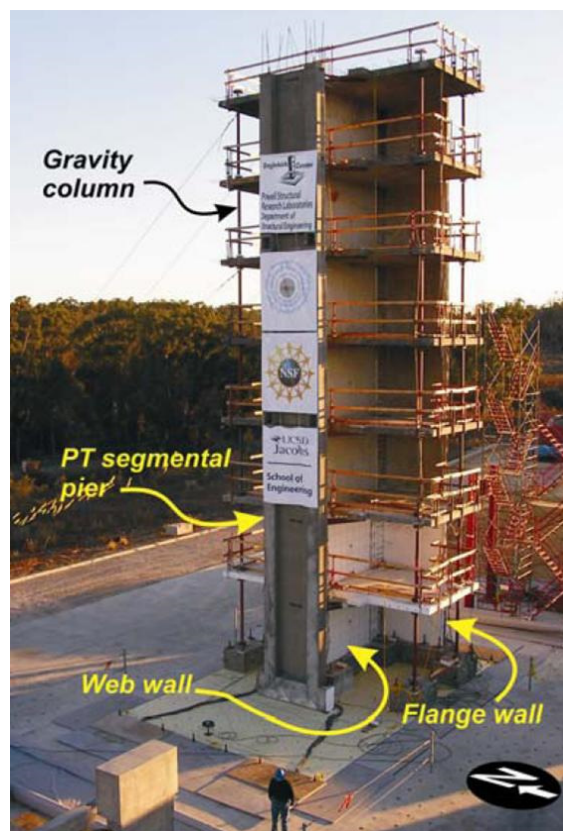
Figure 96 UCSD 7-Story Shake Table Test – Photo of test setup
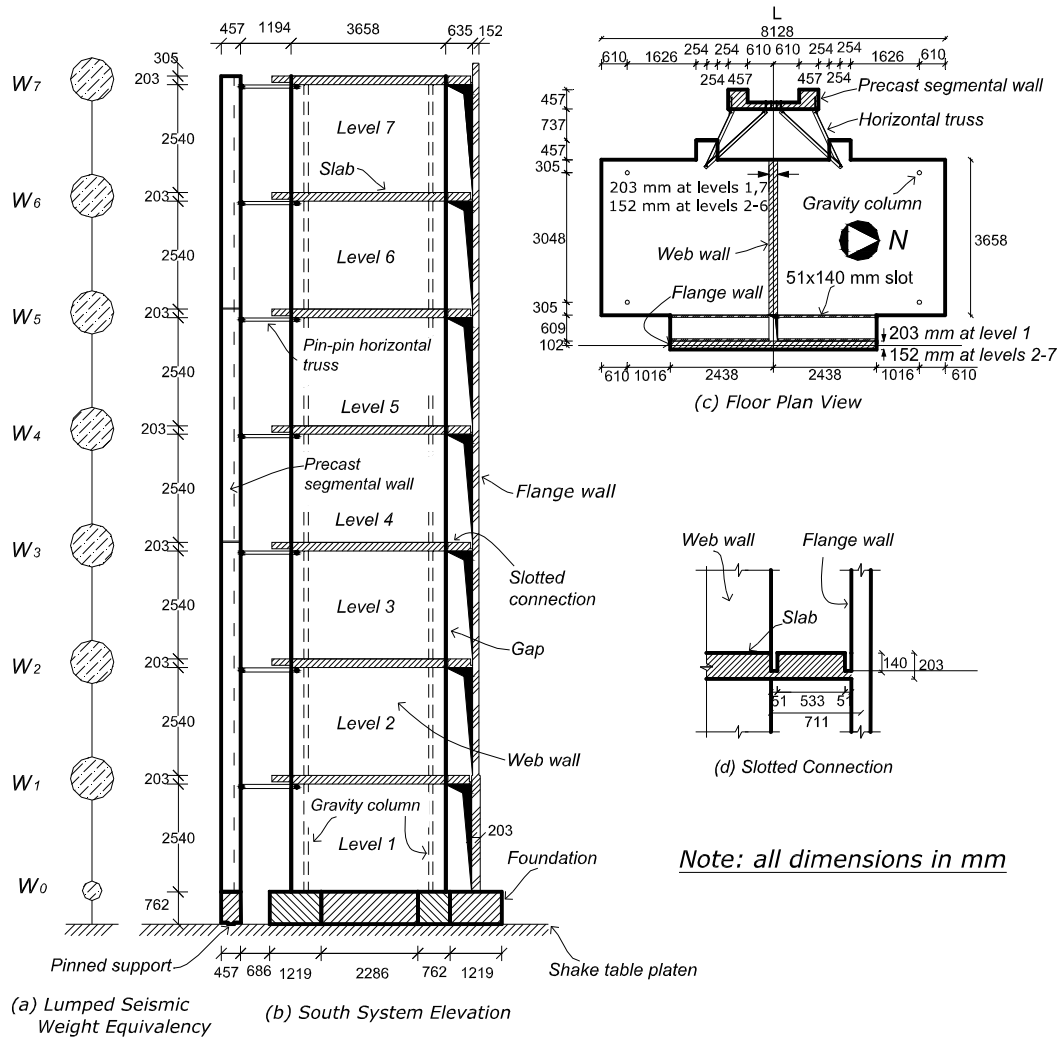
Figure 97 UCSD 7-Story Shake Table Test – Construction drawings

Uni-directional ground motion signals were applied in the east-west direction (see Figure 97(c) for compass) of the building only. The full protocol consisted of four ground motions applied as shown in Figure 98.
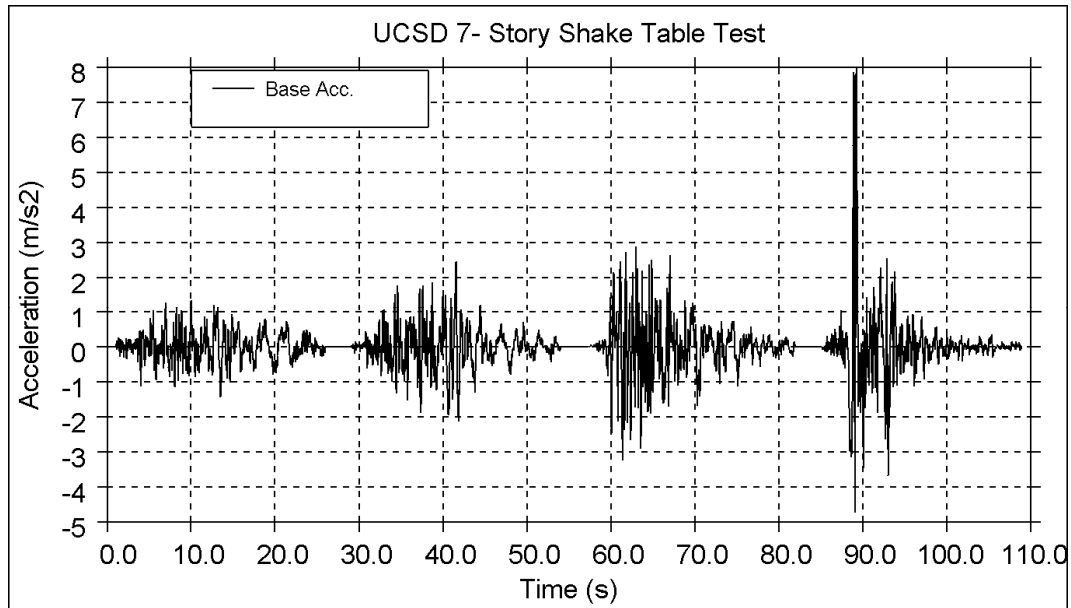
Figure 98 UCSD 7-Story Shake Table Test – Base acceleration time history

The concrete slabs were 8" thick, typically with #4 at 12" O.C. T&B E.W. The level 1 and level 7 shear walls were 8" with #5 at 4" O.C. E.F. in the boundary zones, and typically #4 at 10" O.C. in the middle of the wall elsewhere. The level 2-6 shear walls typically have #4 at 10" O.C. in the middle of the wall. See Table 18 for the unconfined concrete properties.

Table 18 UCSD 7-Story Shake Table Test – Unconfined wall concrete properties

Mass density	2170 kg/m^3
Young's modulus	27.2 GPa
Compressive strength	40.7 MPa
Tensile strength (assumed)	3 MPa
Poisson's ratio	0.2
Strain at peak compressive stress	0.0022
Failure strain (assumed)	0.0024
Aggregate type	Crushed gravel
Aggregate size (assumed)	12 mm

3.3.2   Test Results

Figure 99 UCSD 7-Story Shake Table Test – Crack pattern after full protocol – Level 1

Figure 100 UCSD 7-Story Shake Table Test – Crack pattern after full protocol – Level 2
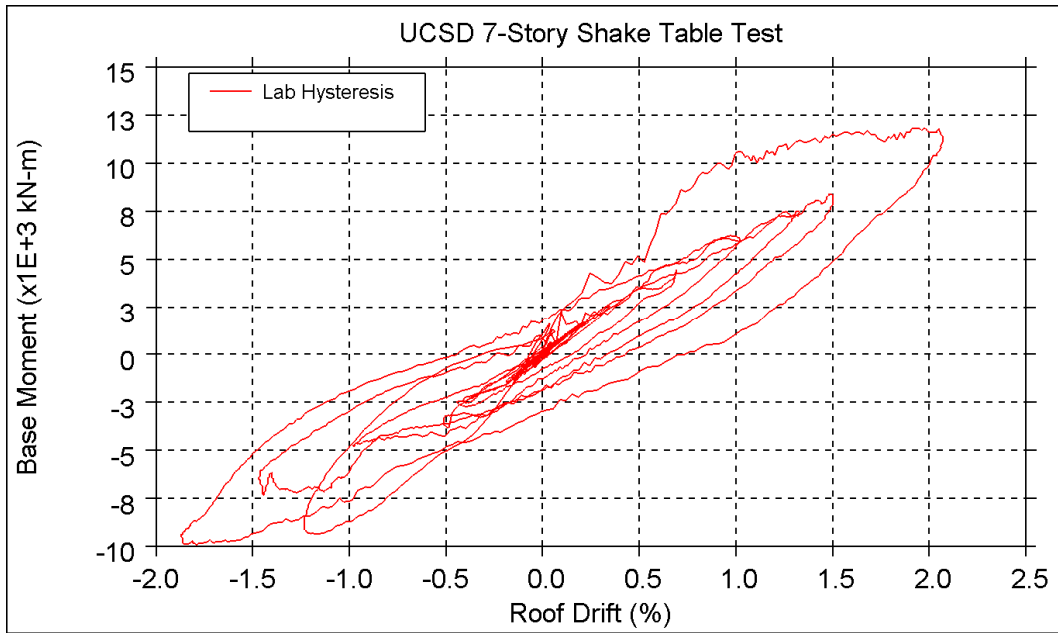
Figure 101 UCSD 7-Story Shake Table Test - Hysteresis loop from lab test for GM4 (last ground motion in full protocol)

3.3.3   LS-DYNA: Model Description
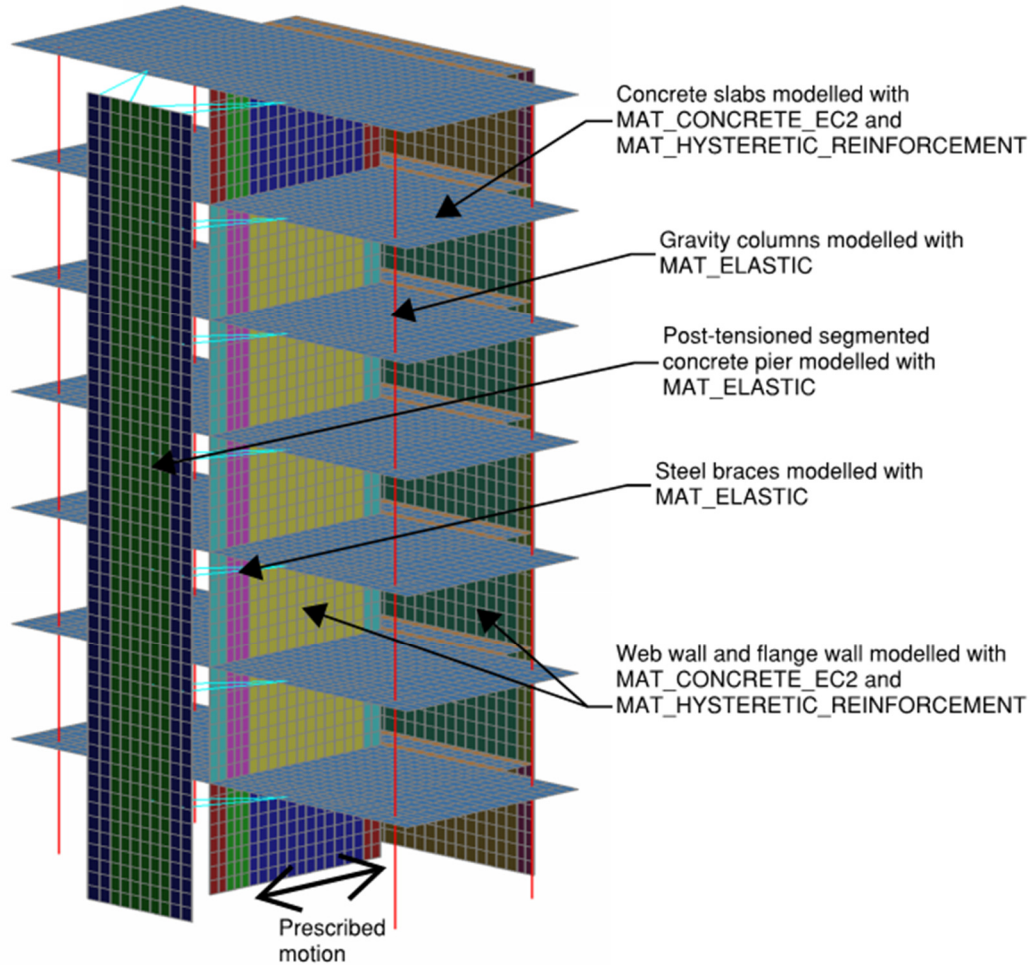
Figure 102   UCSD 7-Story Shake Table Test – LS-DYNA model

Material properties are assigned to each layer through the thickness, for unconfined (cover) concrete, reinforcement and confined concrete. The concrete is modelled by LS-DYNA's *MAT_CONCRETE_EC2 while the reinforcement uses *MAT_HYSTERETIC_REINFORCEMENT.

The LS-DYNA input parameters came directly from the lab, or from Eurocode 2 where lab data was unavailable, except for the following:

- 1% damping applied over a range of 10-50 Hz

- Tensile strength assumed to be 7.5% of compressive strength

- Fracture energy assumed to be 600 N/m

3.3.4 LS-DYNA: Results & Validation

The LS-DYNA results are compared against the laboratory test results in Figure 103 and Figure 104 below.
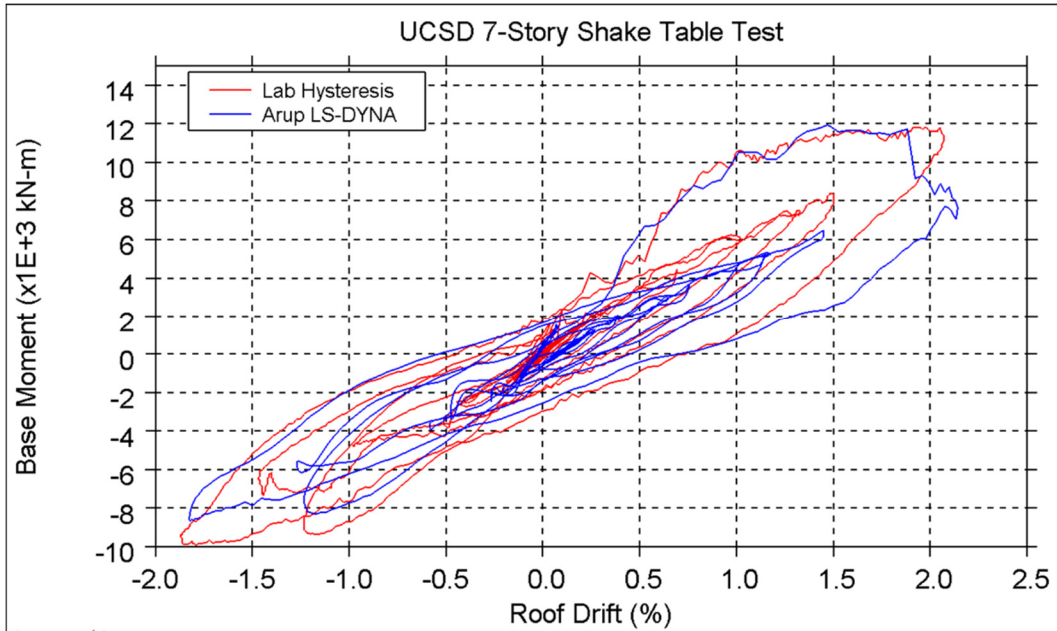
Figure 103 UCSD 7-Story Shake Table Test – Hysteresis loop comparison for GM4 (last ground motion in full protocol)

Level 2 Shear Wall

Level 1 Shear Wall

Analysis Results
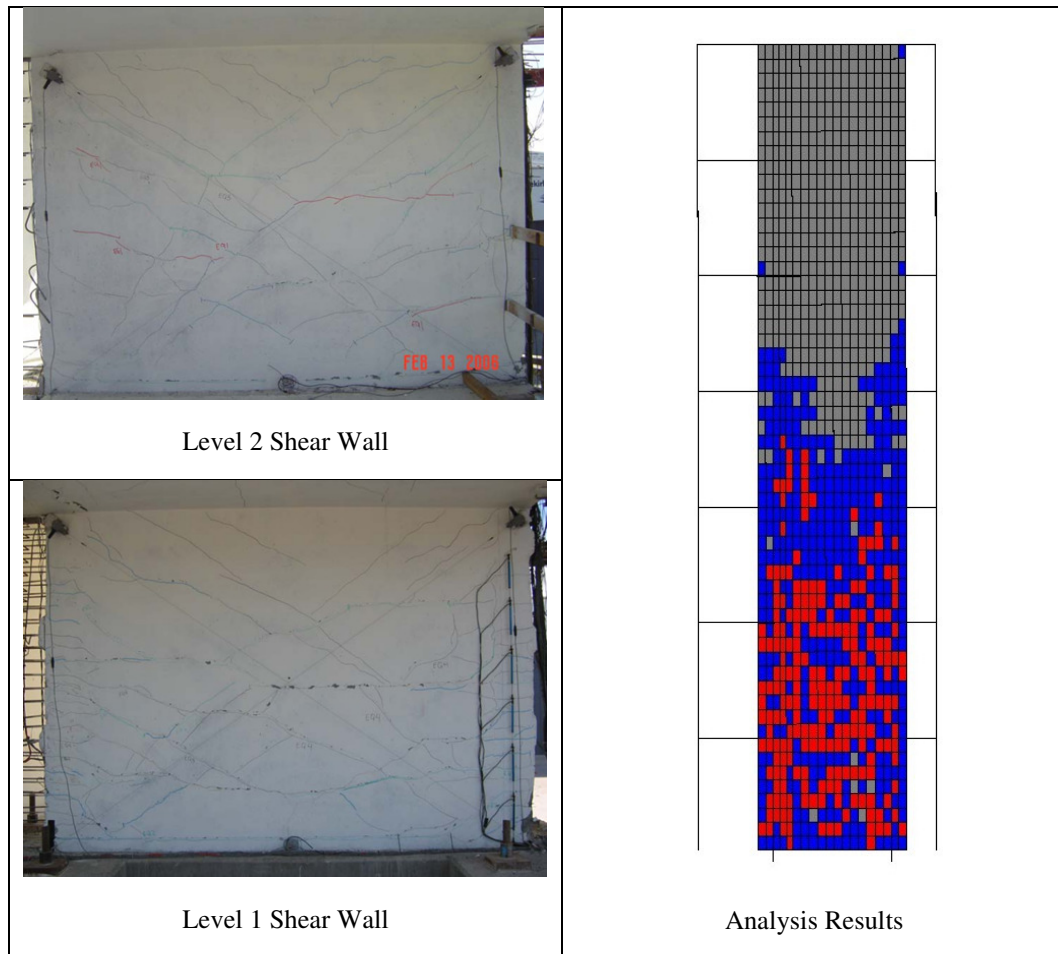
Figure 104 UCSD 7-Story Shake Table Test – Comparison of cracking in test (left) to cracking in DYNA (right). Subfigure on right shows number of cracks by element. Red denotes 2 or more cracks, while blue denotes 1 crack.

3.3.5   Conclusion

The hysteretic behaviour in the LS-DYNA simulation provides a good match to experimental data. The degree of cracking in each storey also agrees with the experimental result.

The building was not taken to collapse in the experiment, and therefore the accuracy of collapse prediction by LS-DYNA could not be accessed.

4 Modelling Foundations with MAT_HYSTERETIC_SOIL

4.1 Bearing Capacity of Shallow Footings

The purpose of this study is to demonstrate the accurate prediction of the resistance of long strip footings when the soil domain is modelled using 3D solid elements with LS-DYNA model MAT_HYSTERETIC_SOIL.

4.1.1 Test case

The reference bearing capacity and failure surfaces have been obtained using the theoretical work by Terzaghi (1943), and results obtained from PLAXIS 2D, a widely known geotechnical finite element program.

This test case comprises an infinitely long, 8m wide rigid strip footing on the surface of a uniform cohesive soil domain having undrained shear strength of 30kPa. Three loading conditions have been examined, as follows:

(i)   a vertical load at the centroid of the footing,

(ii)   an inclined load with varying angles

(iii)   a vertical load with eccentricity of 2m.

These cases were chosen to investigate loading conditions for which theoretical solutions are available and which might arise in practice.

4.1.2 Theoretical solutions

4.1.3 Terzaghi (1943) Bearing Capacity Equation

The bearing capacity of the 8m wide rigid strip footing has been derived using the bearing capacity equation by Terzaghi (1943). This equation including factors to account for load inclination. For cohesive soils under undrained conditions, the original Terzaghi (1943) equation reduces down to equation (1). It is noted that the original bearing capacity equation was derived based on laboratory and field studies, and assuming plane strain conditions. The load inclination factor was based on the relevant recommendations by DnV (1992), a recognized offshore foundation standard.

$$q_c = cN_c i_i + q \qquad (1)$$

where: q_c = ultimate bearing capacity, s_u = undrained shear strength, N_c = bearing capacity factor = 5.14 (Prandtl, 1921), i_i = load inclination factor and q = effective stress at the bottom of the foundation.

Figure 105 shows the proposed failure mechanism by Terzaghi (1943). This mechanism was developed based on earlier recommendations by Prandtl (1921)

shown in Figure 106. For pairs of vertical and horizontal allowable loads in the form of yield envelopes for all loading scenarios refer to Section 4.1.8.
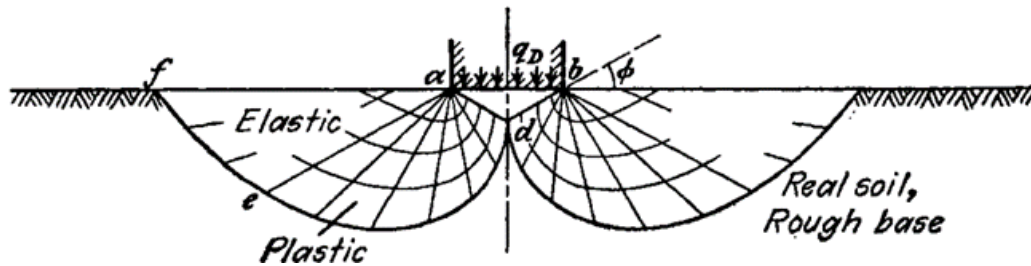
Figure 105 Boundaries of zone of plastic flow after failure of earth support of continuous footings after Terzaghi (1943).
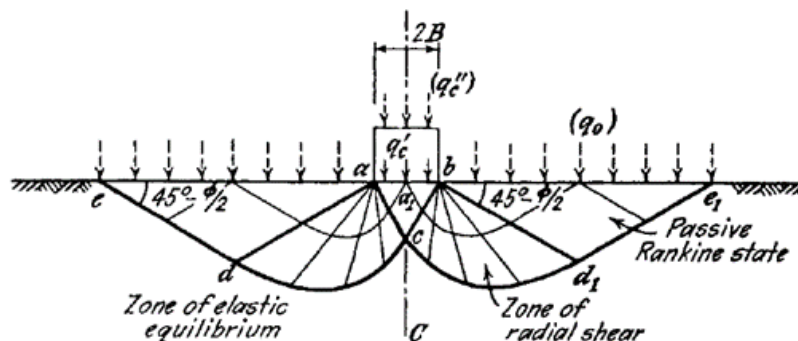
Figure 106 Plastic flow in semi-infinite cohesive weightless soil due to uniformly distributed surcharge for an infinitely long strip after Prandtl (1921)

4.1.4   Finite Element Analysis with Plaxis 2D

The finite element program Plaxis 2D was used to verify the resistances predicted by the Terzaghi and DnV formulae. An initial vertical load of 5 MN/m was assumed to determine the load factor.

The soil domain modelled in PLAXIS comprised a 2D slice of a 50 m wide, 25 m deep deposit of clay. The 8 m wide strip footing was located on the surface. The soil domain was divided into three sections with refined meshing density as shown in Figure 107. The clay was modelled using the PLAXIS Mohr-Coulomb soil model. The footing was modelled as weightless with the elastic properties shown in Table 19. The analysis was performed in four construction stages: (i) generation of initial conditions (pore water pressures and initial stress), (ii) staged construction (placement of the footing), (iii) activation of the point load and (iv) completion of the plastic analysis (application of the point loads to failure).

Contours of shear strain are shown in Figure 108 for the vertical load case without eccentricity. The combinations of vertical and horizontal loads defining the yield envelope for all loading scenarios are shown in Section 4.1.8.

Table 19 Material Properties assumed in the PLAXIS 2D analyses

Property	Clay	Concrete	Unit
Material model	Mohr-Coulomb	Linear Elastic	-
Type of Behaviour	Undrained	Non-Porous	-
Total Unit Weight	18	0	kN/m^3
Young's Modulus, E	5000	2.0×10^7	kPa
Poisson's ratio	0.35	0.15	-
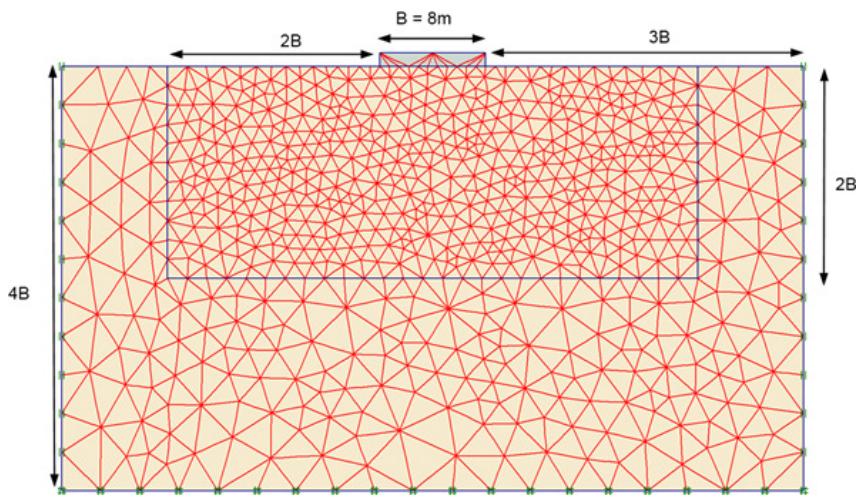
Figure 107 Generated finite element mesh for PLAXIS 2D analysis

Figure 108 PLAXIS Incremental shear strain for pure vertical load without eccentricity

4.1.5 Finite Element Analysis with LS-DYNA

The bearing capacity of the strip footing was predicted using the LS-DYNA model of Figure 109. One element wide mesh with plane strain conditions on the Y faces to simulate an infinitely long footing. The mesh was continued for 5B = 40 m from the edge of the footing, and 40 m in depth. The dimensions of the solid elements for the soil were a constant 0.33 m × 0.33 m × 0.33 m. The footing was modelled as rigid shell elements meshed into the soil surface.
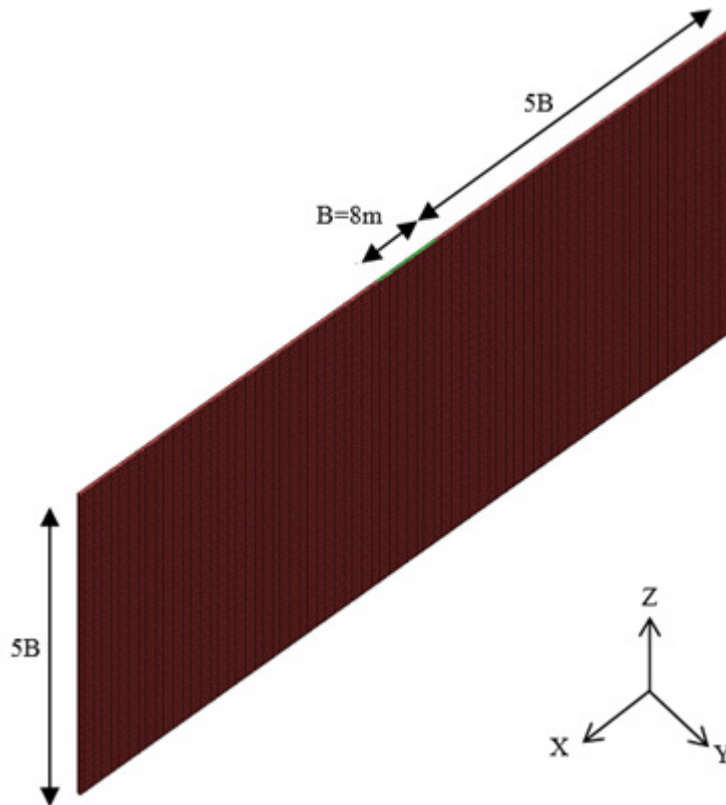
Figure 109 Overview of the LS-DYNA finite element model

The theoretical solution of Terzaghi assumes that soil behaves as a rigid-plastic material. Therefore an elasto-plastic stress-strain curve was simulated in LS-DYNA using the *MAT_HYSTERETIC_SOIL material model with a high initial shear modulus. The bulk modulus was determined from the shear modulus assuming a Poisson's ratio of 0.3. To prevent modification of soil strength due to 'pressure sensitive' features of MAT_HYSTERETIC_SOIL, these features were set to zero or unity, as appropriate.

The LS-DYNA analyses were conducted under displacement control in which the displacements of the centroid of the rigid footing were ramped up over time. The footing was allowed to rotate about the global Y axis to allow the appropriate deformation mechanism to develop.

4.1.6 LS-DYNA analysis results

4.1.7 Deformation mode under vertical loading only

Figure 110 show the maximum shear strain on a deformed mesh for the case where a vertical displacement is applied at the centroid of the footing. The shear strains develop along failure surfaces similar to those illustrated by Terzaghi and predicted by PLAXIS 2D in Figure 108.
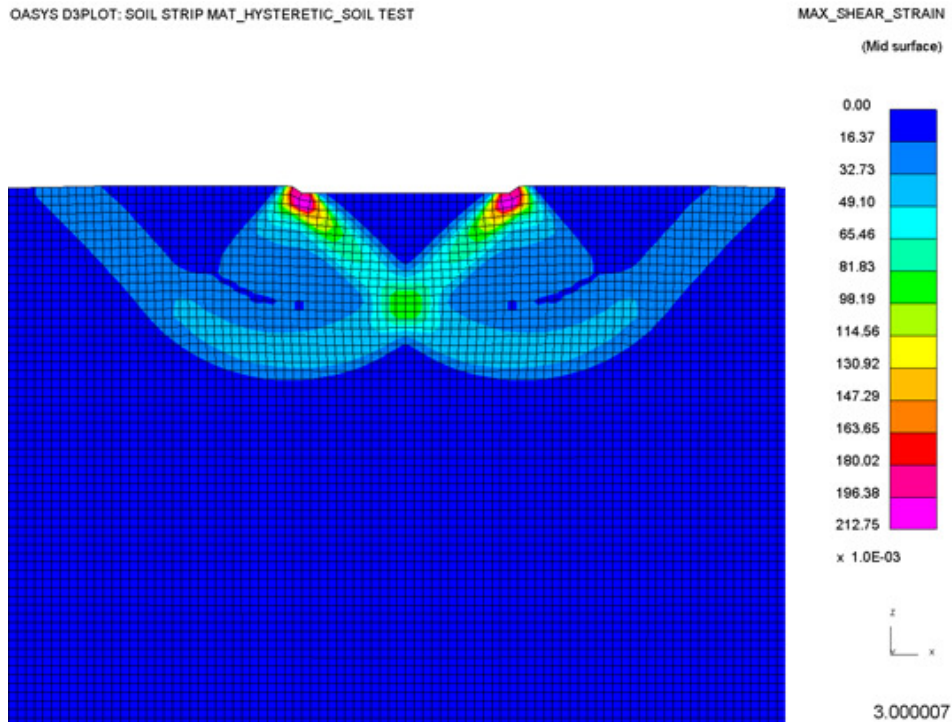
Figure 110 Shear strain distribution for analysis case with pure vertical displacement

Figure 111 shows the corresponding velocity vectors which provide further demonstration of Terzaghi's plastic mechanism (comprising downwards movement of a triangular wedge, and vertical uplift along a radial slip surface.
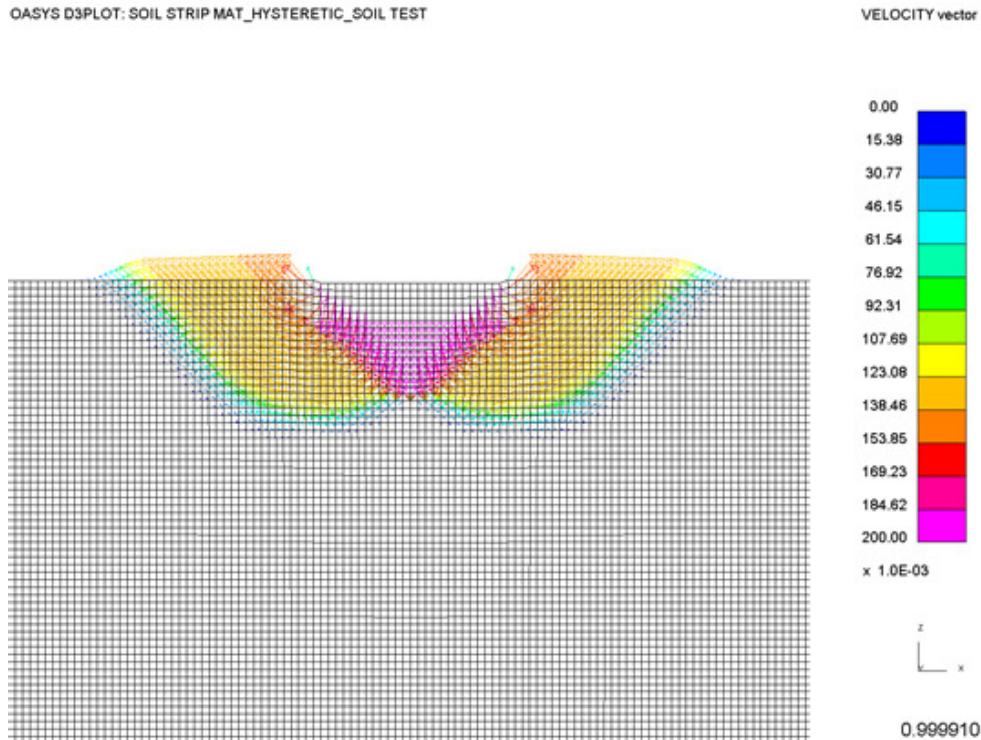
Figure 111 Velocity vectors for analysis case with pure vertical displacement at time of maximum applied velocity

4.1.8 Predicted resistances

The maximum resistances predicted by all three methods described above (in the form of yield envelopes of horizontal and vertical loads) are presented in Figure 112. The results obtained using LS-DYNA are in very close agreement with those derived by PLAXIS 2D and are similar to values predicted by the Terzaghi (1943) equation.
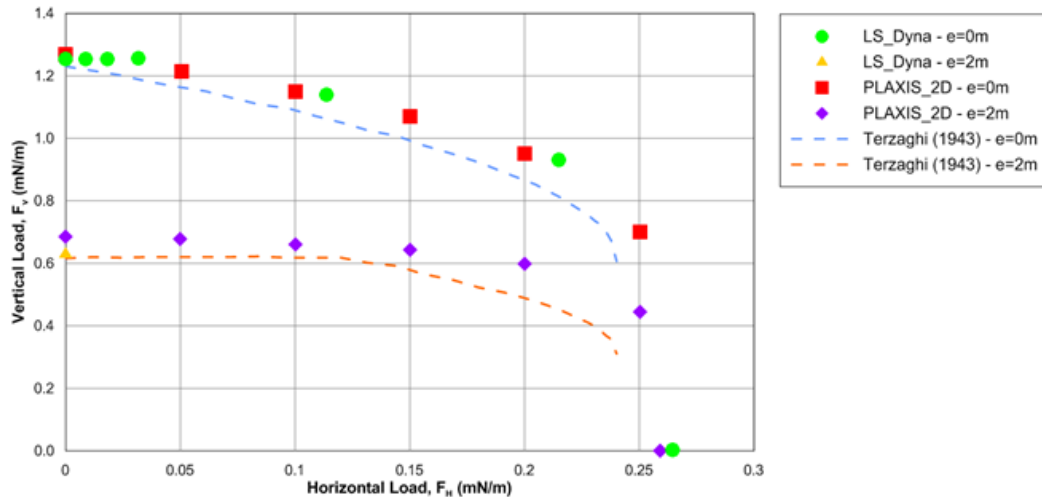
Figure 112 Results from LS-DYNA, PLAXIS 2D and Terzaghi (1943) in the form of yield envelopes of horizontal and vertical loads

The following observations can be made:

1.   The PLAXIS and LS_DYNA finite element models slightly over predict strip footing capacity relative to the Terzaghi (1943) bearing capacity equation. This is consistent with the Terzaghi bearing capacity factors being based on empirical data from laboratory and scale model tests.

2.   As the horizontal load is increased from zero, the finite element model capacities increasingly depart from the Terzaghi failure envelope up to approximately 13%. This is attributed to the fact that in the finite element models a pure sliding surface cannot form immediately under the footing, as assumed by the Terzaghi (1943) solution, since stresses and strains are only checked at element integration points. Furthermore, highly-distorted soil elements at the edge of the footing cannot break off from neighbouring elements, leading to an overall lengthening of the yield surface.

In view of the inherent uncertainty in soil properties in practice, the agreement between the predictions of LS-DYNA and other methods is very satisfactory.

4.1.9   References

[1]   Terzaghi, K. (1943), "Theoretical Soil Mechanics", John Wiley and Sons, New York;

[2]   L. Prandtl, (1921) "Über die Eindringungsfestigkeit (Härte) plastischer Baustoffe und die Festigkeit von Schneiden, Zeitschrift für angewandte Mathematik und Mechanik", 1(1), 15-20;

[3]   Das, B. (2006). "Principles of Foundation Engineering", Thompson-Engineering;

[4]   Det Norske Veritas, (1992). "Classification Notes No. 30.4 Foundations".

5 Modelling Non-Linear Site Response Using MAT_HYSTERETIC_SOIL

5.1 Modelling Principles

Non-linear site response analysis may conducted in LS-DYNA using a 3D soil domain meshed with solid elements. The soil domain may be excited in one, two or three orthogonal directions simultaneously. It is assumed that horizontal motions are transmitted by the 'vertically propagating shear wave' mechanism, and vertical motions by the 'vertically propagating p-wave' mechanism.

The non-linear shear stress vs shear strain backbone curve for each soil layer is the principal input to the MAT_HYSTERETIC_SOIL material model. Hysteresis follows either Masing rules (usually) or a non-Masing algorithm. These rules determine the unloading/re-loading paths, and as a result the hysteretic damping that will be generated. The soil stiffness may be defined as a function of strain rate, which research has shown can be important for cohesive soils subjected to cyclic loading. Small strain damping (for amplitudes lower than those which generate damping from non-linear hysteresis) is introduced using DAMPING_FREQUENCY_RANGE _DEFORM.

The height of the soil elements determines the maximum frequency that can be accurately transmitted. In general the soil domain should be divided into elements small enough to ensure each layer can propagate frequencies of at least 25Hz.

When soil-structure interaction of a structure is also to be incorporated the soil-domain must have substantial lateral extent. However, for the purposes of modelling site response alone it is only necessary to construct a 'column' comprising one single solid element per level, with the (four) nodes at each level constrained to move identically in the horizontal plane. This technique is used in the following validation cases.

5.2 Validation Case - Kashiwazaki-Kariwa Nuclear Power Plan, Japan

The Kashiwazaki-Kariwa Nuclear Power Plant (KKNPP), Japan is a 'non-basin' site with a down-hole array that has been well documented in the literature.

5.2.1 Site data

Site data for the KKNPP site were obtained from the Tokyo Electric Power Company (TEPCO) and re-interpreted by Motamed et al (2015) based on SPT, shear wave velocity, and site specific laboratory testing from Yee et al (2013). The primary change made to the TEPCO interpretation was the incorporation of an updated shear wave velocity profile developed with P-S suspension logging as described by Yee et al (2013). For details on the derivation of the backbone curves and dynamic soil properties for this study refer to Motamed et al (2015). The water table was assumed to be at 45.5m depth.

KKNPP Site		
Formation	Thickness (m)	Unit Weight (kN/m^3)
New Sand Layer	4	16.0
Banjin Sand Layer	41	17.8
Yasuda Layer	25	20.8
Nishiyama Layer	29.4	20.8
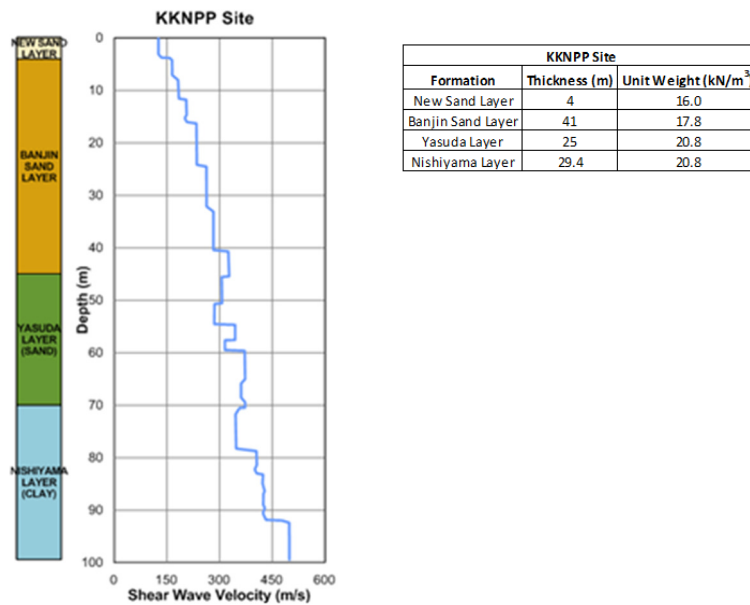
Figure 113 Stratigraphy, unit weight and shear wave velocity profiles for the KKNPP site

5.2.2   Ground motions

This validation study considers ground motions recorded at the Service Hall Array (SHA) near the KKNPP site during the M_w 6.6 Niigata-ken Chuetsu-oki earthquake on July 16th 2007. The SHA recorded motions at 2.4m, 50.8m and 99.4m below the ground surface. The acceleration time histories at a depth of 99.4m were rotated to match the fault normal and fault parallel directions before being used as input to the LS-DYNA soil column. The relevant response spectra of the recorded motions are presented in Figure 114. For further details refer to Motamed et al (2015).

Figure 114 Recorded response spectra rotated to (a) Fault Normal (FN) and (b) Fault Parallel (FP) directions

5.2.3   LS-DYNA model

The soil column used in the study is illustrated in Figure 115.
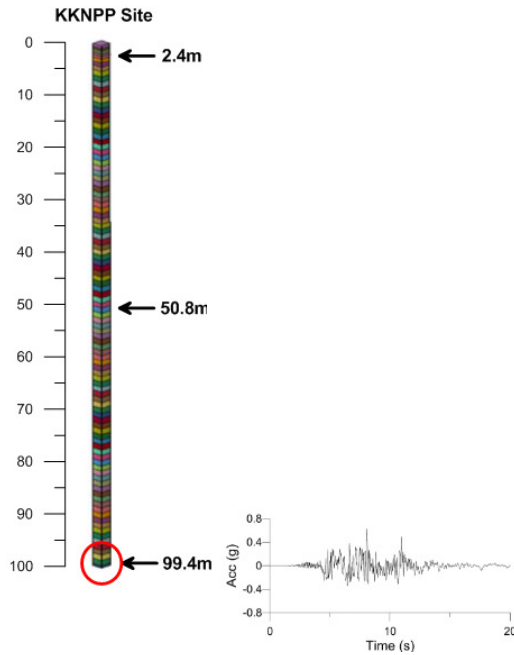
Figure 115 Soil column used to conduct SRA in LS-DYNA for the KKNPP site

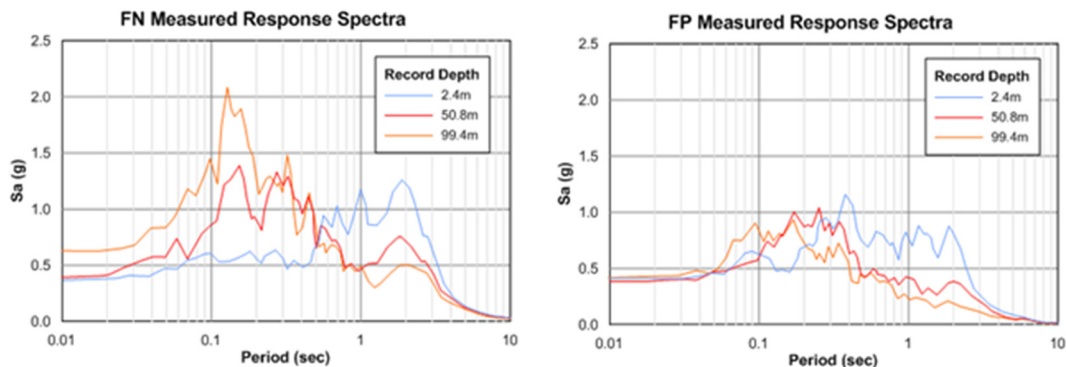The Masing hysteresis rules were used. Small strain damping of 2% of critical was specified, based on typical values estimated by Darendeli (2001). Strain rate correction was incorporated by a 5% increase in stiffness per log cycle of plastic strain rate for cohesive layers at strains greater than 10^{-5}

The recorded bi-directional horizontal motions at a depth of 99.4m were applied as input.

5.2.4   Comparison of predictions with measurements

The response spectra for the KKNPP site derived with LS-DYNA at 2.4m and 50.8m depths are compared in Figure 5 with those recorded from the vertical array.

Also shown are predictions by Yee et al (2013) using a 1D shaking model implemented in DEEPSOIL assuming small strain damping enhanced to 5% to improve comparison with the recordings. For further details on the predicted motions refer to Motamed et al (2015) and Yee et al (2013).

Figure 116 Recorded and computed ground motions spectrum with LS-DYNA and DEESPOIL (KKNPP site)

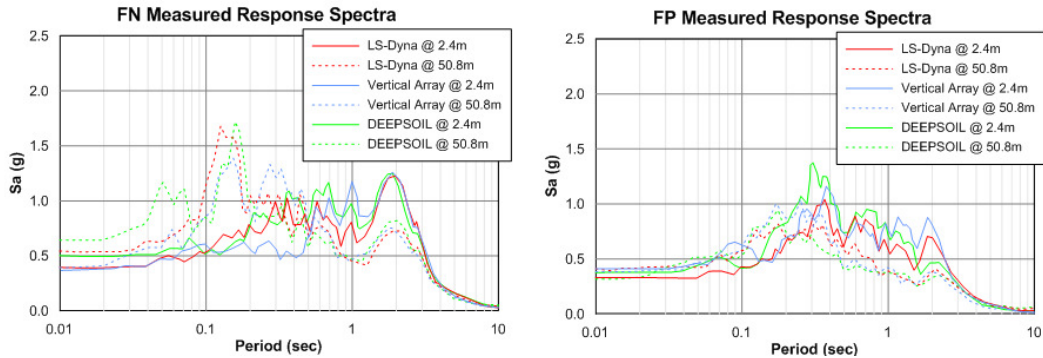The computed surface response spectra are in reasonable agreement with those recorded; the LS-DYNA prediction captures well the distinctive amplification of the response spectra associated with the first modes of the soil column.

5.3 Validation case- Secretariat of Communications and Transportation (SCT) site in Mexico City

The Secretariat of Communications and Transportation (SCT) site in Mexico City, is a 'non-basin' site with a vertical array which has been monitored since 1985. The array consists of accelerometers installed at 0 and 25m depth.

5.3.1 Site data

The stratigraphy of the SCT site was based on Seed et al (1988) and Hernandez-Martinez et al (2002). The idealized shear wave velocity profile was determined by averaging the available data from Hernandez-Martinez et al (2002), Ovando-Shelley et al (2007), Romo (1995) and Seed et al (1988). In addition, the shear wave velocity of the clay layers was increased by 15% in order to account for thixotropic effects. The plasticity index was obtained from Hernandez-Martinez et al (2002). The shear strengths based on the CPT tip resistance data from Ovando-Shelley et al (2007).
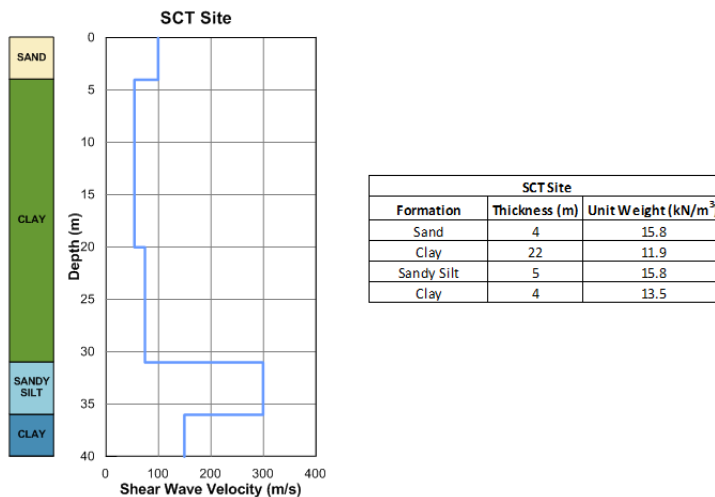

SCT Site		
Formation	Thickness (m)	Unit Weight (kN/m³)
Sand	4	15.8
Clay	22	11.9
Sandy Silt	5	15.8
Clay	4	13.5

Figure 117 Stratigraphy, unit weight and shear wave velocity profiles for the SCT site

5.3.2   Recorded Ground Motions

Ground motions from the Mw 7.3 earthquake recorded on September 14th 1995 obtained from the Mexican Strong Motion Database (MSMD) for the SCT down-hole array site were utilized. For the actual records of these ground motions refer to MSMD.
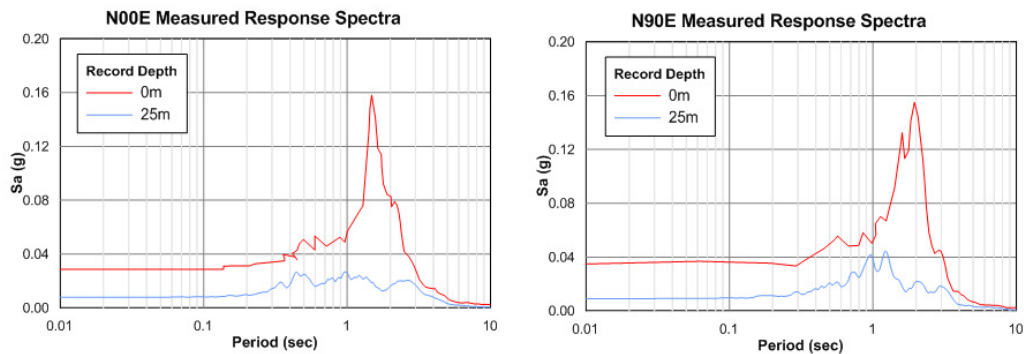
Figure 118 Recorded response spectra in (a) the N00E direction and (b) the N90E directions

5.3.3   LS-DYNA model

The soil column used in the study is illustrated in figure 4.
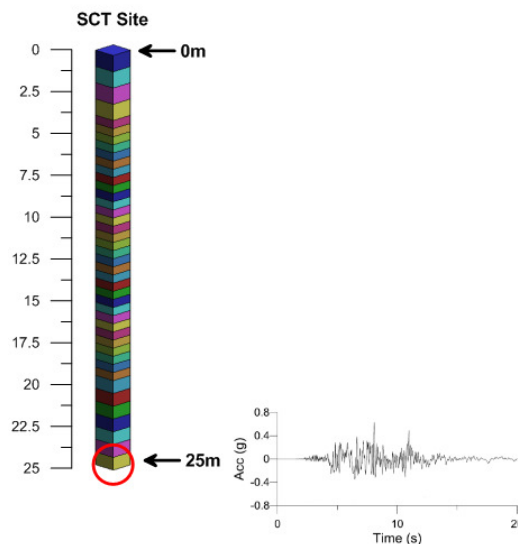
Figure 119 Soil column used to conduct SRA for the SCT Site in Mexico City

The backbone curves in the SCT site were based upon Darendeli (2001) adjusted in order to achieve the correct shear strength at a specified target strain. The Masing hysteresis rules were used. Small strain damping of 2% of critical was specified, based on typical values estimated by Darendeli (2001). Strain rate correction was incorporated by a 15% increase in stiffness per log cycle of plastic strain rate for cohesive layers at strains greater than 10^{-5}

The recorded bi-directional horizontal motions at a depth of 25m were applied as input.

5.3.4   Comparison of predictions with measurements

The surface response spectra for the SCT site derived with LS-DYNA are compared in Figure 92 with those recorded from the vertical array. It is evident that the computed surface response spectra are in good agreement with those recorded; it is seen that the LS-DYNA prediction captures the distinctive "double-peak" of the response spectrum associated with the first two modes of the soil column.
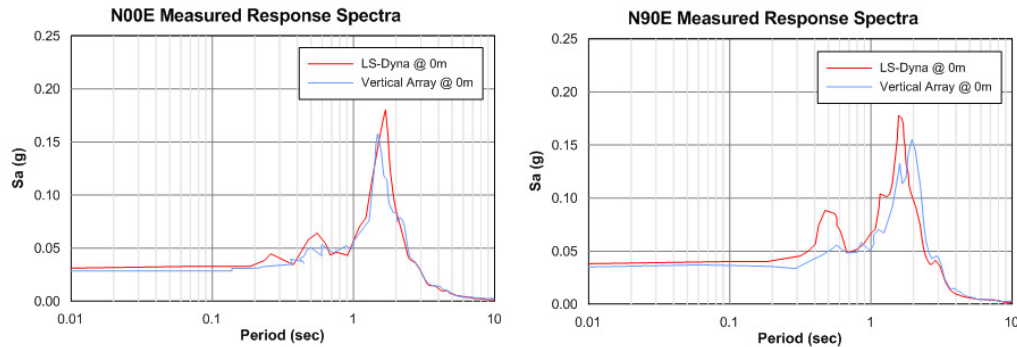

Figure 120 Recorded surface ground motion spectra compared with LS-DYNA prediction

5.3.5   References

[1]   Motamed, R., Stanton, K., Almufti, I, Ellison K. and Willford, M. (2015). "Improved Approach for Modelling Nonlinear Site Response of Highly Strained Soils: Case Study of the Service Hall Array in Japan". Journal of Earthquake Spectra.

[2]   Yee, E., Stewart, J. P., & Tokimatsu, K. (2013). "Elastic and Large-Strain Nonlinear Seismic Site Response Analysis of Vertical Array Recordings". Journal of Geotechnical and Geoenvironmental Engineering, 139, 1789 - 1801.

[3]   Seed. H., Romo, M., Sun, J., Jaime, A., and Lysmer, J. (1988). "The Mexican Earthquake of September 19, 1985 – Relationships Between Soil Conditions and Earthquake Ground Motions". Earthquake Spectra. Vol. 4, No. 4, 687 – 729.

[4]   Ovando-Shelley, E., Ossa, A., and Romo, M.P. (2007). "The sinking of Mexico City: Its effects on soil properties and seismic response". Soil Dynamics and Earthquake Engineering, 27(4), 333-343.

[5]   Romo, M.P. (1995). "Clay Behavior, Ground Response and Soil-Structure Interaction Studies in Mexico City". In Proceedings: 3rd Int. Conf. on Recent Advances in Geotech. Earthquake Eng. and Soil Dynamics, St. Luis, MO.

[6]   Darendeli, M. (2001). "Development of a new family of normalized modulus reduction and material damping curves". Ph.D.

Dissertation, University of Texas, Austin, Department of Civil Engineering.

[7] Hardin, B.O. and Drnevich, V.P. (1972). "Shear Modulus and Damping in Soils," Journal of Soil Mechanics and Foundations Division, ASCE, 98(7), 667-692.

[8] F. G. Hernández-Martínez, V. M. Taboada-Urtuzuástegui, A. W. Elgamal, M. P. Romo, "Linear analysis to evaluate dynamic soil properties at SCT site in Mexico City", Paramètres de calcul géotechnique. Magnan (ed.) 2002, Presses de l'ENPC/LCPC, Paris

6 Modelling Timber Diaphragms and Connections

6.1 Nail Connection Modelling

6.1.1 Test Description

Lin and LaFave (2012) conducted experiments to study the behaviour of connections between brick walls and timber diaphragms. Specimens comprised a small section of brick wall including a pocket in which a timber joist was supported, as shown in Figure 121. The masonry was constructed of clay bricks using Type S Portland cement mortar.

The selected specimen for this study had traditional wall-joist anchors comprising a steel strap and a threaded rod welded together. The wall anchor and wood joist were connected by two 10d bright common nails, and the threaded rod was anchored outside the masonry with a standard hex nut and washer. Figure 122 illustrates the size and characteristics of the specimen.

The brick masonry portion of the assembly was held by two vertical clamps. Two additional horizontal steel clamps were used: a lower clamp to prevent the brick masonry assembly from cracking, and an upper clamp to apply a normal compression force between the joist and the base of the brick wall pocket, as shown in Figure 121. This force was set to a representative value of around 3.78-4.0 kN at the beginning of each test, but was sometime varied during certain tests. The specimens were tested under uniaxial loading (in the joist longitudinal direction) in a testing machine.
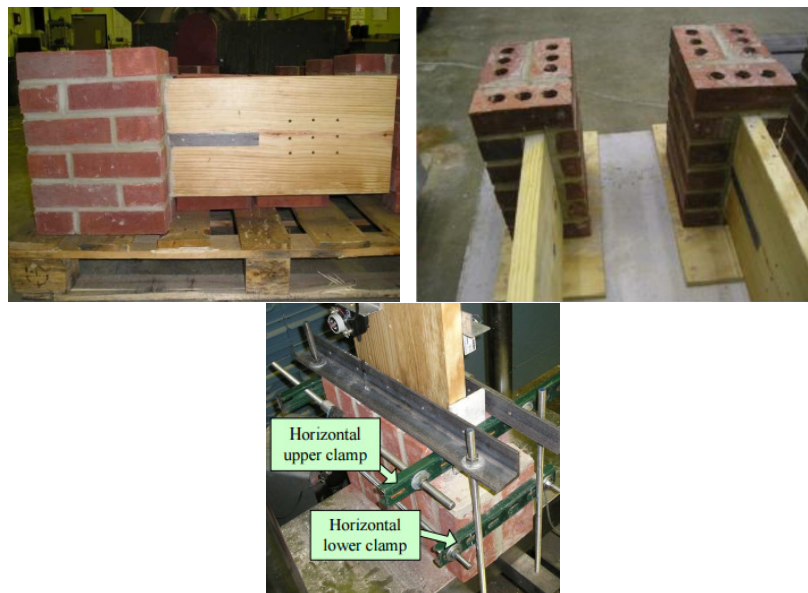

Figure 121 Test specimen of wall-diaphragm connection. (Lin and LaFave, 2012)
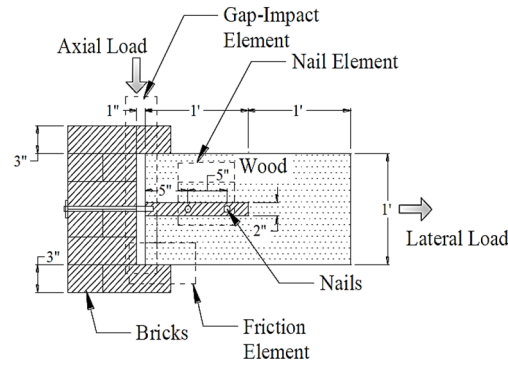
Figure 122 Size of the specimen tested

A lower bound value for the friction coefficient of 0.2, average value of 0.5, and an upper bound value of 0.8 was determined.

6.1.2   Test Results

Figure 123 shows the force-displacement backbone curves generated for the specimen under static monotonic loading. This represents the actuator force at the free end of the wood joist versus relative displacement between the wood joist and brick assembly. Both specimens failed as the two nails sequentially sheared off at the head. Failure of each nail was accompanied by a steep drop in the force vs. displacement curve.
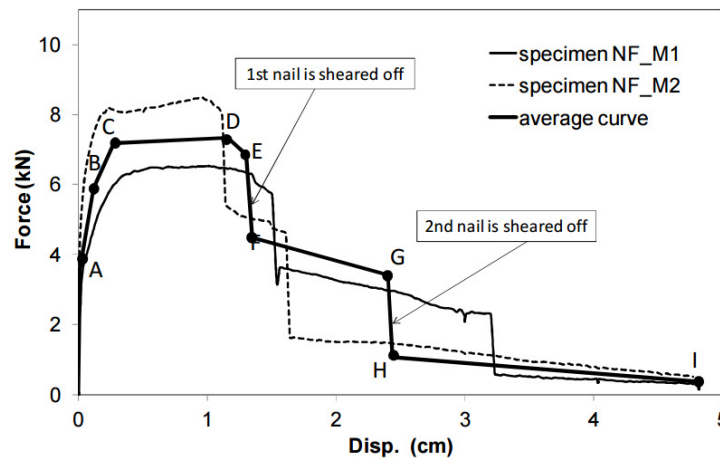

Figure 123 Force vs. displacement curves for the specimens (Lin and LaFave, 2012)

6.1.3   LS-DYNA Modelling

A detailed finite element (FE) model of the specimen was modelled in LS-DYNA (Figure 124). The nails are considered the weakest link whereas the brick walls, steel anchors and straps are expected to remain elastic and almost rigid during loading. Therefore, it is assumed that the nonlinear behaviour will come from the nail-slip deformation. This assumption is primarily consistent with the results of the experimental program and those in the literature.
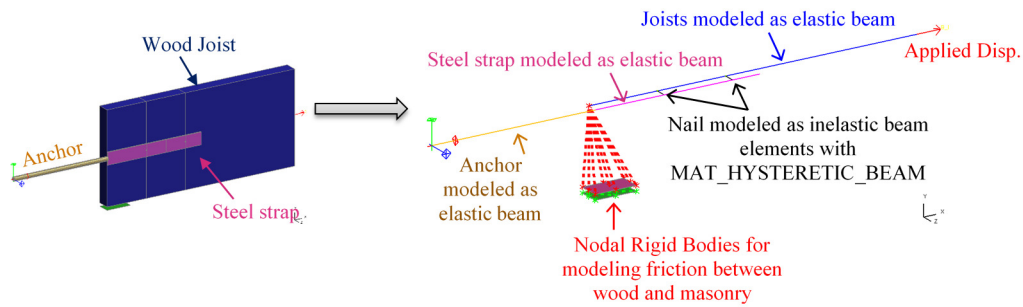
Figure 124 LS-DYNA model of the nail connection test specimen

The nails were modelled as nonlinear beam elements using MAT-HYSTERETIC-BEAM elements in which the shear force vs. plastic strain backbone curve for the nail is defined.

The behaviour of the nail depends on many factors including the properties of the side members, nail size, material, etc.. MacLain (1975) developed a procedure for predicting the load-slip curves of laterally loaded nailed wood joints as shown below:

$$V_n = A \, log_{10}(1 + B \, e_n) \tag{1}$$

where:

V_n = Lateral load, kN

A, B = Empirically-derived constants, kN and mm$_{-1}$, respectively

e_n = Interlayer slip, mm (relative displacement of joint members)

McLain found that parameter A could best be predicted as a function of the specific gravities (SG) of the main and side members (SG model). The equation recommended for joints with only solid wood members is:

$$A = I[0.2053 + \frac{0.232}{SGS} - 0.0324 SGS \times SGM] \tag{2}$$

where:

I = 4.448 for A in kN (1.0 for A in kips)

SGS= Specific gravity of side member

SGM = Specific gravity of main member

Parameter B can be determined from Eq. (3) which requires a known point on the V_n-e_n curve. An approach was developed based on the theory of beams on elastic foundations that enables the prediction of the load associated with a joint slip of 0.38 mm (for more information the reader is referred to Appendix A in Peralta, 2003)

$$B = 10^{Vn/A} - 1/e_n \tag{3}$$

This method was developed for one nailed joint specimen configuration which was a single-shear joint consisting of a solid-wood main member and a 3/4-in.-thick side member connected with an 8d common wire nail. This method was later improved by Pellicane et al. (1991) to incorporate the effects of nail size (6d to 10d common nails), side-member thickness, side-member specific gravity, main-member specific gravity, and interlayer gap (0-0.9 mm).

The backbone curve adopted for the shear force vs. interlayer slip displacement of the nail is shown in Figure 125, based on the method proposed by MacLain (1975). It is scaled to match the "Connection Yield Force" predicted using "Connection Calculator" of the American Wood Council for the current test setup. The failure displacement point was selected based on the experimental results.
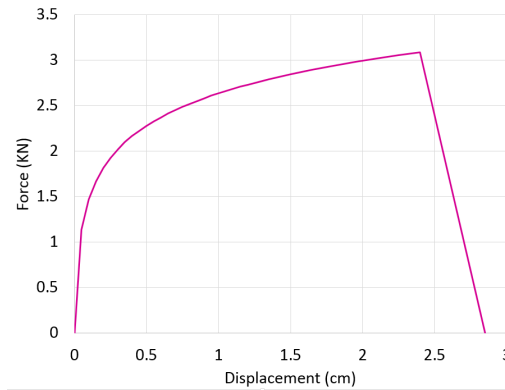

Figure 125 Force-displacement backbone curve for nails

Young Modulus for the wood joist was taken as 12400 MPa, based on Peralta, (2003). A friction coefficient of 0.25 between wood and masonry was used.

6.1.4   LS-DYNA: Results & Validation

Figure 126 shows the force displacement behaviour of the model as compared to the experiments.

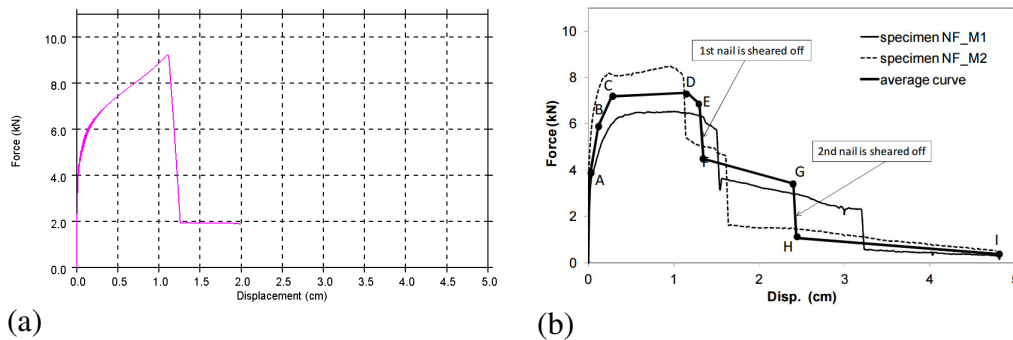
(a)   (b)

Figure 126 Load vs. applied displacement: (a) LS-DYNA, (b) Experiments

6.1.5   Conclusion

A reasonable level of agreement is observed between the LS-DYNA model and the experiments. It should be noted that MacLain's method does not provide any information about the behaviour of the nail after failure.

6.1.6   References

[1]   Dolan, J.D and Madsen, B. (1992), "Monotonic and Cyclic Nail
Connections Tests", Canadian Journal of Civil Engineering,
1992, 19(1): 97-104.

[2]   Lin, T., and LaFave, J. M. (2012). "Experimental Behaviour and
Modelling of Wall-Diaphragm Connections for Older
Masonry Buildings." *15th World Conference on Earthquake
Engineering.* Lisbon, Portugal.

[3]   Mclain, T. E. (1975). "Curvilinear Load-Slip Relations in Laterally
Loaded Nailed Joints." Ph.D. Report, Colorado State
University, Fort Collins, CO.

[4]   Patrick J. Pellicane, Jeffery L. Stone, M. Daniel Vanderbilt (1991).
"Generalized Model for Lateral Load slip of Nailed Joints",
Journal of Materials in Civil Engineering (ASCE), 3:60-77.

[5]   David F. Peralta, Joseph M. Bracci and Mary Beth D. Hueste, (2003).
"Seismic Performance of Rehabilitated Wood Diaphragms",
Department of Civil Engineering, Texas A&M University.

6.2   Timber Diaphragm

6.2.1   Test Description

Peralta et al (2003) performed displacement-controlled quasi-static reversed cyclic tests on existing and rehabilitated floor and roof wood diaphragms under in-plane lateral loads. Two experimental specimens were chosen for the validation studies in this report:

1. a square edged single straight sheathed diaphragm (MAE-2) designed to represent a typical roof diaphragm in pre-1950's URM buildings,

2. the retrofitted diaphragm with an unblocked plywood overlay (MAE-2B) designed for improving the diaphragm's in-plane lateral stiffness.
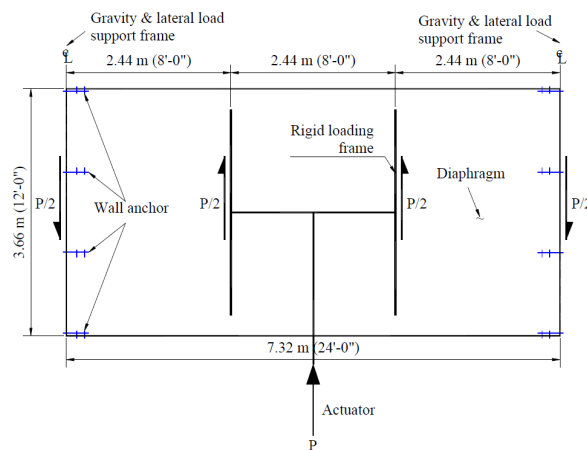
Figure 127 shows the experimental setup.

Figure 127 General diaphragm test setup

Figure 128 shows details of the MAE-2B model and panel arrangements. Specimen MAE-2 was similar to MAE-2B without plywood overlay.

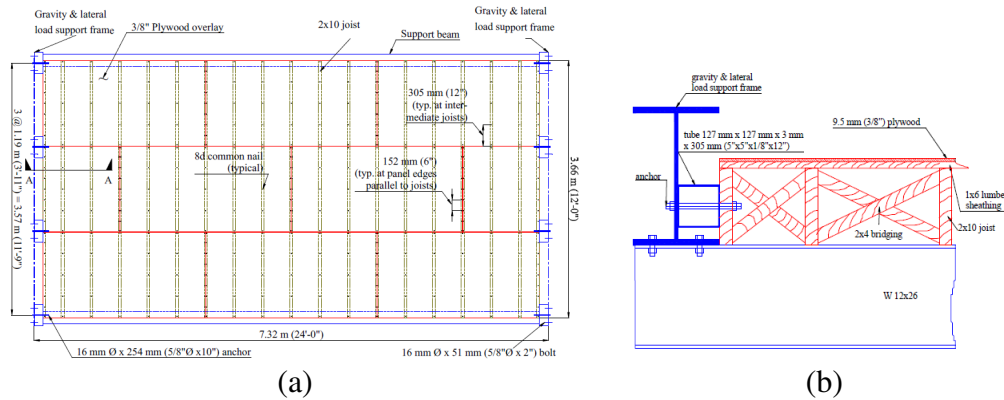(a)   (b)

Figure 128 MAE-2B test specimen: a) plan view details; b) connection details

Southern Pine lumber was used for the solid wood elements. The material properties were determined from AF&PA (1997) and APA (1986) and are listed in Table 20.

Table 20 Material Properties (Peralta et al., 2003)

Property	Solid wood	Plywood
Young's Modulus, MPa (ksi)	12400 (1800)	1490 (216)
Poisson's Ratio	0.2	0.2
Specific Gravity	0.55	-

8d common nails were used with diameter of 3.33 mm and length of 6.35 cm.

Displacement-controlled quasi-static reversed cyclic testing was performed on each diaphragm applying two cycles for each lateral displacement amplitude (a total of 10 displacement amplitudes with maximum value of 76.2 mm). These displacement amplitudes were determined to be appropriate for determining the elastic and inelastic lateral response of the diaphragm specimen.

6.2.2 Test Results

Figure 129 shows the in-plane lateral responses measured for the diaphragms representing the actuator load versus average displacement at the loading points (Figure 127).
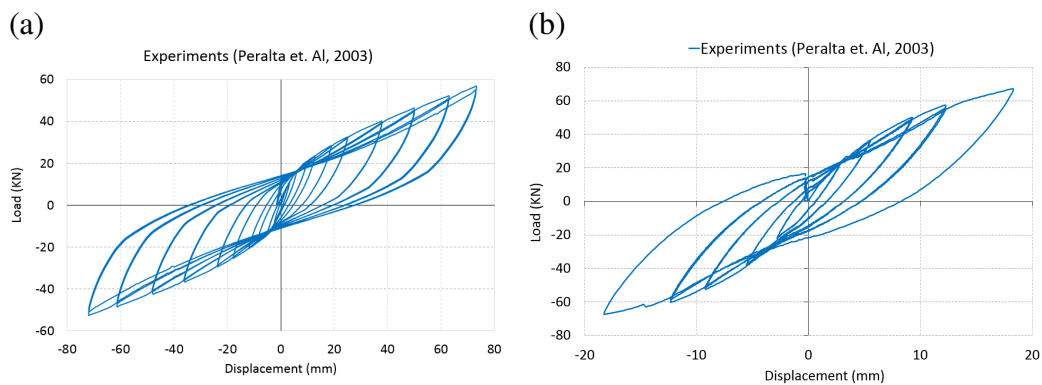
Figure 129 Load-displacement curves for the diaphragm from experiments: a) MAE-2; b) MAE-2B

6.2.3 LS-DYNA Modelling

Detailed finite element (FE) models of the specimens were modelled in LS-DYNA (Figure 130).
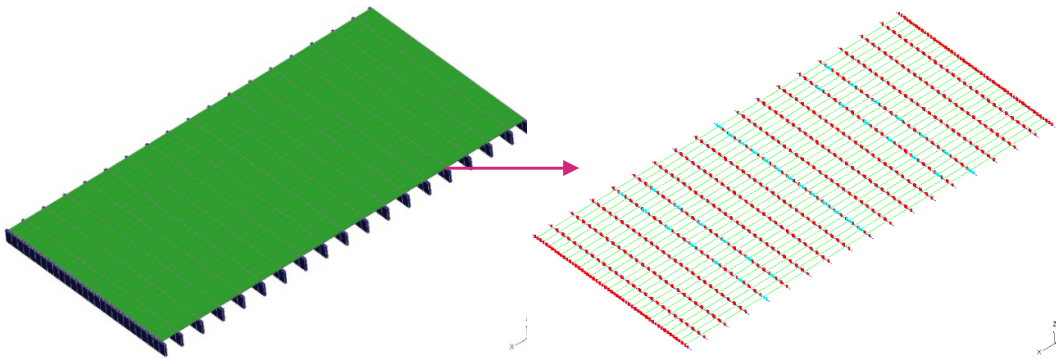

Figure 130 LS-DYNA model for timber diaphragm

It was assumed that the fasteners were the only source of material nonlinearity in the system; this is consistent with the results from the experimental program and those in the literature. The diaphragm specimens were idealized as an assemblage of elastic beams and shell elements connected by nonlinear beam elements representing nails as follows (Figure 131):

1- Sheathings were modelled as elastic beams.
2- Joists were modelled as elastic beams.
3- Plywood in case of MAE-2B was modelled as elastic shell elements.
4- Nails were modelled as nonlinear beam elements using MAT-HYSTERETIC-BEAM with parameters calculated as per Section 6.1
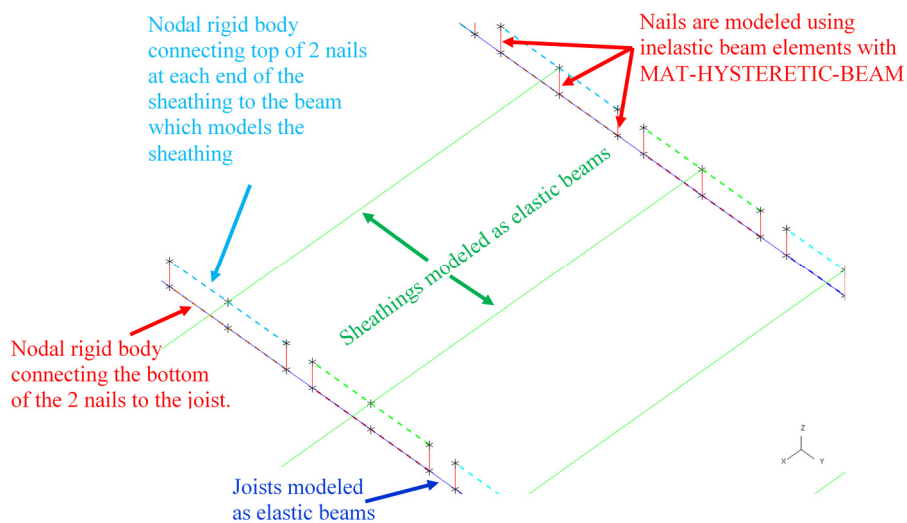
Figure 131 Details of the LS-DYNA model

6.2.4   LS-DYNA: Results & Validation

Figure 132 compares the predicted force-displacement hysteresis of the two specimens to the experimental measurements.
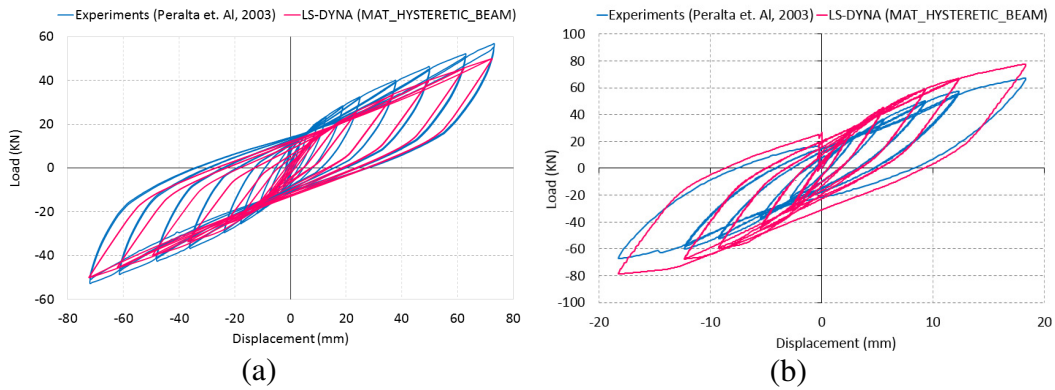

(a)   (b)

Figure 132 Load vs. applied displacement: a) MAE-2, b) MAE-2B

6.2.5   Conclusion

A good level of agreement is observed between the LS-DYNA model and the two experiments. The results presented in this report were obtained using the actual Modulus of Elasticity of the materials without further calibrations to match the results better.

6.2.6   References

[1]   American Forest & Paper Association (AF&PA) (1997). "National Design Specification for Wood Construction." NDS, Washington, D.C.

[2]   APA – The Engineered Wood Association (APA) (1985). "Design/Construction Guide -Residential and Commercial." APA, Tacoma, Washington.

[3]   David F. Peralta, Joseph M. Bracci and Mary Beth D. Hueste, (2003). "Seismic Performance of Rehabilitated Wood Diaphragms", Department of Civil Engineering, Texas A&M University., Texas, USA.